Thermally-Induced Deformations and Stresses in a Steel

Trapezoidal Twin-Box Girder Bridge

by

Michael Gene Lopez, B.S.

Thesis

Presented to the Faculty of the Graduate School of

The University of Texas at Austin

in Partial Fulfillment

of the Requirements

for the Degree of

Master of Science In Engineering

The University of Texas at Austin

May, 1999

Thermally-Induced Deformations and Stresses in a Steel Trapezoidal Twin-Box Girder Bridge

Approved by
Supervising Committee:

Supervisor: Karl H. Frank

Joseph A. Yura

Dedication

This thesis is dedicated to my parents, who personify all that I wish to be.

Acknowledgements

Abstract

Thermally-Induced Deformations and Stresses in a Steel Trapezoidal Twin-Box Girder Bridge

Michael Gene Lopez, M. S. E.

The University of Texas at Austin, 1999

Supervisor: Karl H. Frank

Curved-span steel bridges are becoming increasingly popular. Box girders are optimal for use on such spans, as the large torsional stiffness of a closed section is often more economical than the use of several "open" sections.

Pot bearings are often used with box girders in such bridges. These bearings can accommodate relatively large rotations, and, when used with sliding surfaces, can accommodate significant translations, as well.

The bridge under investigation uses both box girders and pot bearings. It is desired to know what deformations--translations and rotations--may be reasonably expected to occur at the bearings during the year due to temperature changes within the structure. This thesis describes the analytical and experimental investigation of the bridge under study to determine what deformations develop at the bearings. Measured deformations are compared to theoretical values, and other findings are discussed.

Table of Contents

List of Tables

List of Figures

List of Illustrations

Chapter 1

Introduction

1.1   Texas Department of Transportation Project 1395

Trapezoidal steel box girders are finding more frequent use because of their pleasing appearance and large torsional stiffness, which makes them optimal on curved spans. Because there is no specific design specification for such girders, the Texas Department of Transportation (hereafter referred to as "TxDOT") sponsored a research study, Project 1395, on various aspects related to their design and behavior. Investigators on this research project are examining the thermal deformations of such bridges, lateral bracing of the compression flanges of the girders used, stiffener use on the bottom flange of such girders in the negative moment region, and stresses arising during bridge erection.

The study reported herein focuses on the thermal translation and rotation behavior at the pot bearings used on a twin trapezoidal curved steel box girder bridge in Houston, Texas. The continuous three-span bridge is at the intersection of Interstate 45 and Beltway 8, and was opened to traffic in 1996. In a location such as Houston, with its mild winters and very hot summers, it is expected that such motions would be significant and should be accounted for in bearing design, although larger temperature ranges and motions may occur at other U.S. sites.

1.2 Current Bridge Temperature Specifications

The American Association of State Highway and Transportation Officials (AASHTO) currently recognizes the effects that thermal changes will impart upon a bridge structure. The AASHTO *LRFD Specification* (1998) provides for two different climates and specifies the temperature ranges to be used when calculating thermal deformations, as shown in the Table 1.1:

Table 1.1 AASHTO-Specified Temperature Ranges

CLIMATE	STEEL OR ALUMINUM	CONCRETE	WOOD
Moderate	-18° to 50° C	-12° to 27° C	-12° to 24° C
Cold	-35° to 50° C	-18° to 27° C	-18° to 24° C

AASHTO specifies that the temperature ranges used to calculate thermal deformations should be the differences between the upper and lower extremes and the temperature at the time of construction, which is to be taken as the mean air temperature over the twenty-four hour period immediately preceding the setting of the bridge or any of its components. These temperature ranges are used to calculate uniform expansions and contractions of the bridge.

AASHTO also provides thermal gradients to be applied through the depth of the bridge section, in order to determine rotations associated with temperature changes, and their effect on the bridge structure. AASHTO divides the country into four solar radiation zones and provides temperature gradients to be applied to

2

the bridge, depending on the bridge's geographic location and deck surface condition. The gradient specified by AASHTO for a bridge in Houston, Texas, which has a plain concrete deck, is shown in Figure 1.1 by solid lines.
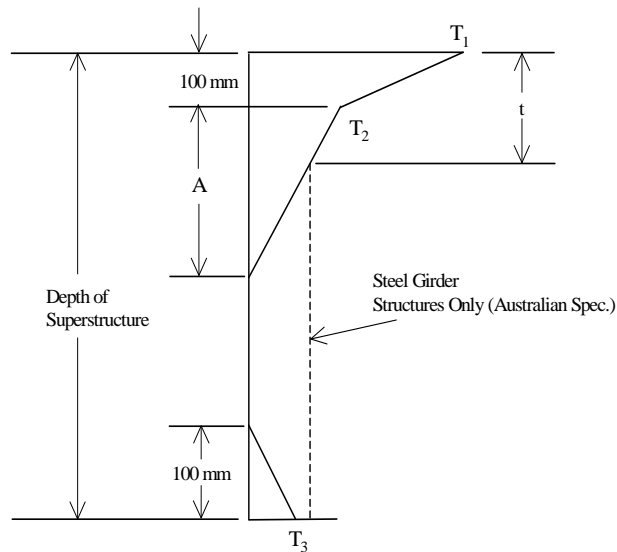
Figure 1.1 AASHTO-Specified Temperature Gradient

where: A = 0.30 m,

t = the depth of the concrete deck,

$T_1 = 25°$ C,

$T_2 = 6.7$ °C.

T_3 shall be taken as 0° C, unless a site-specific study is made to

determine an appropriate value, but shall not exceed 3° C.

AASHTO also specifies that negative curvature-inducing temperature gradients equal to one-half the positive gradients be considered. The dashed line represents the thermal gradient for steel bridges specified by the Australian bridge

specification, *Austroads*. These temperature ranges and gradients will be examined in more detail in Chapter 3.

In order to illustrate the thermal effects on deformations and stresses, consider a three-span simply-supported beam, subjected to a uniform increase in temperature. The bridge under study consists of two trapezoidal box girders with a concrete slab providing composite action in bending. The bridge is continuous over three spans, with support conditions idealized as rollers at three supports and a pinned fourth support. For this illustration, assume three equal span lengths, as shown in Figure 1.1. Pertinent quantities, which approximate those of the bridge under study, are tabulated in Table 1.2.

For a uniform temperature rise of 68°C, which is the AASHTO-specified temperature range to be considered for uniform expansion of a steel bridge in Houston, the maximum horizontal displacement of this bridge would occur at the left-most support shown in Figure 1.2 and would be equal to:

$$\Delta = \alpha L (\Delta T)$$
$$= (1.17 \times 10^{-5} \text{ °C}^{-1})(130 \text{ m})(68 \text{ °C})$$
$$= 0.102 \text{ meters, or } 102 \text{ millimeters.}$$
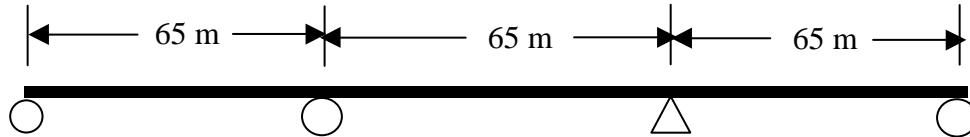
Figure 1.2 Beam Used In Example Problem

Table 1.2 Values Used In The Example

Cross-Sectional Area	Elastic modulus	Coefficient of thermal expansion
0.25 m^2	200 GPa	0.0000117 °C^{-1}

Conversely, if the roller supports are replaced with pinned supports and no expansions or contractions are allowed, the system will undergo a maximum stress change of:

$$\sigma = E\alpha(\Delta T)$$
$$= (200 \times 10^3)(1.17 \times 10^{-5} \, °C^{-1})(68 \, °C)$$
$$= 159.1 \, \text{Mpa.}$$

It is clear, then, that significant displacements will tend to occur in this bridge system, and that, if these motions are not properly accommodated, significant thermal stresses will arise.

Consideration of thermal variations through the depth of this indeterminate structure will lead to induced stresses within the structure. Moments and rotations will be induced over the supports, as will vertical reactions, even in the absence of applied gravity loading. This further illustrates the effects of temperature changes within a structure. In general, bearings are used to accommodate the thermal movements so that thermal stresses are minimized.

1.3   Pot Bearings: Use, Function, and Requirements

Pot bearing systems can accommodate large reactions, along with large rotational displacements. The essential elements of such bearings are a cylindrical (pot-shaped) housing, an elastomeric pad, sealing rings, and a piston (Roeder and Stanton, 1996). Top and bottom bearing plates are typically used to provide for attachment of the bearing unit to the bridge pier caps and to increase the bearing support area on the cap.

The various elements of a pot bearing fit together to form a viable load-bearing unit. The elastomeric pad is confined within the system by the sealing rings. Sealing rings protect the elastomer from leakage and deterioration from contaminants, extending the useful life of the elastomer. The vertical load reactions imposed upon the bearing are carried through compression of the elastomeric pad, which, although it has some shear stiffness, is often idealized as behaving hydrostatically.

Pot bearings are ideal for use when expected bridge bearing rotations are relatively large. Pot bearings are particularly well-suited for these applications, as they will allow rotations to occur about any axis. This is accomplished through deformation of the elastomeric pad housed within the pot. Large cyclic rotations can quickly damage pot bearings due to abrasion and wear of the sealing rings

and elastomer, but pot bearings can withstand many cycles of very small rotations with little or no damage (Roeder and Stanton, 1996).

Pot bearings can also be made to accommodate significant lateral translations, as well. Unless used with a polytetraflourthylene (PTFE) sliding surface, a pot bearing will not allow any translation. However, where PTFE surfaces are used, relatively large translations can be tolerated across the bearing. Table 1.3 shows force and deformation capacities of both pot bearings and PTFE sliding surfaces.

Table 1.3 Force And Deformation Capacities Of Pot Bearings And Sliding Surfaces

Element Type	Load		Translation		Rotation	Costs	
	Min. (kn)	Max. (kn)	Min. (mm)	Max. (mm)	Limit (Rad.)	Initial	Mainten-ance
Pot Bearing	1200	10,000	0	0	0.02	Moderate	High
PTFE Slider	0	> 10,000	25	> 100	0	Low	Moderate

Table 1.3 shows that both bearing elements have attractive attributes. Polytetrafluorthylene surfaces can be used to accommodate large vertical forces and lateral translations at relatively low-to-moderate cost, while pot bearings will accommodate large vertical forces and moderate rotations at relatively moderate-to-high cost. It can be concluded that the use of the two elements in conjunction with one another will provide the bridge designer with several attractive bearing features, at moderate-to-high cost.

Other optional accessories often used with pot bearings are guides which dictate in which direction girder translations are allowed to occur. Motions are not allowed to occur in a direction normal to the orientation of the guides, but are

only allowed to occur in the guided direction. These are often necessary to provide stability to the bridge superstructure system with respect to rotation about a vertical axis. They may also be used where the dominant direction of bridge motion is already known. For example, the bridge under study has guided bearings near the relatively straight off-ramp. As the bridge has a relatively long expansion length leading to this ramp and is much longer than it is wide, deformations may thus reasonably be expected to occur in the longitudinal direction and not in the transverse direction. This would thus be a suitable location for such guides.

However, guides may be freely oriented in the structure. An important question thus facing the engineer is how to properly orient the guides to accommodate thermally-induced deformations in dominant directions while preventing damage caused by inhibiting deformations in other directions. This would be a venerable question to resolve in the design of a curved bridge such as the one under study.

1.4 Previous Thermal Studies

Most previous work has been related to temperature-induced stresses more rather than induced displacements. Thepchatri, Johnson, and Matlock (1977) provided a means of predicting temperatures and stresses in bridges using weather reports, with the inclusion of solar radiation, air temperature, and wind speed. Moorty and Roeder (1992) performed a finite element heat-transfer analysis in the determination of bridge temperatures to be used in a temperature-induced displacement analysis. Emerson (1981) developed a relation for the average temperature of a bridge, based on equilibrium principles, which accounts for different materials and material properties within the same bridge. Her formula will be presented and used later.

A most straightforward description of how temperature variations within a bridge at a given time will lead to stresses and displacements has been provided by Will, Johnson, and Matlock (1977). They found that thermal stresses and displacements in bridges may be divided into three categories:

1. Longitudinal and lateral expansion and contraction, which is mostly related to uniform heating or cooling.

2. Vertical displacements and rotations, usually caused by a temperature gradient through the depth of the bridge cross-section, which may be restrained by the indeterminancy of the structure.

3. Bending stresses due to the nonlinear distribution of temperature through the depth of the bridge cross-section.

It is assumed by the AASHTO *LRFD Specification* that the first type of stress and displacement occurs when the mean bridge temperature rises or drops. This is the most straightforward and familiar of the bridge motion concepts described herein.

The second type of motions may be attributed to the low thermal conductivity of concrete (Billington, 1952). Heat entering the concrete bridge deck only slowly passes through the depth of the deck to the girders below, resulting in temperature differentials through the depth of the bridge section. Steel, however, has a thermal conductivity fifty-four times that of concrete, so heat travels through the steel girders much more rapidly than it travels through the concrete deck. As a result of the bridge experiencing differing temperatures through its depth, vertical displacements are induced within the span, and rotations will occur at the bearings. The nonlinear temperature distribution is also a result of the differing conductivity properties through the bridge depth (Will, Johnson, and Matlock; 1977). The implication of this temperature distribution is that, if

deformation is restrained, a nonlinear stress distribution through the depth of the bridge will occur if plane sections remain plane.

1.5   The Scope of this Study

This study focuses on the thermal deformation behavior at the pot bearings in service in an existing bridge. Specifically, it is desired to know what magnitudes and ranges of thermally-induced displacements and rotations may reasonably be expected to occur in such a structure. It is also of interest to ascertain in which direction(s) movements tend to occur at unguided bearings, to facilitate future orientations of guides in such pot bearings.

The bridge was instrumented for temperature distributions and deformations for 11 months. Data was collected via a remote instrumentation scheme on an hourly basis during this period. This study does not concern deformations induced by gravity loading. Only thermally-induced deformations are considered. Of interest are displacements and rotations occurring at the bearings on two instrumented piers. A finite element model was developed to predict analytical results for comparison to measured values. The instrumentation scheme used is described in Chapter 2. The temperature data is analyzed in Chapter 3, while the displacement data is illustrated in Chapter 4. Analytical displacement predictions are investigated in Chapter 5. Induced rotations are considered in Chapter 6. Experimental girder stresses were not obtained, but analytical predictions are considered in Chapter 7, along with pier deflections. Conclusions are summarized in Chapter 8.

1.5.1   The Bridge Under Study

The bridge under investigation is at the northern edge of Houston, and is the curved portion of Beltway 8 as it passes over Interstate 45. The instrumented portion are the two spans that feed into northbound I-45. The structure is a twin-box girder bridge in which the girders are linked with diaphragms at the supports. A typical girder cross-section is shown in Figure 1.3.
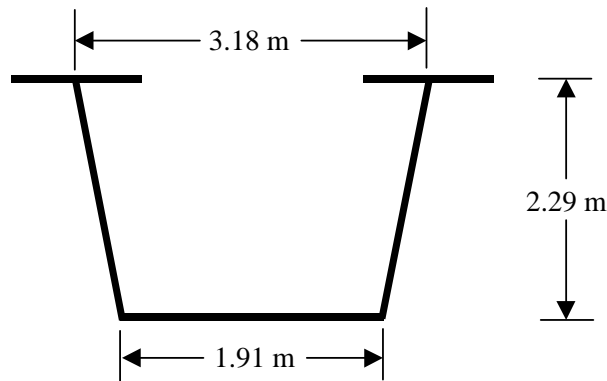
Figure 1.3 Typical Trapezoidal Box Girder Section

Although only two spans were instrumented for this study, the twin-box girder system comprises three spans, of lengths 87.2, 56.7, and 54.9 meters, all topped with a 240-millimeter-thick slab. The bridge is curved in plan, with a radius of approximately 274 meters. The diaphragms linking the girders mentioned above are different at the two piers instrumented for this study. The end instrumented pier (the northern pier) has a truss diaphragm composed of double angle steel members, as shown in Figure 1.4, while the inner instrumented pier (the southern pier) has a steel plate diaphragm, as shown in Figure 1.5. There are also

11

transverse stiffeners throughout the structure and internal diaphragms at the supports.
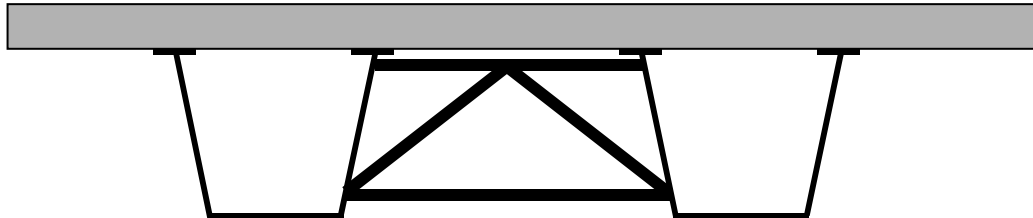
Figure 1.4 Bridge Cross-Section At End Pier, Showing Truss Diaphragm
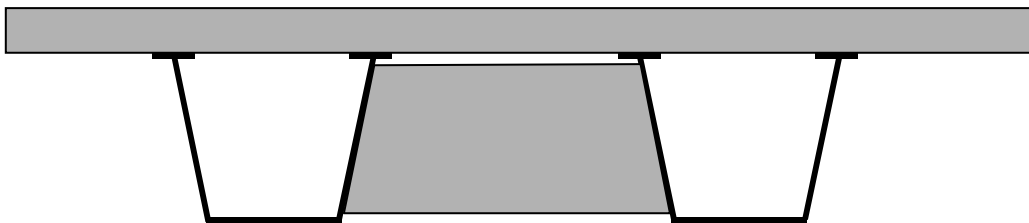
Figure 1.5 Bridge Cross-Section At Inner Pier, Showing Steel Plate Diaphragm

A plan view of the bridge, showing relative instrumentation locations, is shown in Figure 1.6.

"Southern" pier

10 m

North

KEY:

—··—··— Cross-section 1

------- Cross-section 2

Guided bearing

"Free" bearing

"Northern" pier
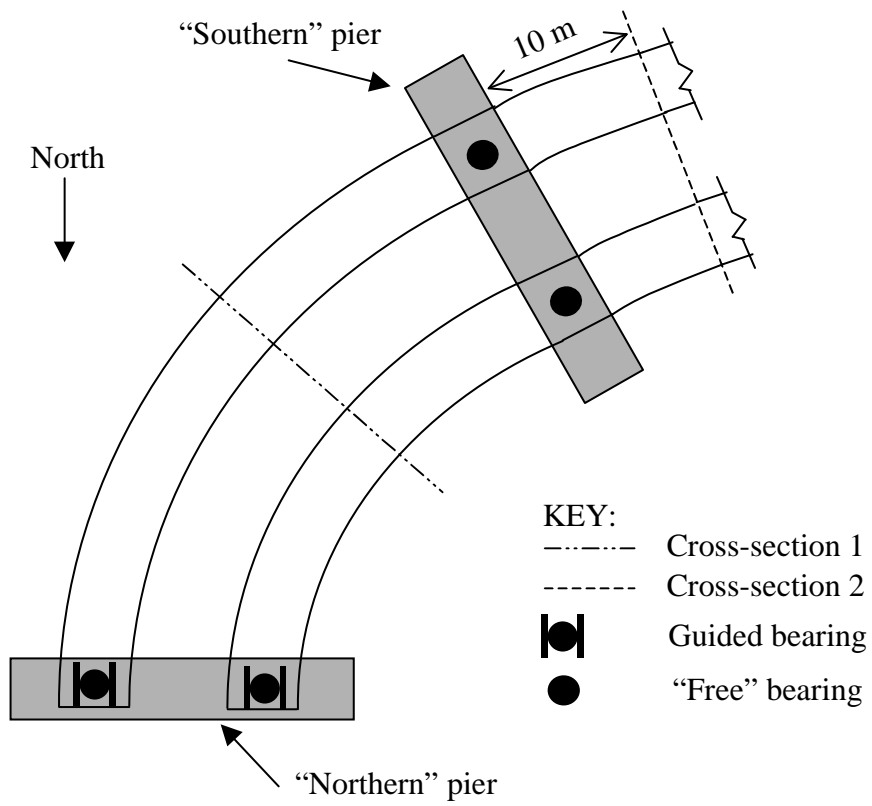
Figure 1.6 Plan View Of Bridge, Showing Instrumentation Locations

Chapter 2

Instrumentation Procedure

2.1   Background

Two spans and two bridge piers were instrumented with thermocouples and linear potentiometers for this study.   The instrumentation schemes used are described herein. It will be recalled that this study does not involve deformations induced by gravity loading. Only thermally-induced deformations are considered. Also, a strategic instrumentation scheme was necessary due to limited instrumentation resources.

2.2   Instrumentation

Thermocouples are very versatile devices used to measure temperatures of air, solids, or liquids. A thermocouple is formed by joining two wires of dissimilar metals together at one end. When the junction point undergoes a thermal change, a voltage is generated. When that voltage is read by a data collection device, it is converted into a temperature, which is the temperature of the junction point. The wires are otherwise insulated along their lengths to prevent electrical "shorts" from occurring.   For this study, thermocouples constructed of copper and constantan wires were used. The thermocouples were able to record temperatures accurate to within 0.01° Celsius.

Linear potentiometers were used with a gage length of 50 mm to determine bearing plate rotations and radial girder translations, and 100-millimeter potentiometers were used to determine longitudinal girder translations.   The

excitation voltage used with the potentiometers was 5 volts, which was provided by a battery powered by a solar cell. The nominal output of the 50-millimeter potentiometers under this excitation voltage was 100 mV/mm, while the nominal output of the 100-millimeter potentiometers was 50 mV/mm.

2.2.1 Girder and Thermal Instrumentation

It was decided to instrument the interior of both girders for temperature distributions, along with the slab between the girders, and the outside upper flanges of each girder. A thermocouple was also left to hang in the air between the girders to record ambient air temperatures.

In order to gain a thorough record of temperature distributions within the girders, two locations in each girder were instrumented with eight thermocouples each, for a total of thirty-two thermocouples between the two girders. A typical cross-section of the two girders is shown in Figure 2.1. This diagram shows one instrumentation location out of the two in place. The second instrumented cross-section is shown in Figure 2.2.
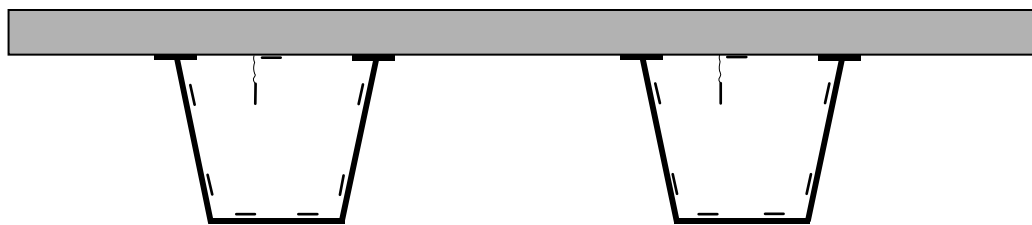
Figure 2.1 Bridge Cross-Section Showing Thermal Instrumentation.

In order to follow the temperature variation from the girders to the slab, and from the girders to the ambient air temperature, several thermocouples were

attached to the slab between the girders. An additional thermocouple was attached to the outer top flange of each girder. The thermocouples between the girders were attached to the stay-in-place slab forms, while the thermocouples attached to the flanges were attached to the bottom face of the flange. Wherever a thermocouple is shown attached to steel (girders or the form), the connection was made by mounting a horseshoe magnet to the steel element, with a small piece of rubber inside the magnet, which applied pressure to the thermocouple, ensuring a tight fit. Two thermocouples attached to the stay-in-place form between the girders are shown in Figure 2.3.

The thermocouple installation outside the girders was done beyond the interior pier, approximately ten meters into the interior span. This is shown in Figure 2.4.
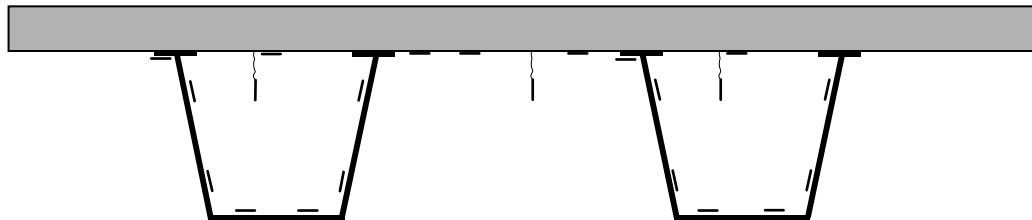
Figure 2.2 Southern Instrumented Cross-Section, Showing Slab Thermal Instrumentation
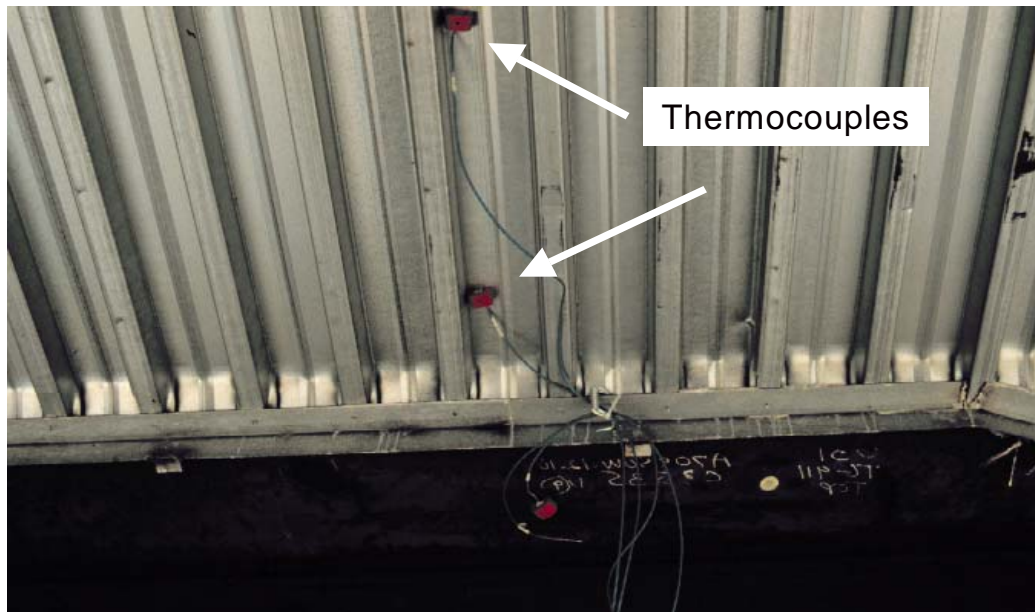
Figure 2.3 Thermocouples Attached To Stay-In-Place Form

A total of thirty-eight thermocouples were installed in various components of the two spans instrumented. This thermal instrumentation scheme provides an accurate description of the temperature variations and gradients throughout the bridge.

"Inner" pier

North

10 m

KEY:
—··—··— Cross-section 1
------- Cross-section 2
Guided bearing
"Free" bearing

"End" pier
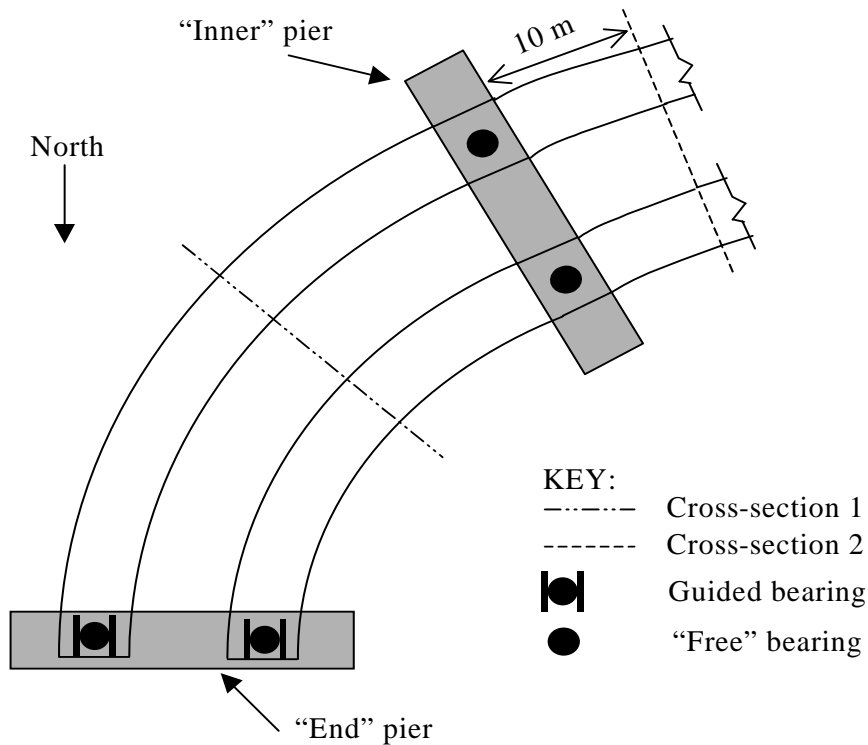
Figure 2.4 Plan View Of Bridge Showing Instrumentation

Translation Instrumentation

Extensive use of linear potentiometers was made to measure bridge deformations. Because both translations and rotations at the bearing plates of this bridge are quantities of interest, the problem was to devise a way in which to use potentiometers to calculate the desired quantities. The task was facilitated by the fact that pot bearings make use of rectangular steel bearing plates both below and on top of the cylindrical pot which houses the elastomer. By using these plates as bearing surfaces for the potentiometers, displacement and rotation data became easier to gather, as described below.

Because both longitudinal and transverse girder translations are of interest in this study, it was necessary to instrument the bearing plates for motions in both of these directions. A method by which to support the potentiometers that would allow unattended operation at the bridge site for an extended period of time had to be devised. Aluminum brackets were machined which held a potentiometer in a snug position, restraining it from moving in any direction. By holding the position of the potentiometers constant, a reliable displacement-measuring datum was established, providing accurate measurements of girder translations. Stands were also fabricated for each potentiometer out of steel plates and rods. Tripod mounts were used to prevent rocking of the potentiometer stand. The mounts were positioned on the bridge pier caps such that the potentiometers were left to bore against the bearing plates, monitoring displacements of these plates. Because the motion across the bearing is of interest, that is, the displacements of the top bearing plates relative to the bottom ones, only the top bearing plates required instrumentation. The bottom bearing plates are firmly attached to the pier caps, and only the top bearing plate displacements relative to this datum were measured. Where conditions were too cramped to facilitate the bearing of a potentiometer upon a bearing plate, small pieces of steel plate were clamped to the bearing plates, and the potentiometers were set to bear against these smaller plates. A typical potentiometer set-up used for measuring transverse translations is shown in Figure 2.5.

Rotation Instrumentation

Because the bearing plates on a pot bearing are oriented in a horizontal plane, vertically-oriented potentiometers were used to measure the plate rotations. It should be noted that the quantity of interest is not a torsional twist in the plane of the plate, but a rotation of the girders at the bearing. Thus, by monitoring the

elevations of various points on a bearing plate, plate rotations could be followed in time. In order to separate rotations occurring in the longitudinal and transverse directions, a large T-square was used to ensure that transverse rotations were obtained in an orthogonal direction to the bridge curvature. The separation of rotation components is described in further detail in Chapter 6.

Potentiometer for recording transverse displacements
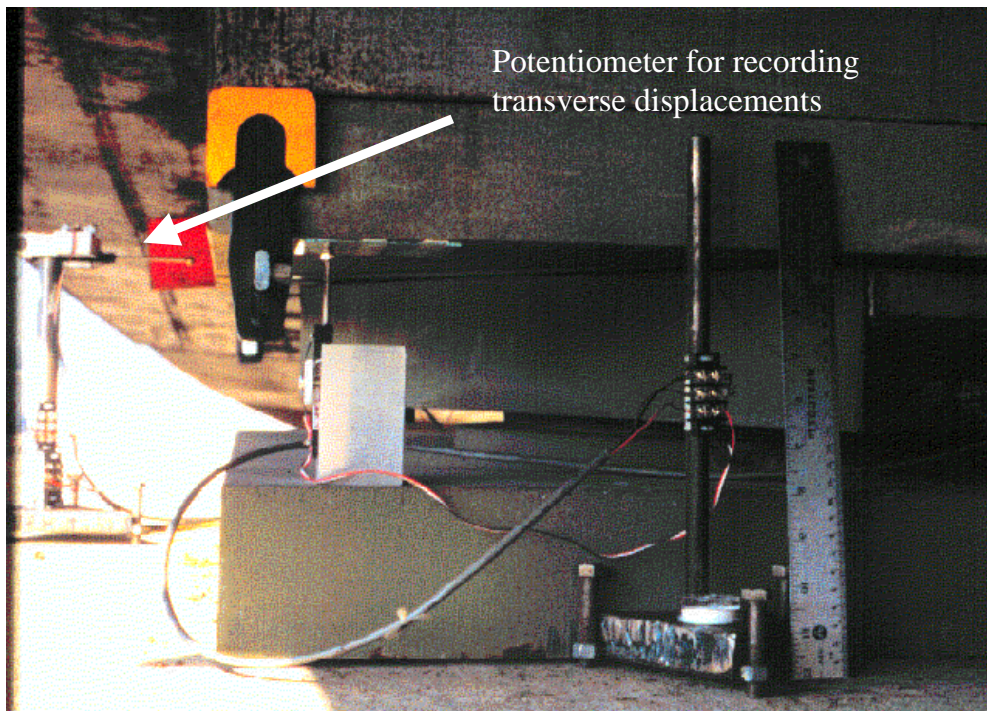
Figure 2.5 Potentiometer Used To Measure Transverse Girder Displacements

In order to measure the vertical plate displacements, 50-millimeter potentiometers were used. The potentiometers were placed between the bearing plates, as shown in Figure 2.6. At the location where the stands were used, the potentiometers were allowed to bear upon the bottom flange of the girder. Inclinometers were also considered for use in monitoring girder rotations, but

these proved to be prohibitively expensive and did not offer the accuracy which could be obtained with potentiometers.
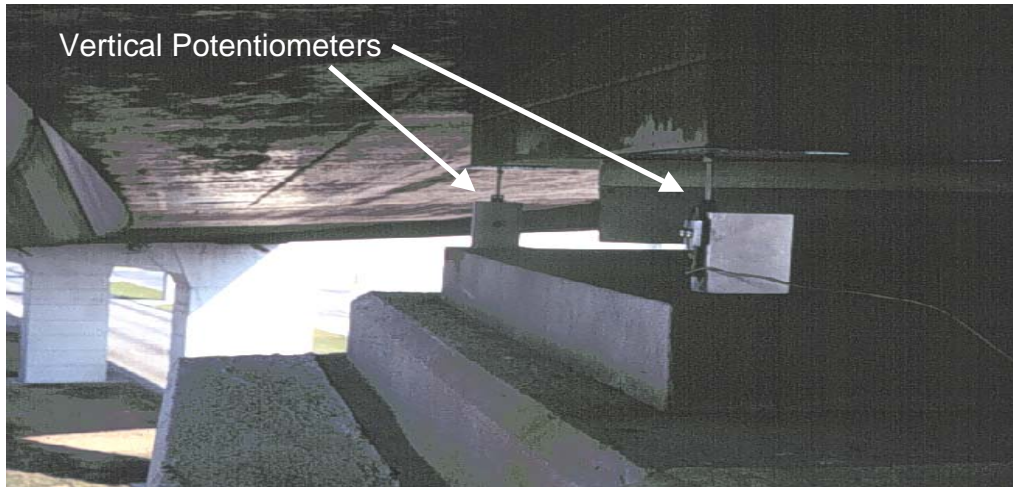
Figure 2.6 Detail Showing Vertically-Oriented Potentiometers To Measure Girder Rotations

2.3 The Data Collection Procedure

Readings of the thermocouples and potentiometers were taken each hour. The only practical data collection procedure for a study such as this would be one which provides for remote acquisition. A data collection scheme which did not require a "hard-wired" connection to the instrumentation was necessary, as it was also necessary to provide for the collection of data without access to the bridge.

A cellular telephone link was used. Because all measured quantities described thus far are measured by voltage changes, an electric data acquisition system was needed. Similarly, a data-logging system is required for the collection and interpretation of the voltage changes. Measurements such as these, therefore, occur in three stages, as listed below:

1. Voltage change (from thermocouple or linear potentiometer);
2. Switched input of voltage change to data-logger channels (via multiplexers);
3. The data-logger controls the multiplexers, reads, and stores voltage changes.
4. The data-logger is programmed and the data is downloaded by a modem through a cellular phone attached to the data-logger.

A Campbell Scientific 21X Datalogger was used, which could be programmed to read the voltage values of the various instrumentation elements, through the multiplexers, every hour. The data is stored in the Datalogger for collection via a cellular phone attached to the 21X unit. When a call is received by the 21X, the current data in storage is transferred through the air waves to the a personal computer. Similar to the thorough instrumentation scheme, it is believed that the sophistication of this data collection procedure is unprecedented in a study of this type.

There are multiplexers in two general locations, that is, there are multiplexers both inside and outside of the bridge girders. Those multiplexers inside the girders (there is one in each girder) are used to read the voltages of the thermocouples which are mounted to the inner walls of the girders. The thermocouple leads were strung to the multiplexers. One multiplexer was left outside the girders to read voltages associated with the thermocouples outside the girders. Two more multiplexers were left outside the girders to read voltages associated with the linear potentiometers. The multiplexers were then all led to the 21X Datalogger unit, which was left inside the inner girder. In order to complete the relay of the data, an antenna was attached to the cellular phone, and the antenna was left to hang outside of the interior girder through the existing access hole in the girder's bottom flange. Finally, the entire instrumentation setup was powered by the use of a solar-charged 12 volt battery, which was placed on the as-yet unfinished access ramp near the ends of the steel girders. The

instrumentation scheme worked very well for the duration of the study. The collection of data over a long distance worked well throughout the duration of this study.

2.4   Pier Instrumentation

The possibility of pier motions was also considered. The piers supporting this bridge are relatively tall, and are composed of reinforced concrete. It was hypothesized that, under thermal changes, the piers could deflect laterally, moving with the girders as shown in Figure 2.7. This would reduce the relative displacement measured at the bearings.

A second instrumentation system was needed. It was decided to suspend plumb bobs, with fishing line, from the two instrumented pier caps to discern whether pier motions are occurring, and their directions. The possibility of monitoring total girder displacements with a laser and detector was also examined, but was rejected for three reasons. First, powering the laser proved to be a substantial problem. Also, the effects of sunlight might have proved detrimental to such a system. Finally, a proprietary laser system was investigated on consignment, and it was simply too difficult to obtain a high degree of accuracy in displacement measurements, even under controlled conditions.

It was decided to use a system of buckets, framing squares, and oil to record the plumb bob positions over time. The motion of the plumb bobs was damped by immersing the plumb bobs into buckets filled with gear oil. A framing square was tack-welded to each bucket. The framing squares serve as coordinate axes, so that a plumb bob's position at a given time can be measured with respect to the "origin" and compared to the bob's previous positions. A small T-square was used to transfer the position of the bob to the framing square. The system is shown in Figure 2.8.
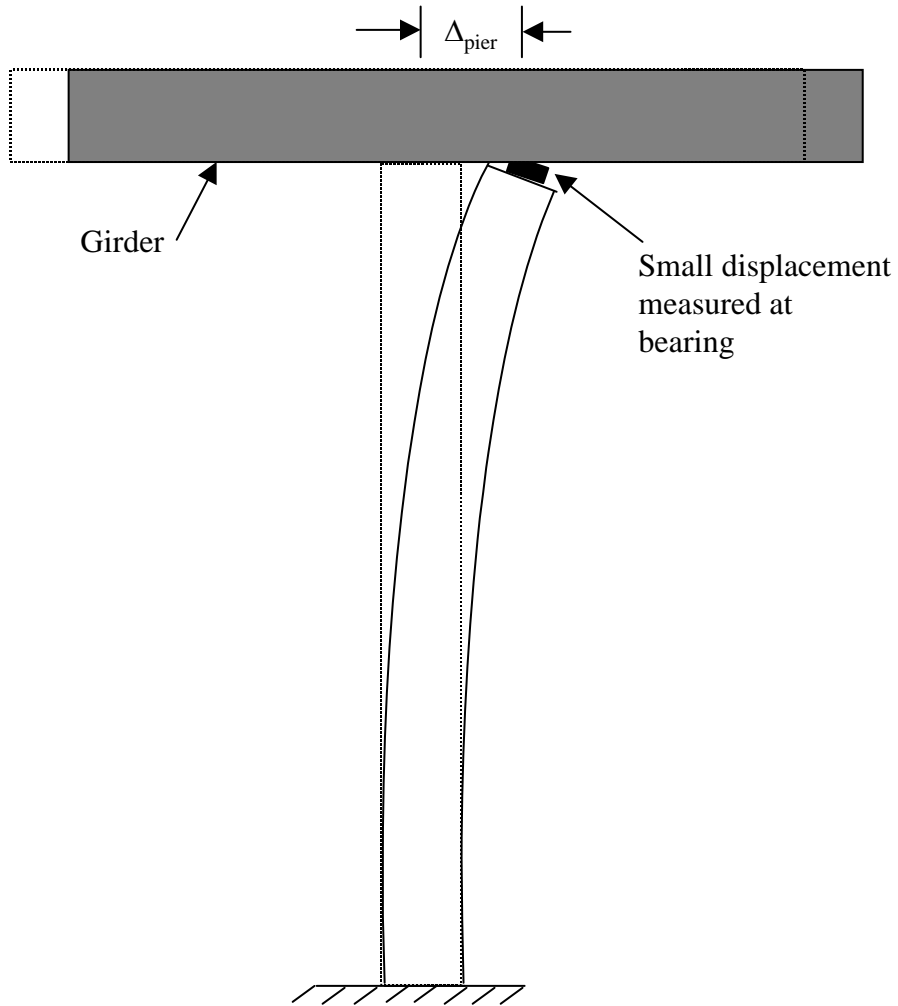
Figure 2.7 Effect Of Pier Deflection On Deformations Measured At The Bearing

Figure 2.8 Pier Deflection Monitoring System

The bucket sits upon a frame, which was cast in concrete to prevent movement of the frame for the sake of reliability in plumb bob measurements. Because pier motions are recorded over time, it is important to have a fixed reference frame for measurements. It was also necessary to protect the bucket and its mounting bracket from vandalism. It was decided to cast the mounts in concrete at the base of the columns and only install the buckets when they are being used, that is, when plumb bob positions are being recorded. Two steel

angles were welded to each mount, with a hole drilled through each one. Two pins were then welded to each bucket, which fit into these holes and located the system. The buckets can be removed when they are not in use, yet replaced in the same position each time measurements are to be made. This is vital, as relative pier positions are of importance. Finally, it was also desired to protect the plumb bobs from theft, and from becoming damaged over time when they are not in use. The plumb bobs were removed after each period of reading and the fishing lines were wrapped around the piers at a sufficient height to prevent theft.

The accuracy of this system was governed by the smallest division on the framing squares used, which was approximately 1.6 mm (1/16-inch). Also, it was impossible to completely dampen the effects of wind on the bob measurements. This will be illustrated further in Chapter 7.

2.5   Problems with Instrumentation

The initial instrumentation for longitudinal displacements of the inner girder at the end pier failed. No displacements were recorded at this location for the first five months of the instrumentation record. The problem was investigated during the second instrumentation site visit by displacing the potentiometer known amounts and reading its output. It was discovered that the multiplexer channel in use for this potentiometer was not functioning. The potentiometer was then wired to a functioning channel so that displacements could be measured and recorded through the remainder of the study.

It was also discovered during the course of the study that the potentiometer measuring longitudinal displacements at the end pier for the outer girder exhibited very erratic behavior. At times, the potentiometer seemed to lock in place, with no recorded displacements for several weeks. At other times, the potentiometer would record relatively large displacements over a relatively brief time and small

temperature changes. This behavior was also investigated during the second site visit. It was found that the potentiometer malfunctioned frequently.

The potentiometers measuring transverse and longitudinal displacements of the outer girder at the interior pier seemed to have problems, as well. The potentiometer measuring transverse displacements at this location repeatedly measured near-zero displacements, while the potentiometer measuring the same quantity at the inner girder measured reasonable displacements. At the same time, the potentiometer measuring longitudinal displacements of the outer girder at the interior pier seemed to exhibit some of the behaviors of the potentiometer on the outer girder at the end pier-large, unreasonable displacements at some times, and null displacements at others. Wherever possible, measurements of this potentiometer have been salvaged and analyzed. It should be noted, though, that a continuous record of transverse and longitudinal displacements of the inner girder at the interior pier were obtained, as was a record of longitudinal displacements of the inner girder at the end pier, after the second instrumentation procedure. Thus, a reasonably thorough record of bridge translations was obtained. Figure 2.9 shows the potentiometers which provided reliable data. No reliable displacement data for the outer girder was obtained.

Inner Girder

End pier   Inner pier

Figure 2.9 Illustration of functioning potentiometers

In this figure, functioning potentiometers are represented by arrows. The girder has been shown as straight for simplicity. Both transverse and longitudinal displacements are monitored at the inner pier and longitudinal displacements only are monitored at the end pier on the inner girder. As described in Chapter 1, the girders are linked by stiff diaphragms at the piers, so that transverse displacements of the girders at the inner pier should be nearly equal.

Also, the potentiometer measuring longitudinal girder translations at the end pier became "stuck" in November in a constant position, i.e., no displacements were recorded after this occurred. When the instrumentation was removed from the bridge, it was discovered that most of the potentiometers were in poor condition. Long-term exposure to the elements caused most potentiometers to exhibit at least some degree of "jamming," that is, the shafts of the potentiometers were fixed in place. However, a substantial amount of useful deformation data was obtained, and will be described in this thesis.

Chapter 3

Thermal Data and Analysis

3.1   Heat Transfer Principles Applied to Highway Bridges

As described in Chapter 1, yearly temperature cycles at a bridge site play a role of vital importance in bridge engineering. It was shown that failure to account for reasonable temperature changes from the conditions under which a bridge was constructed can lead to the development of stresses within the bridge. These stresses can be detrimental to the bridge structure if not accounted for in design.

The main concerns of this study include the determination of what temperature ranges and extremes can reasonably be expected to occur in this structure. However, it will be illustrative to first examine the various mechanisms by which heat flows into, out of, and throughout a bridge. This will be needed so that it will be understood why bridge temperatures do not usually match ambient air temperatures. The following concise explanation of these mechanisms is due to Roeder (1998).

Heat flow in bridges occurs due to radiation, convection, and conduction. Radiation, or, in the case of highway bridges, solar radiation, is the transfer of heat energy from a warm body to a cooler body over long distances. In the case of a highway bridge, the bridge both receives radiant heat energy from the sun and radiates heat energy to the environment at night.   The bridge under investigation is made of weathering steel, which is particularly well-suited for absorbing radiant energy, as its surfaces have no reflective paint or coating.

Convection is the transfer of heat from a body to a moving fluid, such as air. In the case of a bridge, this mechanism is influenced by the ambient air temperature and is driven by wind and air currents near the bridge. The convection mechanism is responsible for reducing high temperatures of the bridge in the summer and for lowering the bridge temperatures in the winter, as well. Conduction is the flow of heat within the bridge itself. Because various points of the bridge will receive differing amounts of radiant heat energy throughout the day, heat will flow throughout the bridge as the bridge moves toward a point of thermal equilibrium. In the absence of additional energy input by radiation and convection mechanisms, the bridge will reach a uniform equilibrium state; however, the constant presence of these mechanisms prevents this state from occurring. Roeder also notes that the accurate determination of the bridge temperature requires consideration of all three transfer mechanisms, as well as cloud cover, air temperature, wind speed, and the time of day, along with other factors.

As noted, this study is not concerned with the prediction of bridge temperatures, although several techniques for such predictions have been proposed [see, for example, Moorty and Roeder (1992) or Fu, et al. (1990)]. It will be seen, however, that various elements of the bridge under study are scarcely at the same temperature at a given time. This has implications in the finite element analysis of this bridge, as will be explained later.

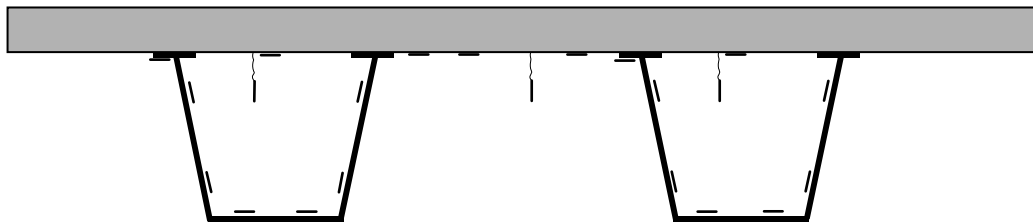## 3.2   Thermal Analysis: Data Collection

As described in Chapter 2, a total of 38 thermocouples were used to gather temperature records of the bridge and its surrounding air. Thermocouples were positioned such that complete temperature distributions could be obtained at two

bridge cross-sections and slab temperature variations could be obtained at one cross-section. Thermocouple layouts are shown again here for convenience.
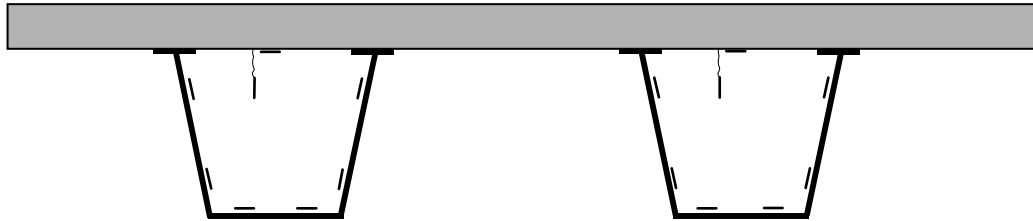
Figure 3. 1 The Northern Thermal Instrumentation Location

Figure 3. 2 The Southern Thermal Instrumentation Location, With Additional Thermocouples On The Slab And Top Flanges

It is seen that the instrumentation scheme used for thermal data collection is quite thorough and should provide an accurate description of temperature variations within the bridge.

3.3   Thermal Analysis: Data Presentation

Much useful temperature data was gathered during the course of this investigation. It was described in Chapter 1 how the American Association of State Highway and Transportation Officials (AASHTO) specifies that

temperature effects be accounted for in the design of bridges. Specifically, AASHTO mandates that a uniform temperature increase or decrease from the actual air temperature averaged over the 24-hour period preceding the setting of the bridge or its components be used. The range specified for the bridge under consideration, a steel structure in a moderate climate, was shown earlier to be bounded between -18° C and 50° C. This range will be examined.

It has been shown that one thermocouple was installed hanging between the two girders of this bridge, in order to record the ambient air temperature. This provided a site-specific temperature record for the bridge location with more accuracy than could be obtained from weather reports for Houston. The tabulation of this temperature data made it simple to pinpoint the extreme weather conditions at the bridge site for the period of investigation. It was found that the lowest ambient air temperature recorded was 2.5º C, on March 10, with a corresponding high temperature of 13.6º C. It was also determined that the highest air temperature recorded was 39.8º C, occurring on August 2, with a corresponding low temperature of 27.5º C. The thermal history of the bridge on these two days will now be examined in detail, and comparisons between the two days will be made.

Descriptive Conventions

Thermocouple layouts through the bridge cross-sections were shown earlier. The relative locations of the instrumented locations are shown below in Figure 3.3. This shows the two instrumented portions of this three-span bridge. For convenience, the northern thermocouple instrumentation location will hereafter be referred to as the "northern" section, and the southern location will be referred to as the "southern" section. Also, the box girder on the outside of the curve (the longer girder) will be referred to as the "outer girder," while the shorter girder

will be referred to as the "inner girder." Finally, the northern pier instrumented for displacements and rotations will be referred to as the "northern pier," while the southern pier will be referred to as the "southern pier."
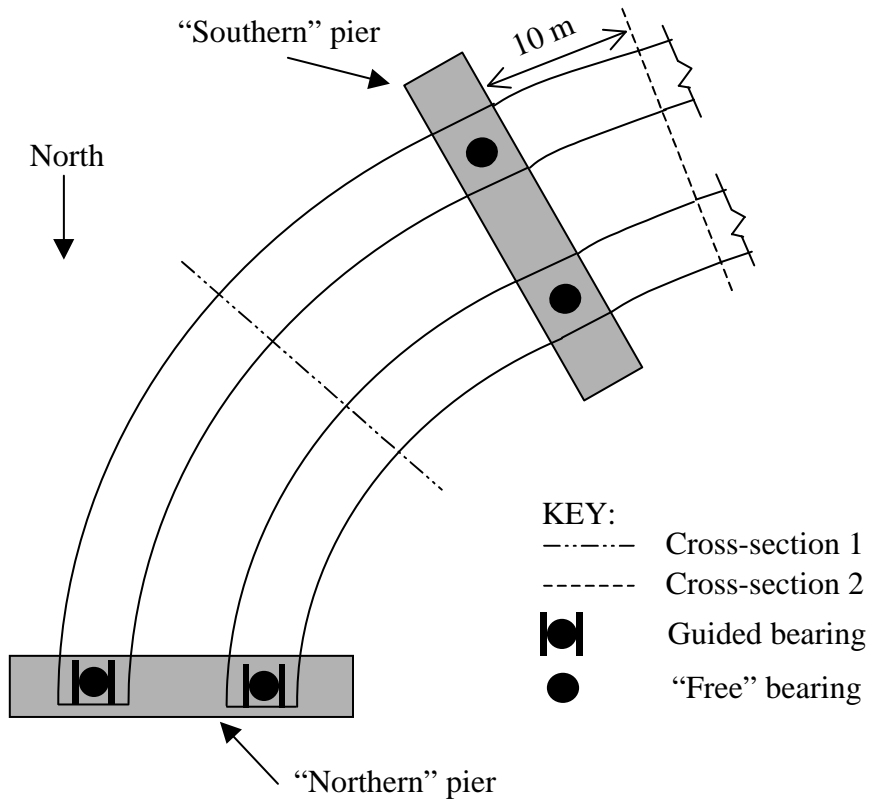
Figure 3.3 Plan View Showing Instrumentation Locations

3.3.1   Temperature Variation Across The Northern Cross-Section

Shown in Figure 3.4 are plots of the mean cross-sectional temperatures of both girders at the northern section during March 10, and in Figure 3.5 are shown the same quantities for August 2. For clarity in this thesis, all horizontal time

scales will use a 24-hour time scale convention, that is, midnight will be denoted as "0:00" and noon will be denoted as "12:00." In calculating the mean temperature of a girder at a particular cross-section, the six thermocouples in contact with structural steel at that location were used; that is, the thermocouples attached to the stay-in-place form and hanging within the girder were not included in the calculation.
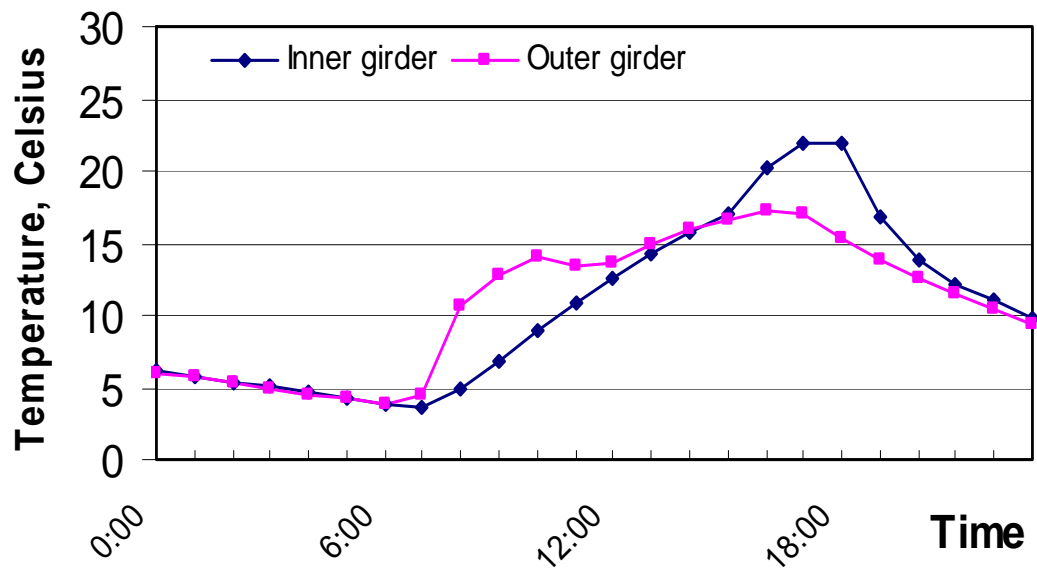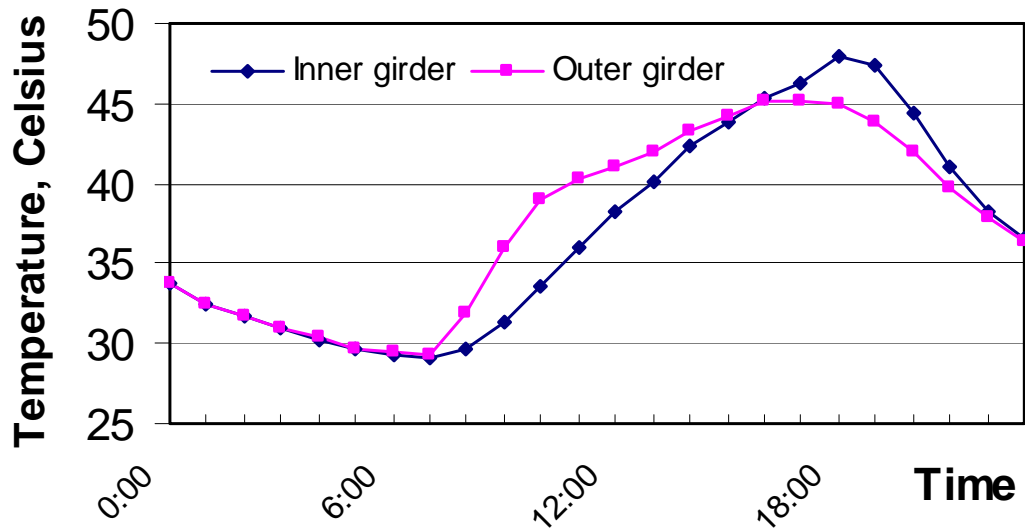

Figure 3. 4 Mean Temperature Variation Across The Northern Section For March 10, 1998

Figure 3. 5 Mean Temperature Variation At The Northern Section For August 2, 1998

The thermal behavior shown in these plots is typical observed behavior of the bridge at these locations. It is seen in both plots that the inner and outer girders are at nearly the same temperature in the early hours of the morning at cross-section 1. As expected, the mean temperatures of both girders decrease through the early-morning hours, and reach a minimum at approximately 7:00. What occurs next illustrates the effect of radiation heating due to direct exposure to the morning sun. It is seen that the temperatures of both girders at cross-section 1 start to increase at about 7:00 but that the temperature of the outer girder increases much more quickly than that of the inner girder. This is to be expected, as the outer girder is directly exposed to the east, the direction of the rising sun. Because the inner girder is still shaded at this time, its mean temperature does not increase as rapidly as the mean temperature of the outer girder does.

The inner girder, however, will still reach a maximum daily temperature greater than that of the outer girder. What allows this to happen is the change in the sun's position over the course of the day. The plots show that, although the outer girder's mean temperature at this cross-section continues to rise for several hours after its initial rapid increase, it does so at a slower rate after only one or two hours. This is because as the sun moves through the daytime sky and passes over the bridge deck, moving from east to west, the outer girder receives increasingly less direct sunlight exposure. At the same time, the inner girder's mean temperature at this cross-section continues to increase at nearly the same rate. When the mean temperature of the inner girder finally does equal and then pass that of the outer girder, it is because it is now receiving direct sunlight at the hottest time of the day—the afternoon. The more intense heating is evidenced by the increase in the rate at which the inner girder's temperature increases, which occurs at approximately 15:00. Upon reaching their respective thermal maxima, both girders then begin cooling to nearly the same temperature. It is apparent that at several times during the course of a day, there is a temperature difference between the two girders, even at the same cross section, where the temperatures are being measured only a few meters apart. This is further illustrated in the table below.

Table 3.1 Maximum Mean Temperature Differences At Northern Section During March 10 And August 2.

Day	Time	Outer Girder Mean Temp.	Inner Girder Mean Temp.	Difference
March 10	8:00	10.2° C	4.8° C	5.4° C
March 10	18:00	15.3° C	23.0° C	7.7° C
August 2	10:00	39.1° C	33.6° C	5.5° C
August 2	19:00	43.8° C	47.3° C	3.5° C

3.3.2 Temperature Variation Across The Southern Cross-Section

Shown in Figures 3.6 and 3.7 are plots of the thermal variation across the southern section for the same days, March 10 and August 2. It is immediately clear that this cross-section exhibits the same general thermal characteristics as does the northern section. On both days, both girders spend the first several hours of the day at nearly the same temperature, until a temperature increase begins, at which point the outer girder's mean temperature at this section increases much more rapidly than the inner girder's temperature does. The temperature of the outer girder is warmer than in the inner girder until the middle afternoon hours, at which time the inner girder's temperature passes that of the outer girder and continues to rise under the influence of direct solar heating. There is again a temperature difference between the two girders through most of the day, even though the instrumentation locations are at the same point in the span for both girders. This is further illustrated in the Table 3.2.

Table 3.2 Maximum Temperature Differences At The Southern Section During March 10 And August 2.

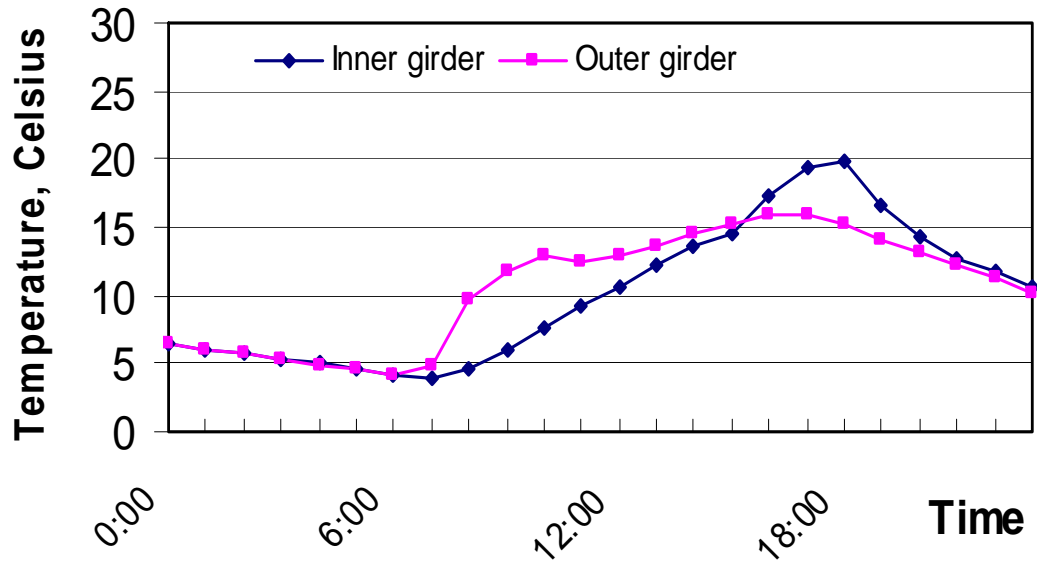| Day	Time	Outer Girder Mean Temp.	Inner Girder Mean Temp.	Difference
March 10	8:00	9.5° C	5.0° C	4.5° C
March 10	18:00	15.1° C	21.1° C	6.0° C
August 2	10:00	32.7° C	37.6° C	4.9° C
August 2	19:00	43.4° C	46.5° C	3.5° C

37

Figure 3. 6 Mean Temperature Variation Across The Southern Section For March 10, 1998
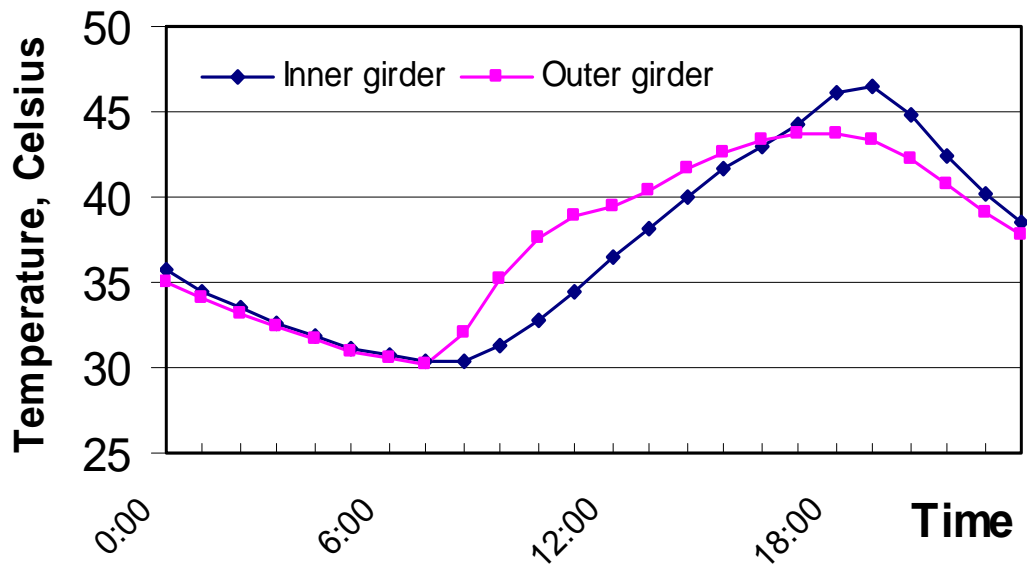

Figure 3. 7 Mean Temperature Variation Across The Southern Section For August 2, 1998

It is clear that the behaviors of both thermally-instrumented locations are similar, both in the heating and cooling characteristics of the two girders, and in the fact that there is, with the exception of the early morning hours, always a temperature difference laterally between the girders.

3.3.3   Temperature Variations Within the Inner Girder

Having made comparisons between the observed thermal histories between the two girders at the same location, it will now be instructive to examine the thermal behavior within the individual girders on the two days under study. Figures 3.8 and 3.9 show the measured thermal behavior of the inner girder on March 10 and on August 2, respectively.   Mean sectional temperatures were calculated as before, that is, all thermocouples in contact with structural steel at a particular section were included in the calculation of that section's mean temperature.   From these plots, it can be seen that, on both days, the southern section starts the day at a slightly higher mean temperature than does the northern section.   The temperatures at both cross-sections steadily decrease in the early morning hours, with the southern section warmer than the northern by nearly the same amount through these hours.   The temperatures of both sections reach minima at approximately 7:00, at which time the temperatures in both girders begin to rise.   The southern section remains warmer than the northern until around 9:00, at which time the temperature of the northern section rises above that of the southern.   Both cross-sections continue to increase in temperature, with the difference in the two cross-section temperatures gradually increasing.   The temperatures of both girders continue to increase until approximately 18:00, and the temperatures of both girders reach their peaks at approximately the same time. Finally, at approximately 19:00, the temperature of the northern section drops slightly below that of the southern, and the temperatures steadily decrease for the

remainder of the day, at which time another daily temperature cycle ensues. Again, it is important to note that the mean cross-sectional temperatures are almost always different, albeit slightly so, within the inner girder from one span to the next.
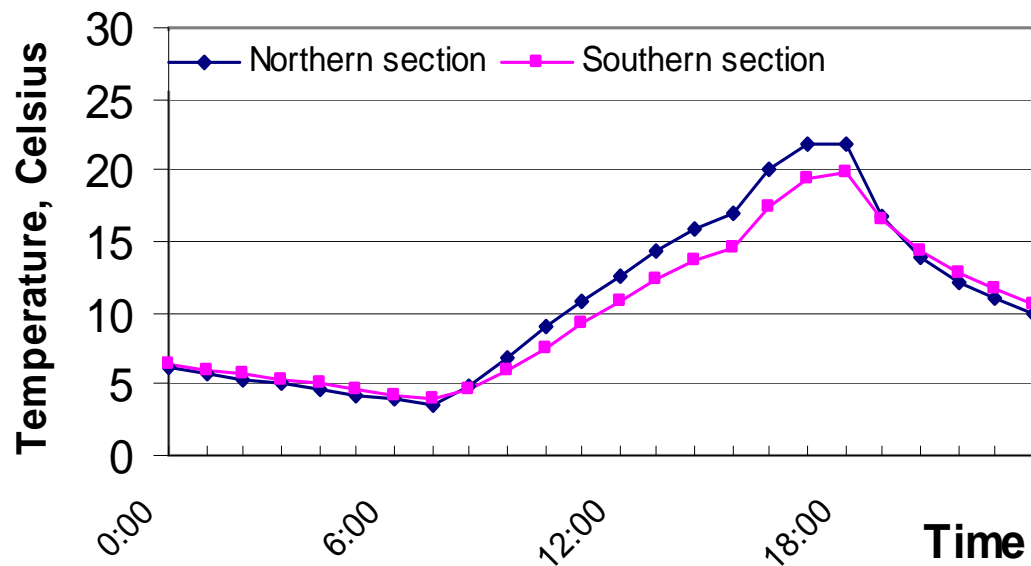

Figure 3. 8 Mean Temperature Variation Within The Inner Girder For March 10, 1998

3.3.4   Temperature Variations Within the Outer Girder

As can be seen in Figures 3.10 and 3.11, the outer girder exhibits thermal behavior similar to that of the inner girder. On both days under study, the southern section starts the day at slightly higher temperatures than does the northern section, and both temperatures steadily decrease until roughly 7:00. Both cross-sectional mean temperatures then begin to increase, with the northern

section surpassing the temperature of the southern shortly after the temperature increase begins. Both sections then increase in temperature until the late afternoon hours, with the northern section cooling to a lower temperature than the southern, as seen in the inner girder. Again, the temperatures of both girders continue to steadily decrease, with the southern section remaining slightly warmer than the northern, until another day's thermal cycle begins. It is clear that the thermal behaviors of both girders are very similar, and that temperature differences are almost always present within the girders along their spans.
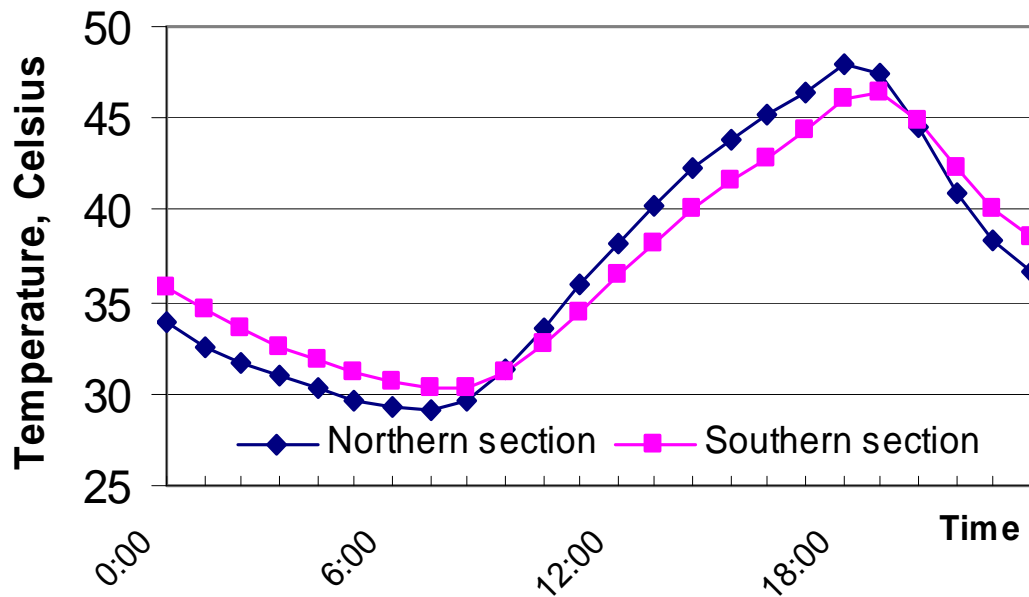

Figure 3. 9 Mean Temperature Variation Within The Inner Girder For August 2, 1998
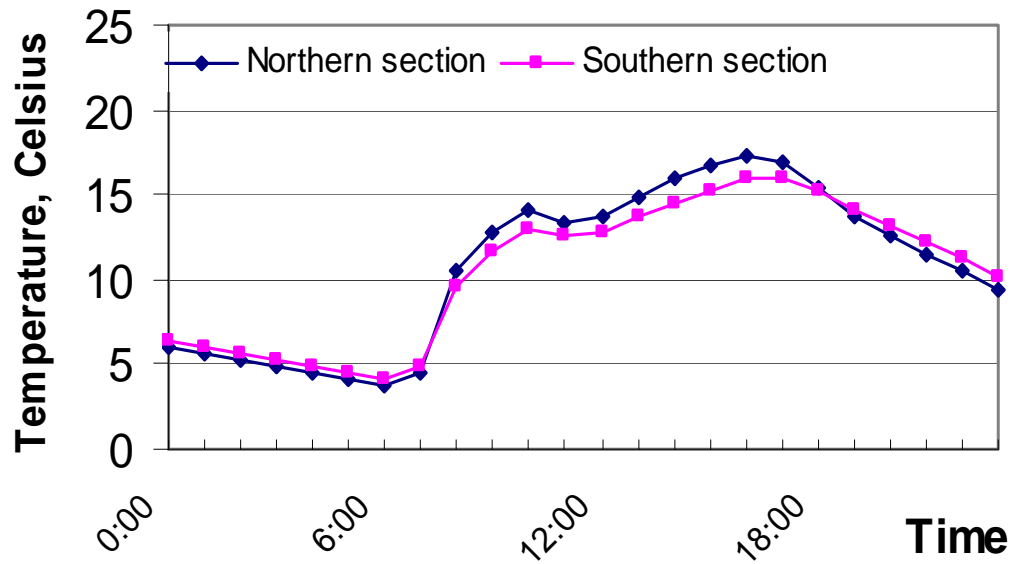
Figure 3. 10 Mean Temperature Variation Within The Outer Girder For March 10, 1998
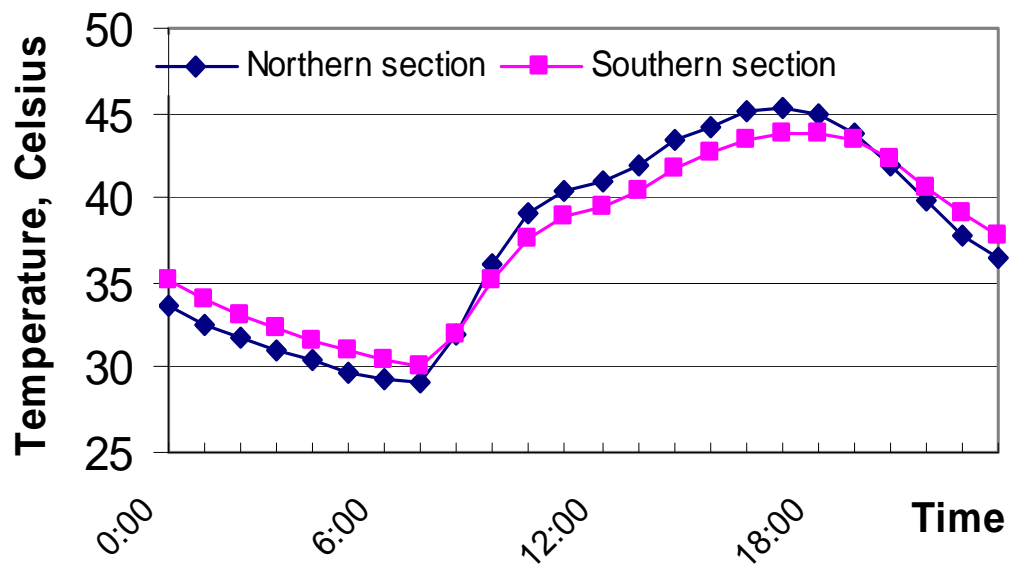

Figure 3.11 Mean Temperature Variation Within The Outer Girder For August 2, 1998

3.3.5   Temperature Variations Between The Girders and Ambient Air

It is also of importance to examine the observed differences between the mean temperatures of the girders and the recorded ambient air temperature at the same times. For this purpose, the thermal behavior of March 10, the coldest recorded day in terms of mean bridge temperature, will be examined in detail for both girders. The temperatures referred to as "ambient" are those recorded by the thermocouple left to hang between the girders.

It is first of importance to define "mean" bridge temperature as it pertains to this study. It has been shown that rates of heating and cooling for the girders and slab are substantially different. Because this bridge utilizes composite action, the differences in the thermal and elastic properties of steel and concrete must be considered when computing mean bridge temperatures. As mentioned earlier, Emerson (1981) provided an equation to determine the mean bridge temperature at a given time, based on equilibrium principles. Her equation is:

$$T_{AVG} = \frac{\Sigma A_i E_i \alpha_i T_i}{\Sigma A_i E_i \alpha_i}$$

where the subscripts refer to different materials or layers in the bridge; A is the cross-sectional area of the segment; E is the elastic modulus of the segment; α is the coefficient of thermal expansion of the segment, and T is the temperature of the segment. This equation was used to determine all reported mean bridge temperatures presented here. The concrete elastic modulus was taken as 30.4 GPa and the steel elastic modulus was taken as 200 GPa. The coefficient of thermal expansion of steel was taken as 1.17×10^{-5} /ºC and the concrete coefficient of thermal expansion was taken as 1.08×10^{-5} /ºC. Further, all mean bridge temperatures will be referred to as "EMBT" henceforth. Finally, where mean

girder temperatures are described, these temperatures were computed as the arithmetic mean of all thermocouples in contact with structural steel in the girder, i.e., both instrumented sections were included in the computation.

Shown in Figures 3.12 and 3.13 are plots of the thermal histories of the girders and the recorded air temperature for March 10. It is clear that the girder temperatures are always higher than the air temperature, but in varying amounts over the course of the day. The girders are only slightly warmer than the surrounding air in the early morning hours. All temperatures are steadily decreasing through this time, with the quantities reaching minima near 7:00. This decreasing trend has been observed in all thermal histories examined thus far and is not surprising. What is interesting to note are the relatively large differences between the girder and air temperatures, and that they occur at different times of the day.

Beginning with the outer girder, note that the girder temperature actually starts to increase one hour before the recorded air temperature increases. This can be attributed to direct solar radiation and the fact that the thermal conductivity of steel is many times that of air. The air temperature then begins to increase, and the girder temperature makes a dramatic increase. Both temperatures then continue to increase, with the air doing so at a more uniform rate than the girder. However, the girder's initial "leap" in temperature allows it to increase to a temperature some eight Celsius degrees higher than the air temperature. This is significant, because it illustrates how actual bridge temperatures often differ substantially from reported air temperatures. It is also clear that both temperatures reach their maxima at practically the same time, namely, at approximately 16:00. At this time, the girder is approximately two Celsius degrees warmer than the surrounding air. This is due to the fact that the air continued a temperature increase at a relatively constant rate, while the rate of outer girder warming dropped from its initial rapid heating trend. Again, this is

44

explained through consideration of the sun's position in the sky through the day. At this point (and throughout the afternoon hours), the sun's radiant energy is no longer reaching the outer girder's surface with high intensity, as the sun has moved to an overhead position and then to a position in the western sky. This leads to the air and outer girder temperatures reaching their maximum temperatures at the same time, as the sun is now shining directly on the inner girder.
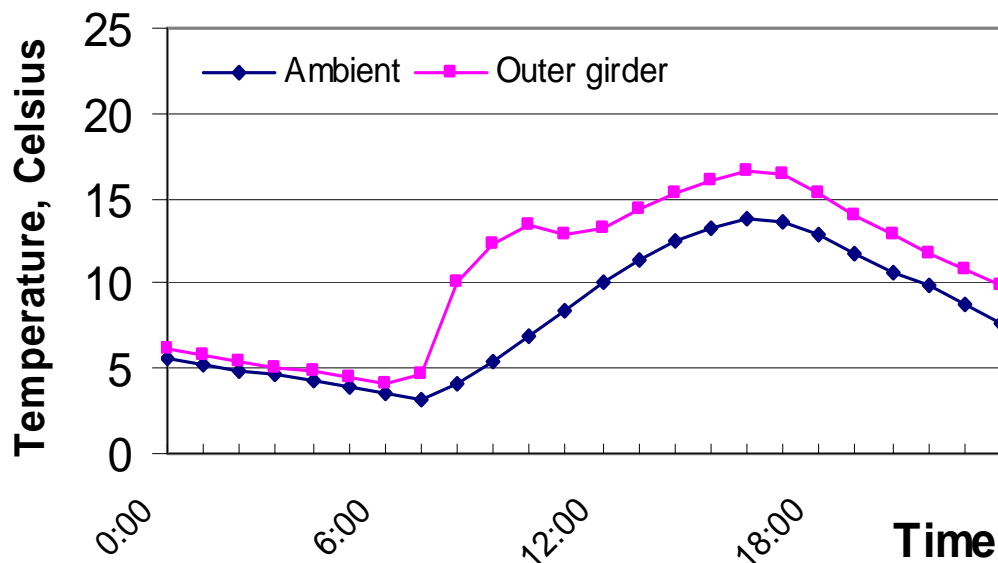
Figure 3.12 Variation Between Mean Outer Girder And Ambient Temperatures For March 10, 1998

Figure 3.13 illustrates the thermal histories of the air and of the inner girder for March 10. The inner girder's early-morning behavior mimics that of the outer girder. The girder starts the day slightly warmer than the surrounding air, and both temperatures are gradually decreasing through this time. It is interesting to note that the inner girder reaches its minimum temperature at the same time that

the air minimizes its temperature. At this point, the sun is shining on the outer girder, and the inner girder is still shaded. The inner girder then increases in temperature at nearly the same rate as the air temperature is increasing. This continues for several hours, until the rate of air temperature increase begins to lag behind that of the inner girder. The girder temperature continues to increase at nearly the same rate, until approximately 15:00. At this time, a sharp increase in the rate of girder temperature rise becomes apparent. It is clear that the afternoon sun is now shining directly onto the inner girder. It can also be seen that the air temperature reaches its maximum value some two hours before the inner girder temperature maximizes. That is, radiant heat energy is still reaching and warming the inner girder, even after the air temperature has begun its descent into the evening hours. This is also illustrative not only of the fact that bridge temperatures usually differ from air temperatures, but it shows that bridge structural elements will continue heating even as the air starts cooling, depending on the orientation and layout of the bridge structure. This also leads to the clear observation that, because the inner girder continues to warm for about two hours after the air has begun to cool, there is a substantial difference between the two temperatures in the early evening hours. The maximum recorded differences between girder temperatures and air temperatures are tabulated below for both girders. Differences during March 10 are tabulated in Table 3.3, while differences during August 2 are tabulated in Table 3.4.
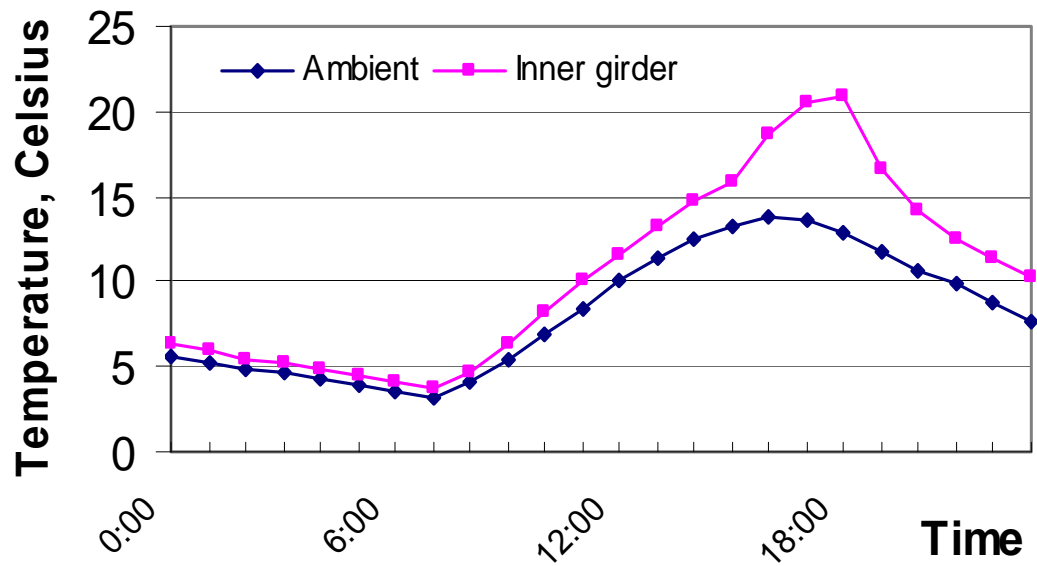
Figure 3. 13 Variation Between Mean Inner Girder And Ambient Temperatures For March 10, 1998

Table 3.3 Maximum Differences Between Girder And Ambient Temperatures During March 10.

March 10	Time	Girder Mean Temp.	Ambient Temp.	Difference
Inner Girder	18:00	22.0º C	12.2º C	9.8º C
Outer Girder	9:00	11.5º C	4.3º C	7.2º C

Table 3.4 Maximum Differences Between Girder And Ambient Temperatures During August 2.

August 2	Time	Girder Mean Temp.	Ambient Temp.	Difference
Inner Girder	20:00	44.7º C	38.5º C	6.2º C
Outer Girder	9:00	38.3º C	31.5º C	6.8º C

3.3.6   Variation Between Mean Girder Temperatures

Having compared and contrasted cross-sectional behavior between the two girders, and having compared overall girder behavior to air temperature trends, it will now be informative to compare and contrast the mean temperature behavior of the girders.

Shown in Figures 3.14 and 3.15 are plots of the thermal behaviors of both girders for both March 10 and August 2. It will be recalled that these mean temperatures were calculated by averaging the recorded temperatures of all thermocouples in contact with structural steel within the girders.   That is, thermocouples in contact with the stay-in-place forms were not included in the calculation, nor were those thermocouples hanging within the girders. It is clear that, on both days, the girders are at essentially the same temperature in the early-morning hours. A state of thermal equilibrium between the two girders has been reached, and both girders are steadily decreasing in mean temperature throughout the early-morning hours. As the girders are at practically the same temperature, they each reach their minimum daily temperature at essentially the same time, at

approximately 7:00. While both girders then begin to increase in mean temperature, it is seen that the outer girder experiences a much more rapid initial increase. This again is due to the fact that the outer girder is exposed to the east, where the rising sun's radiant heat energy strikes it directly. Over the six-seven hours following the beginning of temperature rise in both girders, the outer girder is at a consistently higher temperature than is the inner girder. This further illustrates how a bridge temperature can vary laterally, even though the girders are but a few meters apart.

It is then clear that the rate of temperature increase in the outer girder decreases, while the inner girder continues to warm at an essentially constant rate. This allows the inner girder to reach a higher mean temperature than the outer girder. Again, this is due to the fact that, at this time, the relatively warmer afternoon sun is shining directly onto the inner girder, heating it substantially. It is seen that, when the inner girder reaches its peak temperature at around 18:00, the outer girder has already begun cooling, and there exists a temperature gradient of several Celsius degrees laterally across the bridge superstructure. Maximum observed lateral temperature differences for these two days are tabulated below. It is then seen that both girders will cool to nearly the same temperature in the evening hours, until a new day's thermal cycle can begin. A state of thermal equilibrium between the girders will be reached, until the morning sun begins heating the bridge again, with the outer girder initially warming at a higher rate than the inner girder.
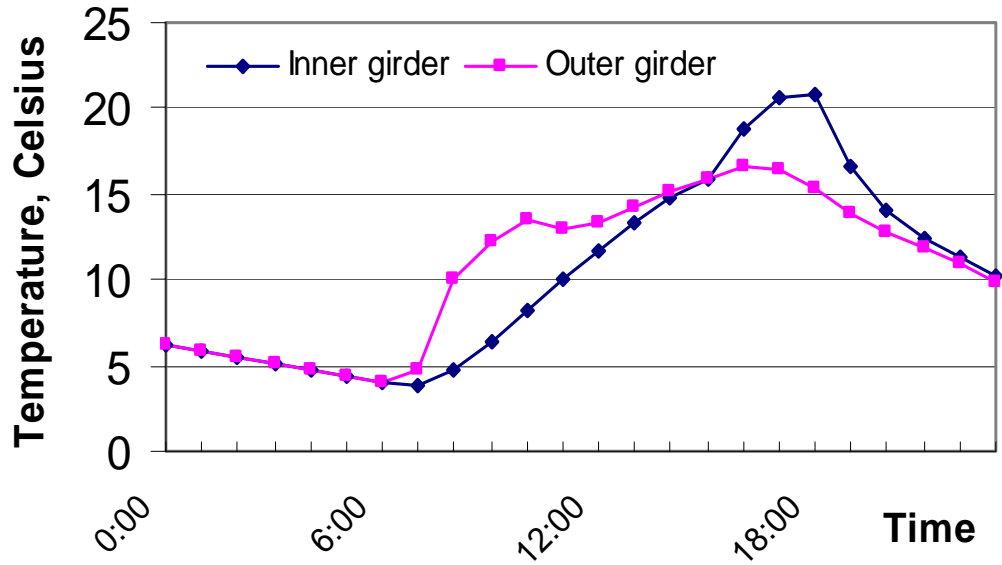
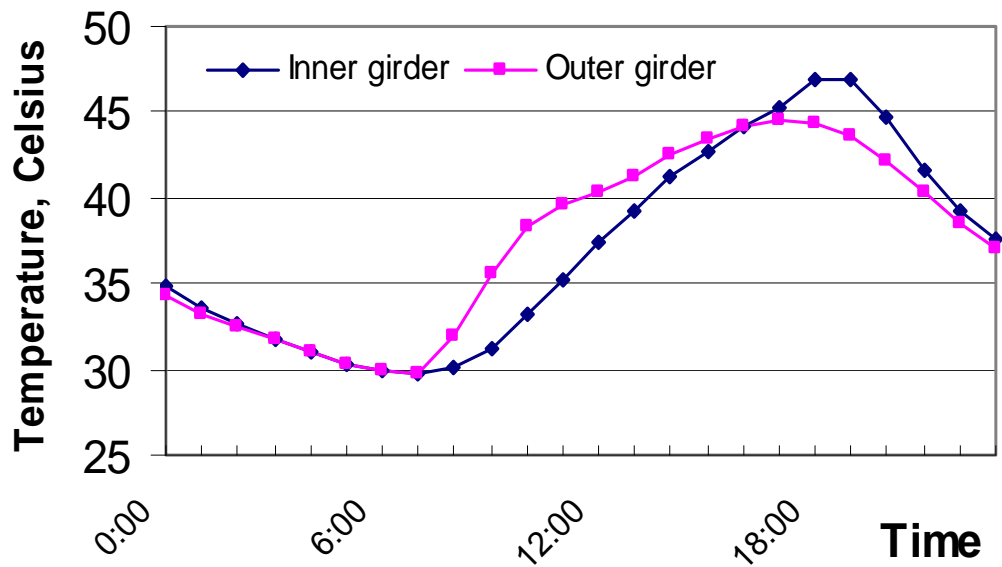**Figure 3. 14 Mean Girder Temperature Variation For March 10, 1998**

Figure 3.15 Mean Girder Temperature Variation For August 2, 1998

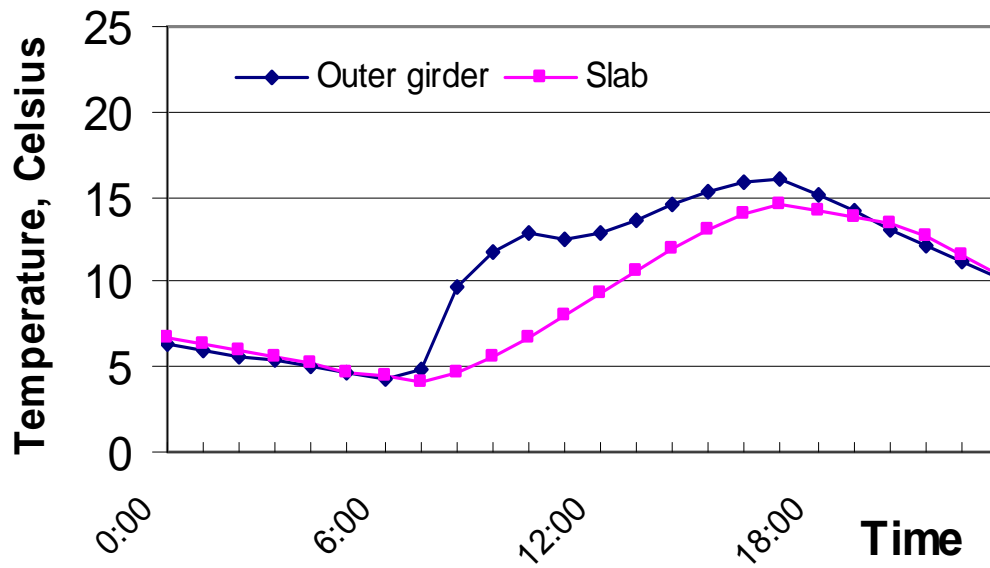### 3.3.7   Variations Between Slab and Girder Temperatures

Having made comparisons between cross-sectional behaviors and overall mean girder temperatures, along with comparisons between girder behaviors and ambient air temperature histories, the thermal behavior of the concrete road deck compared to the behaviors of the girders and the ambient air will now be examined.

As described in Chapter 2, three thermocouples were attached to the bottom of the slab between the two girders by means of attaching the thermocouples to the stay-in-place forms. Also, additional thermocouples were attached to the top flanges on the outside of the curve of each girder. It was not possible to embed thermocouples within the slab of this existing bridge. However, sufficiently different temperatures were recorded between those thermocouples attached to structural steel and those attached to the stay-in-place forms to validate the assumption that temperatures of the bottom of the slab were recorded by those thermocouples in contact with the forms, which conduct heat well. These temperatures will be described presently. For purposes of this study, a mean slab temperature was used, determined as the arithmetic mean of the five thermocouples in contact with the exposed slab forms and top flanges, as shown in Figure 3.2. The thermocouples in contact with the forms within the girders were not included.   It should be borne in mind that the slab temperatures recorded are those of the slab bottom, and that the deck is one of plain concrete. If the deck were covered with a layer of asphalt and thermocouples were attached to the top surface of the deck, substantially warmer temperatures would be recorded, as asphalt absorbs radiant heat well.

Shown in Figure 3.16 is a plot of the thermal histories of the outer girder at the southern cross-section and the slab for March 10. Data collected for the southern section is appropriate for use in considering girder temperatures related

to slab temperatures, because the slab was instrumented at approximately the same location as the southern section instrumentation location for the girders. In all plots of girder temperatures versus slab temperatures, the mean girder temperatures of the southern cross-section will be used. In this manner, the complete thermal history of the bridge at this cross-section is determined.

Examination of this plot shows that the outer girder and the slab begin the daily thermal cycle at nearly the same temperature, with the slab maintaining temperatures very slightly above those of the outer girder. The slab and girder are steadily decreasing in temperature during the early-morning hours, with the slab reaching its minimum temperature approximately one hour before the outer girder minimizes its temperature. The slab then begins steadily increasing in temperature, with this change plotting as a smooth curve. At the time of the onset of temperature increase, the outer girder makes its rapid initial increase described earlier. Because of the different heating trends between the two elements, there exists a substantial temperature difference between the slab and the girder in the mid-day hours. These differences are tabulated in Table 3.4.

Figure 3.16 Variation Between Slab and Mean Outer Girder Temperatures For March 10, 1998 At The Southern Cross-Section
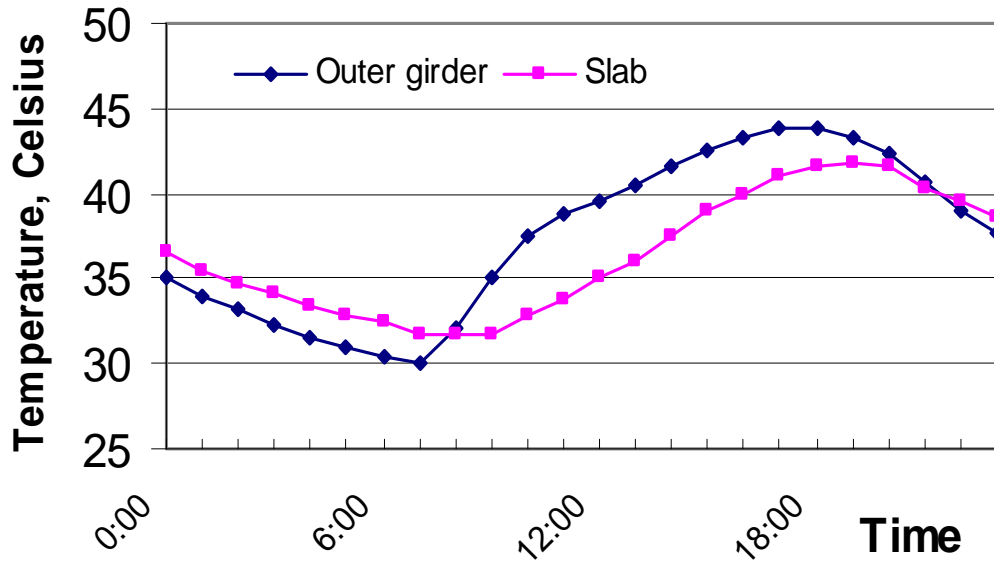
Table 3.4. Differences Between Mean Slab and Mean Outer Girder Temperatures during March 10 At The Southern Cross-Section.

Time	Girder Mean Temp.	Slab Mean. Temp.	Difference
8:00	9.5º C	4.9º C	4.6º C
9:00	11.2º C	5.4º C	5.8º C
10:00	12.8º C	6.7º C	5.9º C

It is clear that the temperatures of both elements continue to rise until the late afternoon hours. As the slab continues to warm at a uniform rate, the rate of warming of the outer girder decreases substantially from its initial rate of temperature increase. As the slab reaches its peak temperature for the day, the outer girder starts to decrease in temperature, thereby decreasing the differences in the temperatures of the elements. Also, it is seen that, as cooling of the girder continues, cooling of the slab is just beginning, allowing the girder temperatures to decrease to values slightly less than those of the slab. Both elements then continue to decrease in temperature, and a new day's thermal cycle can begin for both elements. Examination of these plots also shows that the slab retains heat for significantly longer periods than the girder does. This is an illustration of the fact that the thermal conductivity of concrete is much smaller than that of steel.

The comparisons in the preceding paragraph are for the day of coldest recorded mean bridge temperature, March 10. The behavior described, however, appears to be typical in this bridge. A plot of the same quantities is shown in Figure 3.17 for August 2, the day of warmest recorded EMBT. It can be seen in this graph that behaviors on this day are similar to those recorded for March 10. Although there is a slightly larger initial temperature difference between the slab and the outer girder (the slab is clearly warmer than the girder in the early-morning hours), both elements exhibit the same initial cooling trends described above. One difference that makes itself apparent is that the slab doesn't begin its warming trend until approximately two hours after the girder begins warming, as opposed to the one-hour difference noted above. This is minor, though; all the characteristics observed in the previous comparison are seen in this plot, as well. Temperature differences of several Celsius degrees are readily visible in the graph, and it is also seen again that the outer girder reaches its peak temperature some two hours before the slab does. And it is again seen that, as the outer girder begins its cooling two hours before the slab begins its cooling, the girder will

decrease to a temperature lower than that in the slab, albeit slightly so. Maximum temperature differences between the elements for August 2 are again tabulated, in Table 3.5.

Figure 3. 17. Variation Between Mean Slab And Outer Girder Temperatures At The Southern Cross-Section For August 2, 1998

Table 3.5. Differences Between Mean Slab and Mean Outer Girder Temperatures At The Southern Cross-Section During August 2.

Time	Girder Mean Temp.	Slab Mean. Temp.	Difference
8:00	35.1º C	31.7º C	3.4º C
9:00	37.6º C	32.8º C	4.8º C
10:00	38.8º C	33.7º C	5.1º C

It is also important to compare the thermal behaviors of the inner girder and the slab on the two days under study. Figure 3.18 is a plot of the temperature history of both elements for March 10. It is of interest to note that the elements begin the day at essentially the same temperature. Both elements cool at the same rate, as well, and reach their respective minimum temperatures at the same time, namely, at 7:00. At this point, both the slab and the inner girder begin to warm, with the girder warming at a slightly higher rate, due to its higher thermal conductivity. The girder and the slab temperatures then begin to separate, with the girder warming to higher temperatures than the slab.

The influence of direct sunlight on the warming behavior of the inner girder was described earlier. It was observed before that, in the mid-afternoon hours, the inner girder experiences a dramatic increase in its rate of warming, driving it to peak temperatures often substantially higher than those of other bridge elements. This is seen again here, as the girder's rate of warming sharply increases between 15:00 and 16:00, driving it to a peak temperature several Celsius degrees higher than the peak temperature of the slab. It is also seen that, while the outer girder typically reaches its peak temperature one hour after the slab reaches its maximum, the inner girder reaches its maximum temperature at nearly the same time the slab reaches its maximum, or, at most, one hour later. Thus, the lower thermal conductivity of concrete in comparison to that of steel "stalls" the heating of the slab long enough so that it doesn't reach its maximum temperature until the mid-afternoon sun is imposing relatively intense radiant heat energy onto the inner girder. This is important because it suggests that, although specific temperature differences exist, the inner girder and the slab exhibit the same general trends in heating and cooling, in contrast to the differing trends between the outer girder and the slab. Finally, it is seen in the plot that the girder and the slab cool to nearly the same temperature in the evening hours. In order to do so, the inner girder loses heat at a higher rate than does the slab, indicating that the

girder is re-radiating heat energy to the surrounding air at a higher rate than is the concrete slab.
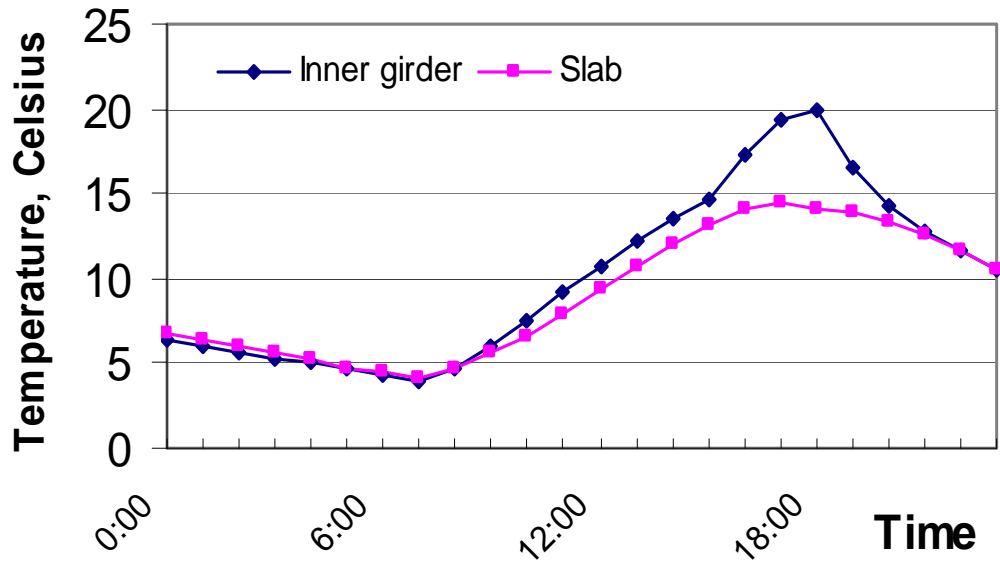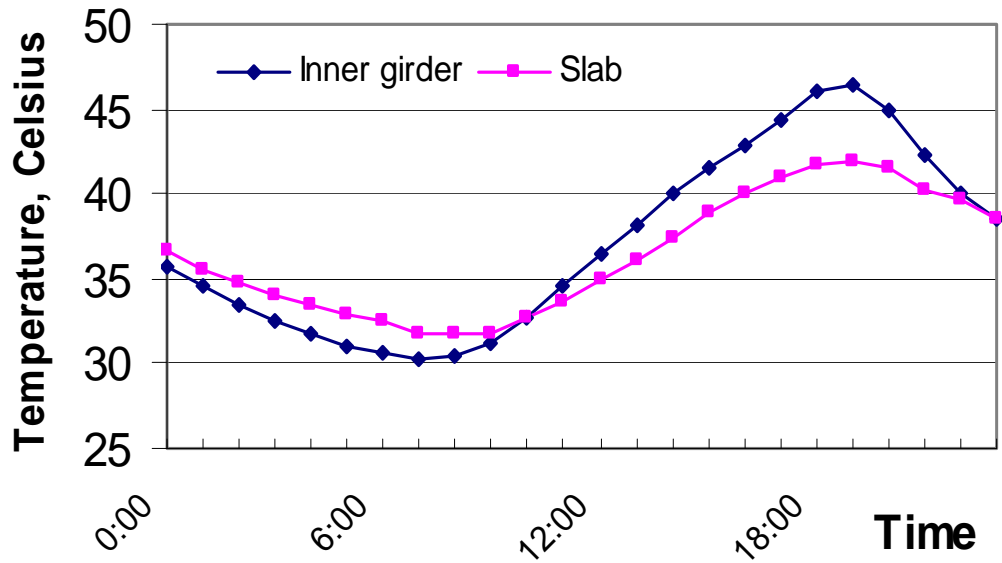

Figure 3. 18 Variation Between Mean Slab And Inner Girder Temperatures At The Southern Cross-Section For March 10, 1998

Table 3.6. Differences Between Mean Slab and Mean Inner Girder Temperatures At The Southern Cross-Section During March 10.

Time	Girder Mean Temp.	Slab Mean. Temp.	Difference
17:00	20.0º C	14.3º C	5.7º C
18:00	21.1º C	14.0º C	7.1º C
19:00	18.2º C	14.1º C	4.1º C

The same behaviors of the inner girder and the slab can be seen in Figure 3.19 for August 2. One difference that is immediately clear is that, on this particular day, the inner girder starts the day at slightly lower temperatures than does the slab. This suggests that, during the evening hours of August 1, the inner girder radiated substantially more heat than did the slab. Also on this day, the girder reaches its minimum temperature some two hours before the slab reaches its minimum. Both elements then warm at nearly uniform rates, with the girder warming at a higher rate than the slab, allowing its temperatures to gradually "pull away" from the slab temperatures. This relatively constant rate of heating continues until approximately 17:00, at which time the girder experiences the sharp increase in heating rate observed earlier. Both elements then reach their maximum temperatures at the same time, namely, 19:00. Just as on March 10, there is a temperature difference of several Celsius degrees between the two elements at this time. It is important to note that the elements still experience the same general heating and cooling trends, despite their temperature differences. The maximum recorded temperature differences are again tabulated, in Table 3.7. Finally, it is clear from the graph that the slab and girder cool to essentially the same temperature as the evening hours progress, further bolstering the observation that the elements undergo the same warming and cooling trends.

Figure 3. 19 Variation Between Mean Slab And Inner Girder Temperatures At The Southern Cross-Section For August 2, 1998

Table 3.7. Differences Between Mean Slab and Mean Inner Girder Temperatures At The Southern Cross-Section During August 2.

Time	Girder Mean Temp.	Slab Mean. Temp.	Difference
18:00	46.1° C	41.7° C	4.4° C
19:00	46.5° C	41.8° C	4.7° C
20:00	44.9° C	41.6° C	3.3° C

3.3.8   Variations Between Slab and Air Temperatures

Having compared the thermal behavior of the slab to the behaviors of both girders, it is also important to compare and contrast the recorded thermal behaviors of the slab and air temperatures. Shown in Figure 3.20 is the thermal history of the slab and ambient air temperatures for March 10.
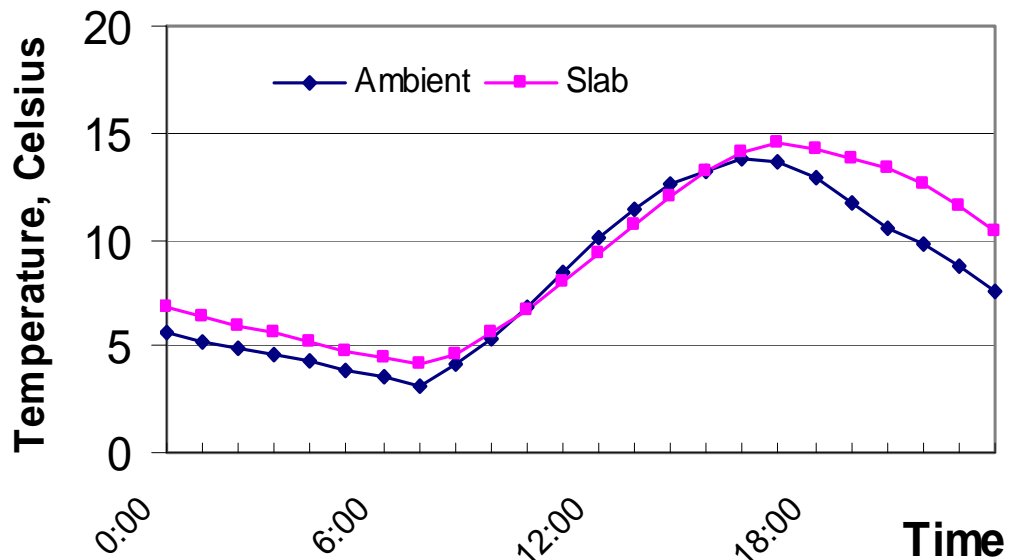

Figure 3.20 Variation Between Slab And Ambient Temperatures For March 10, 1998

It is clear that the day begins with the slab several Celsius degrees warmer than the surrounding air. Both recorded quantities are then seen to decrease practically uniformly, with both temperatures reaching minima at 7:00. At this time, both temperatures begin to rise, with the air doing so at a higher rate than the slab. This continues into the late afternoon hours. What is of principal importance here is that, because the slab starts the day at higher temperatures than

the surrounding air, it will, for all practical purposes, never cool to a temperature lower than that of the air. This is true even when both quantities are at their respective minima and the air temperature is rising, which is the only feasible time the slab could be cooler than the surrounding air. It is clear that the temperatures plot practically on top of each other in the early- to mid-afternoon hours, with both reaching their respective maxima in the late afternoon. At 14:00, it appears that the air is slightly warmer than the slab, but it turns out that this difference is less than 0.25 Celsius degree. The two quantities then decrease in the evening hours, with the air doing so at a higher rate than the slab, allowing for the temperatures to separate from each other in increasing amounts before the next day's cycle begins.

The same general behaviors can be seen in Figure 3.21, which is a plot of the same quantities during August 2. The slab again begins the day several degrees warmer than the surrounding air, and both quantities are seen to be decreasing. On this day, however, the air starts its warming phase two hours earlier than the slab begins its warming. Both quantities then warm at relatively uniform rates through the late-morning and afternoon hours. It can also be seen that, on this day, the slab reaches its peak temperature between one and two hours after the maximum air temperature is reached. However, what is again of prime importance here is that the slab never achieves a temperature lower than that of the surrounding air, as seen in the data recorded for March 10. In fact, it will later be seen that the bridge as a whole never achieves such a condition. It can again be seen in the August 2 plot that the air cools at a more rapid rate than does the slab, allowing for the temperature separation also seen on March 10. The temperatures cool through the evening to finally reach a state similar to those in the early-morning hours, and the thermal cycle begins again the next day.
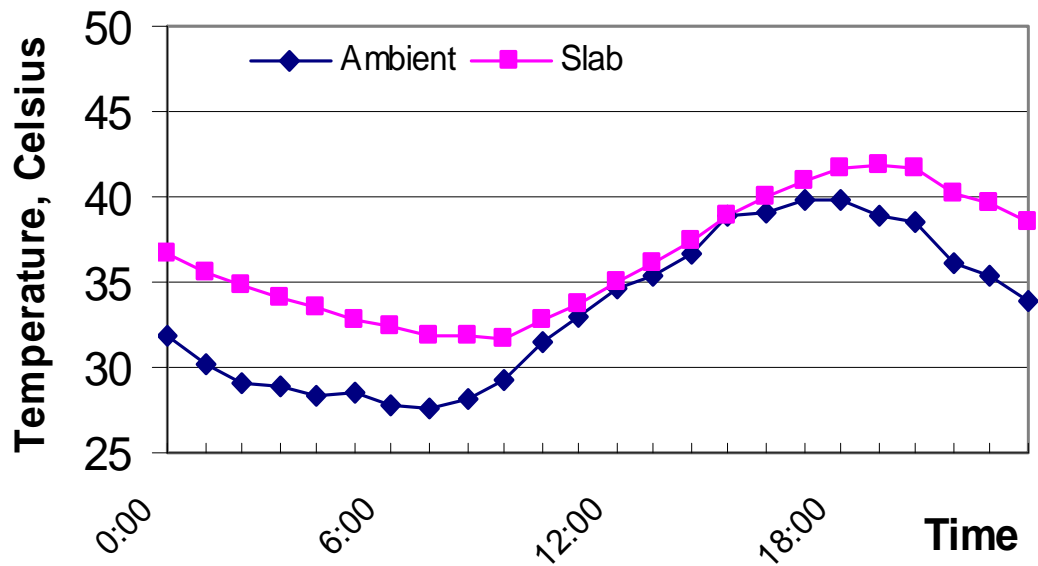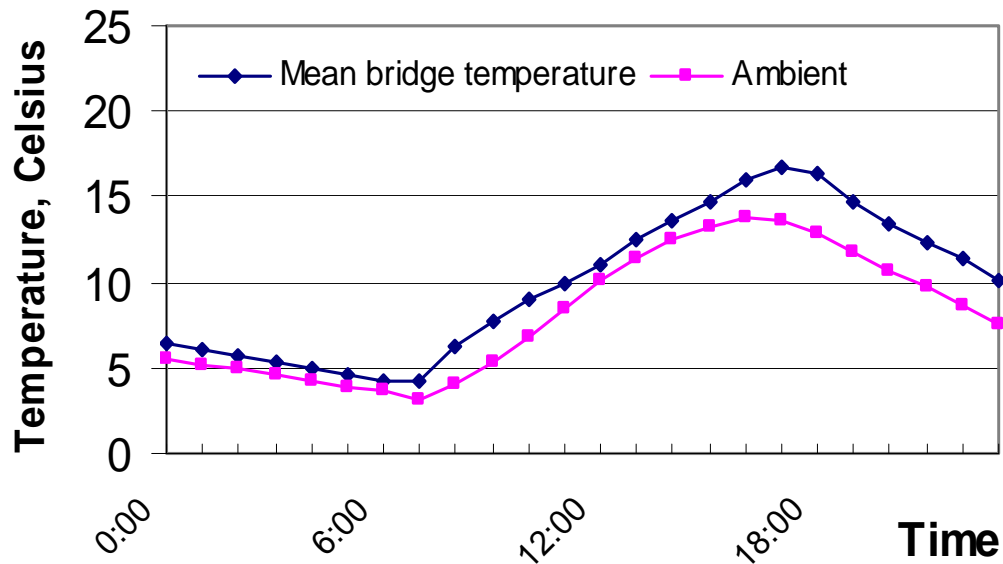
Figure 3. 21 Variation Between Ambient And Mean Slab Temperatures For August 2, 1998

3.3.9   Variations Between Mean Bridge Temperatures (EMBTs) and Air Temperatures

Having examined cross-sectional thermal behaviors, overall girder behaviors, and slab behavior, both individually and as they relate to air temperatures, it is now of the utmost importance to investigate EMBTs as they relate to ambient air temperatures. It will again be recalled that ambient temperatures, as presented here, are those recorded by the thermocouple hanging between the girders. As described earlier, the AASHTO *LRFD Specification* uses mean air temperature ranges in quantifying expected thermal displacements and associated stresses, if stresses are expected to be present. The EMBT histories on the two days under

scrutiny will be studied presently, with specific comparisons to recorded air temperatures at the bridge location.

Figure 3.22 is a plot of EMBT and recorded air temperature for March 10. It can be seen in this plot that, in the early-morning hours, the bridge is between two and three Celsius degrees warmer than the surrounding air. It is also readily observed that the bridge and air both cool through the early hours of the day, and at essentially the same rate, allowing the bridge to maintain a nearly constant temperature margin over the air temperature. Both quantities then reach their minimum values at approximately 7:00. Both measured quantities then begin to steadily increase, with the bridge doing so at a higher rate in the first hour of the warming trend. It is then seen that temperatures continue to increase through the mid-morning and afternoon hours and into the early evening hours. It is important to note that the EMBT then reaches its peak some one to two hours after the maximum air temperature has been achieved. Earlier, it was seen that the outer girder typically reaches its maximum temperature at nearly the same time that the surrounding air it at its maximum temperature. However, it was also shown that the inner girder and the slab both typically reach their daily maxima one to two hours after the maximum air temperature is reached. Thus, the influence of the slight lag in warming of the slab and the inner girder is enough to delay the achievement of maximum bridge temperature until slightly after maximum air temperature is reached. It is then clear that both temperatures gradually decrease at nearly the same rate into the mid- to late-evening hours, and another thermal cycle is ready to begin. It is of prime importance to note, however, that there is always a difference between the mean bridge temperature and the temperature of the surrounding air.

Figure 3.22 Variation Between Mean Bridge and Ambient Temperatures For March 10, 1998

This is also seen in the Figure 3.23, which shows the same quantities on August 2. The same characteristics exhibited in the graph for March 10 are observed again here. The temperatures show the same general cooling trend in the early-morning hours, with the air and mean bridge temperatures both reaching their respective minima on this particular day. Both temperatures then increase, with the bridge doing so at a relatively constant rate. It is also seen that there is a one-hour lag between the time of maximum air temperature and maximum bridge temperature achievement. However, it is again of importance to note that the bridge is never at a cooler temperature than the surrounding air. In fact, at the time of peak bridge temperature, there is a difference of several Celsius degrees between the mean bridge temperature and the ambient air temperature. Maximum temperature differences between the air and the bridge for March 10 and August 2 are tabulated in Table 3.8.
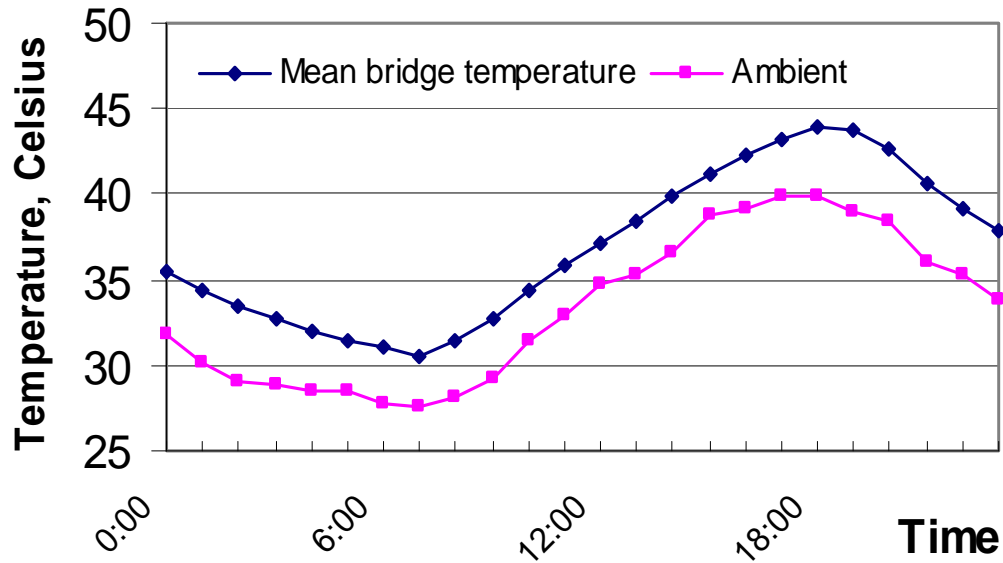
Figure 3. 23 Variation Between Mean Bridge Temperature And Ambient Temperature For August 2, 1998

Table 3.8. Maximum Differences Between Ambient and Mean Bridge Temperatures During March 10 and August 2.

Date	Time	Air Temp.	Mean Bridge Temp.	Difference
March 10	17:00	12.9º C	16.8º C	3.9º C
March 10	18:00	12.2º C	16.6º C	4.4º C
August 2	18:00	39.8º C	43.9º C	4.1º C
August 2	19:00	38.9º C	43.8º C	5.1º C

3.3.10   Further Temperature Variations: "Hot Spots"

It has been shown that there are always temperature differences throughout this bridge structure. At any particular time, there are temperature gradients laterally through the bridge cross-sections, along the girder lengths, and between the steel girders and the concrete slab, as well as differences between the various bridge elements and the surrounding air. It is interesting to note, however, that the large temperature differences which occur throughout the day are between the girder surfaces receiving the most direct sun exposure, namely, the outer webs of the girders. This will be described presently.

It was earlier shown that the outer girder is typically at substantially higher temperatures in the morning hours than the rest of the bridge structure. This was attributed to the fact that during this time the outer girder is receiving more direct radiant heat energy than is the rest of the bridge. It was also shown that in the mid- to late-afternoon hours, the inner girder experiences significantly higher temperatures than the rest of the bridge, due to the sun's position in the western sky, and its direct path of heat transfer to the inner girder. It will be instructive to examine the magnitudes of these temperature differences through a cross-section at various times of the day.

Shown in Figure 3.24 is a temperature profile for the northern cross-section at 8:00 on March 10. This is the time of largest temperature difference between the outer girder and the ambient air. This diagram dramatically illustrates the large variations in temperature which typically occur within the same cross-section of this bridge. It can be seen that there is a relatively large temperature difference between the warmest and coolest points of the cross-section, namely, a difference of 14.6 Celsius degrees. This is quite significant. This is further illustration of the fact that, although girder temperatures are nearly uniform at night, the girders are never at the same temperature during the daylight hours.

19.1   6.8   5.1   5.7

17.6   6.0   4.3   4.5

6.3   5.4   EMBT=6.2º   4.6   4.6
   Ambient=4.6º
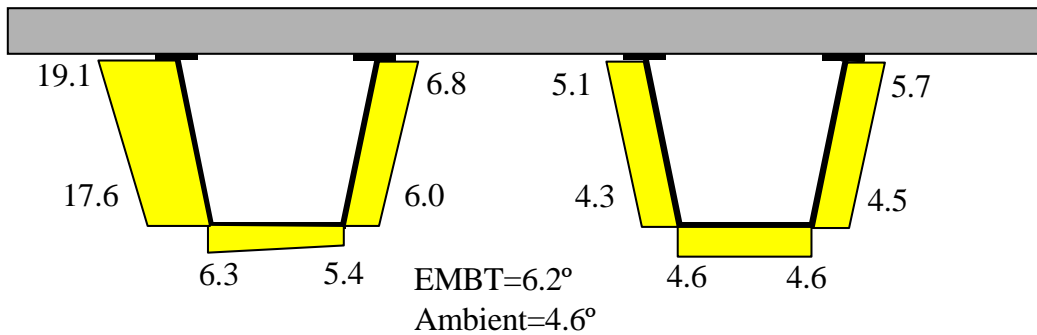
Figure 3.24 Temperature Distribution Across The Northern Cross-Section At 8:00, March 10

These temperature differences are even more substantial later in the day. Figure 3.25 is a profile of the same cross-section at 18:00 for the same day, March 10. It can be seen here that a maximum lateral temperature difference of 19.8 Celsius degrees is present at this time. Further, a temperature difference from the top in the inner web of the inner girder to the bottom of the web of 6.8 Celsius degrees is observed. This is quite significant, as it illustrates not only the large temperature variations which occur between the girders at a given time, but it also shows that significant temperature differences can occur even within a given steel plate.
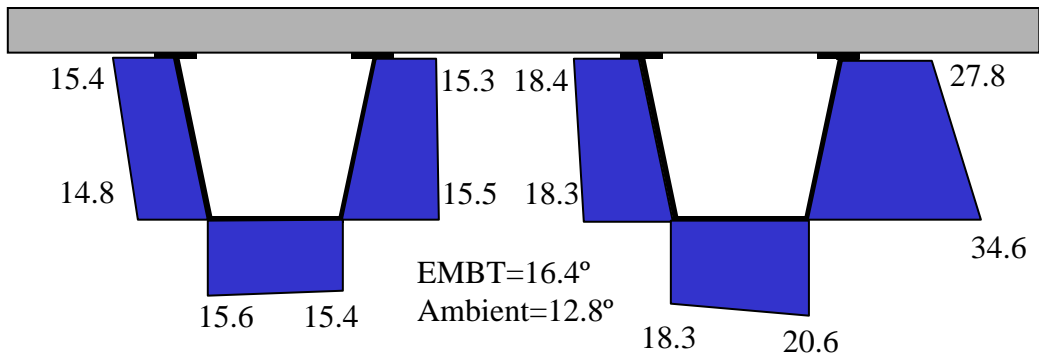
Figure 3.25 Temperature Distribution Across The Northern Cross-Section At 18:00, March 10

Finally, Figure 3.26 illustrates the temperature distribution across the northern cross-section at 3:00 on March 10. It is clear from this figure that girder temperatures are nearly uniform at night.
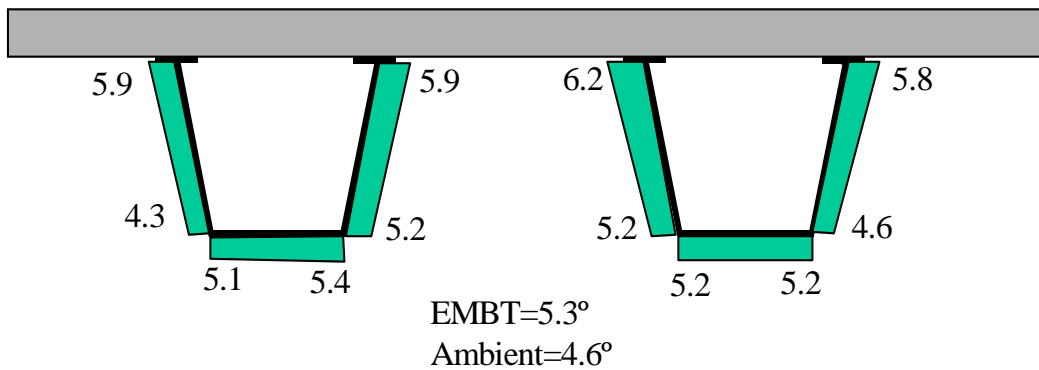
Figure 3.26 Temperature Distribution Across The Northern Cross-Section At 3:00, March 10

3.4   Recorded Temperatures: Maxima, Minima, and Ranges

Having studied in close detail the thermal behaviors of this bridge at various sections, as individual elements, and as whole structure, it is now appropriate to examine the temperature ranges and extreme temperatures recorded during the instrumentation period.

As described earlier, the AASHTO *LRFD Specification* prescribes temperature ranges to be considered in the design of highway bridges. The Specification requires that the designer consider minimum and maximum temperatures in the design of a bridge, and specifies that differences between the actual air temperature at the time of bridge construction and the specified extreme temperatures be considered to compute deformation and displacement effects. It was shown that, for steel bridges in a moderate climate such as Houston, the temperature range to be considered is -18º C to 50º C. Because this bridge was instrumented through extreme temperatures, it is appropriate to examine temperature ranges as they pertain to the bridge under study, as it is necessary to consider both required and expected temperature ranges when calculating thermal-based bridge displacements.

Figure 3.27 is a plot of recorded monthly maxima for both the mean bridge temperature and the surrounding air temperature. Several important attributes of this bridge and its site may be gleaned from this chart. First, it is seen that the maximum mean bridge temperatures for the months under study are always larger than the maximum air temperatures at the site. This is not new; it has been observed in several plots herein that there is always a difference between the mean bridge temperature and the surrounding air temperature. It was also shown that the bridge is, for practical purposes, never at a cooler mean temperature than the ambient conditions. This graph illustrates the differences recorded, while at the same time showing that the bridge always achieves higher maximum

temperatures than the surrounding air. It is possible that in a given month a cold spell followed by a rapid rise in air temperature could leave the bridge at a cooler mean bridge temperature than the surrounding air for a brief time, but this was not observed in this study.

Next, it is seen that the maximum mean bridge temperature achieved is near 44º C (the actual value is 43.9º C). This lends credence to the AASHTO-specified maximum expected temperature of 50º C. This maximum mean bridge temperature is some four Celsius degrees higher than the maximum surrounding air temperature for the same month, August.   The recorded maximum temperatures for the month of July exhibit a very similar relation between the two maxima, and it is during these two months in which the largest temperature differences occur.
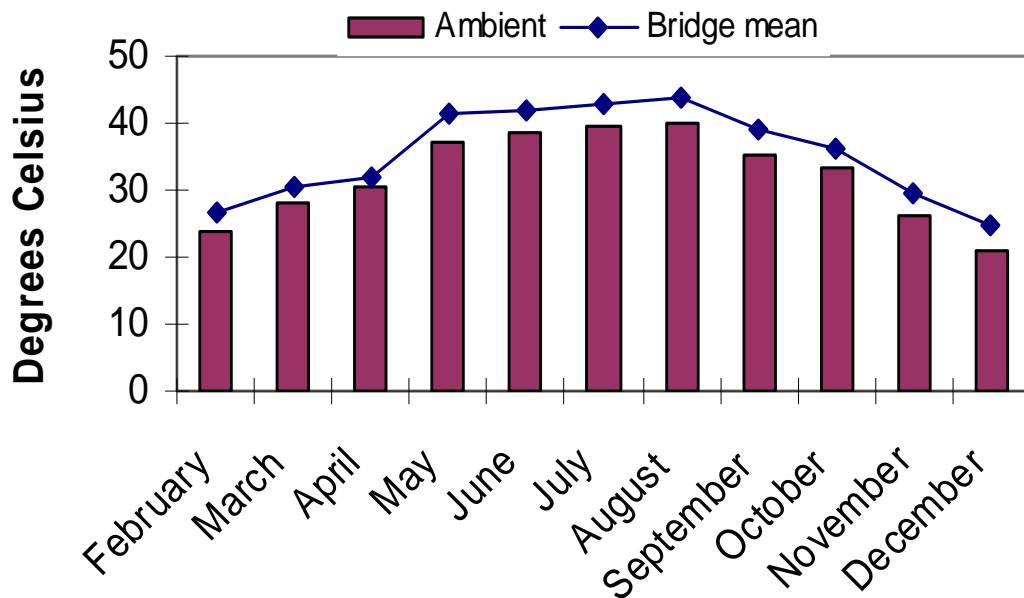

Figure 3. 27 Maximum Recorded Monthly Temperatures

It is also instructive to examine the minimum temperatures recorded as the mean bridge and ambient quantities, as well. Figure 3.28 is a plot of the monthly minimum temperatures, as determined from this study.

It can be seen from this graph that, again, the mean bridge temperature is always at a higher value than the surrounding air temperature. While individual structural elements may reach temperatures cooler than the ambient air, the mean temperature of the bridge is always at least a few Celsius degrees warmer than the air. It will be noted that the minimum mean bridge temperature reached during the period of instrumentation was 4.2º C, which is 1.7 degrees warmer than the minimum air temperature of 2.5º C. Thus, it may be concluded that in both extreme hot and cold conditions at this bridge site, the bridge will remain at a warmer mean temperature than the surrounding air, albeit sometimes only slightly so. There is another important observation to be noted from this chart.
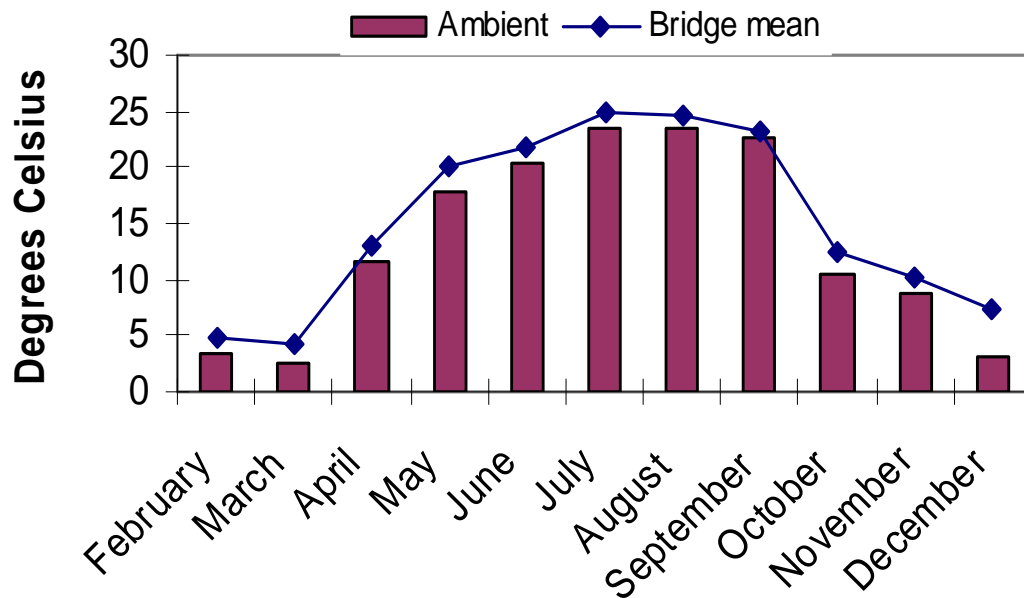

Figure 3.28 Minimum Recorded Monthly Temperatures

The AASHTO *LRFD Specification* prescribes a minimum temperature in moderate climates for the design of steel bridges to be used as -18º C. It is seen in this chart that this is a substantially lower temperature than was recorded at this bridge during the instrumentation period. The bridge never reached a freezing mean temperature, nor did it reach negative values. While this might seem overly conservative, it is to be noted that AASHTO defines a moderate climate as one in which the number of freezing days (defined as a day in which the "average" temperature is less than 0º C) per year is less than fourteen. Because this criterion is applicable to a substantial portion of the United States, it seems reasonable. It should also be borne in mind that studies such as this are impossible for structural designers to perform in the design phase of a bridge. Because of this impossibility, the designer must rely on recorded air temperatures and ascertain the average of these quantities, rather than more reliable bridge temperature measurements. Regions of the country further to the north than Houston might experience fewer than 14 freezing days in a given year, but may also experience negative temperatures when freezing does occur. Thus, bridges in Houston may be "insulated" from the extreme low temperatures considered by AASHTO for moderate climates, but, unless more extensive climate ranges are specified in the future, the specified extreme temperatures seem reasonable.

Finally, the recorded monthly temperature ranges should be examined. The chart below (Figure 3.29) shows measured temperature ranges for each month during the instrumentation period. These are maximum ranges occurring in each month, and not daily ranges. This is a more appropriate quantity to examine, as the bridge and its bearings will be expected to accommodate long-term temperature ranges, which are always larger than daily ranges. It has been seen that the mean bridge temperatures are always higher than the surrounding air temperatures, at both extremes on the temperature scale. It is interesting to note here that the range of mean bridge temperatures isn't necessarily larger than the

range of air temperatures at all times. It can be seen that, in the month of December, the recorded range of air temperatures is almost one Celsius degree larger than the range of mean bridge temperatures for the month. However, the bridge usually experiences larger ranges of temperatures than the surrounding air does, and this may be attributed to the higher thermal conductivity of steel in comparison to air, and to the bridge's absorption of solar radiation. It is interesting to observe that the maximum ranges of both quantities occur in the relatively mild spring and fall months. It can be concluded by inspection of the graph that in the warmer summer months the bridge remains warm relatively continuously, and that there is little change in its thermal state. This directly contrasts the observed thermal range behavior for the spring and fall months, where both cool and warm periods occur, thereby increasing recorded temperature ranges.
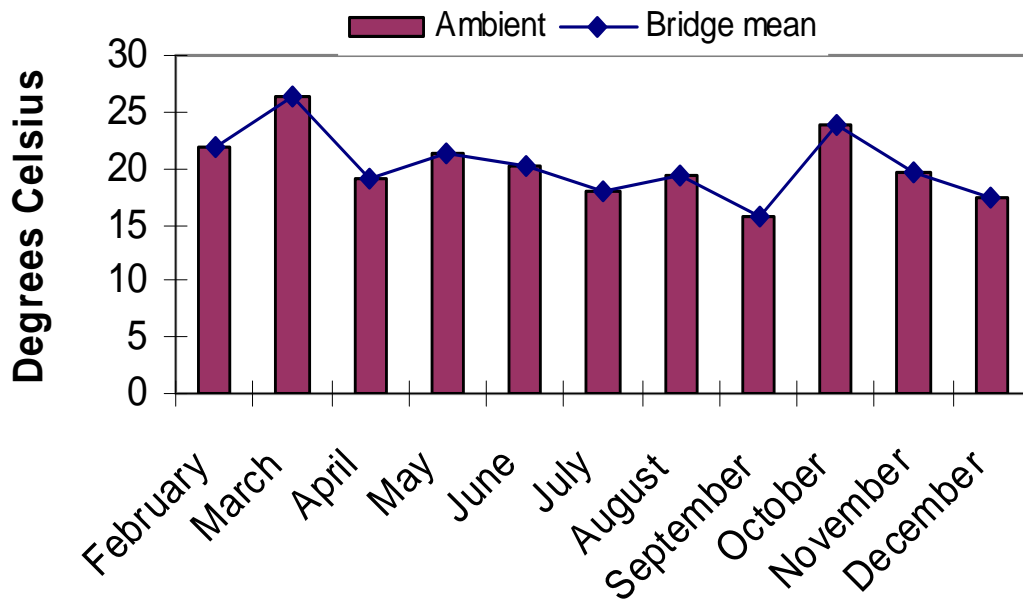

**Figure 3. 29 Recorded Monthly Temperature Ranges**

3.5   The Effects of Cloud Cover

The two days examined earlier were the days of coldest and warmest mean bridge temperatures for the instrumentation period. In examining the thermal trends of the bridge on those days, the effects of solar radiation were referred to several times in describing how it is that some bridge elements can be significantly warmer than others at given times. In particular, large temperature differences were shown to occur between the outer walls of the girders at those times of the day during which the sun is not directly overhead—i.e., when the sun is rising or setting. It is of the utmost importance to note that on those two days, the skies were reported to be clear in Houston for the duration of both days. This is what allows the solar radiation phenomenon to differentially warm the various parts of the bridge. Lack of cloud cover provides a clear path for the sun's radiant energy to reach and warm the girder walls.

It then becomes important to examine thermal behaviors on a day during which significant cloud cover prevented the radiation from occurring, or at least from occurring as effectively. A good day for examining the effects of cloud cover was June 6. Hourly weather reports for this day indicate that an overcast condition prevailed nearly every hour. Relevant temperature measurements will be studied presently.

Shown in Figures 3.31 and 3.32 are plots of mean cross-sectional temperatures of the girders at instrumentation locations 1 and 2, respectively. The girders begin the day at nearly the same temperature, as observed before, and decrease steadily through the early-morning hours. However, the thermal trends of the girders over the next several hours are drastically different from what was observed on the clear days. It is seen that, at both cross-sections, there is almost no difference in mean temperatures between the girders, at any time of day. Where there were large temperature differences between the exposed walls of the

74

girders in the morning and afternoon hours on the clear days, the girders are seen here to behave very similarly at both cross-sections throughout the day. In fact, the largest temperature difference between the girders occurs at the southern cross-section at 11:00 and is equal to slightly less than one-half of one Celsius degree, which is a minimal difference when compared to quantities observed earlier. This supports the argument that substantial cloud cover prevents either girder from absorbing any appreciable "extra" solar radiation compared to the other girder. Finally, Figure 3.30 shows a temperature profile, similar to Figures 3.24-3.26, of the southern section at 18:00 on June 6. This time was shown earlier to be one during which substantial temperature differences are present across the cross-section. Inspection of this figure dramatically illustrates the effects of cloud cover. The cross-section is clearly near uniform in temperature.
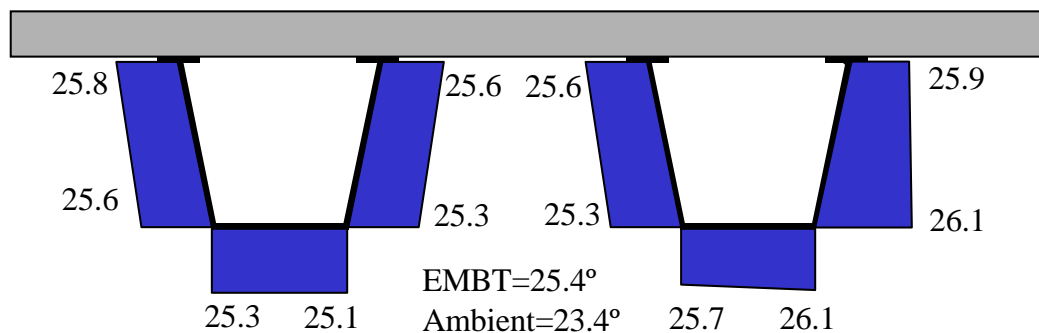
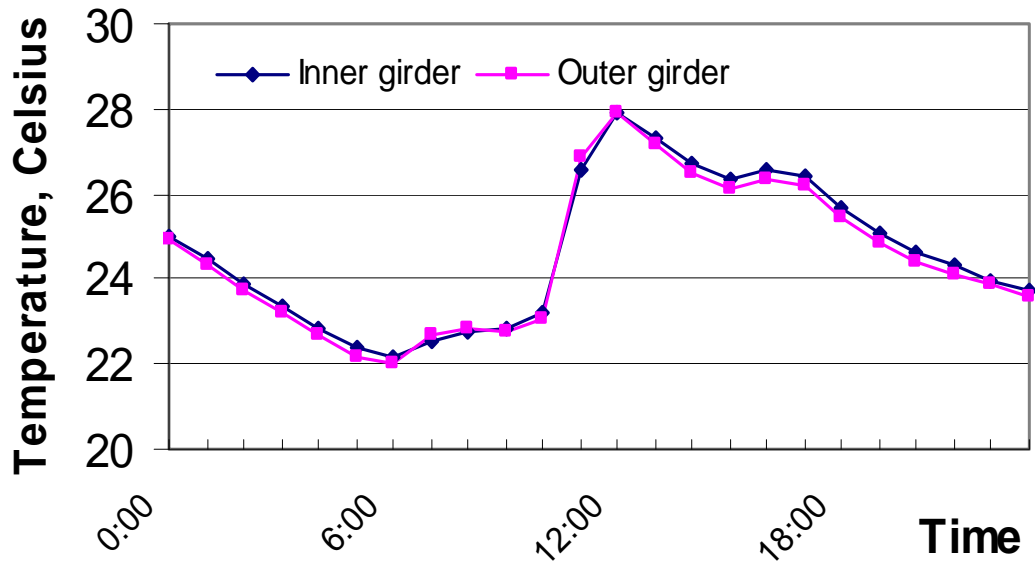**Figure 3.30 Temperature Distribution Across The Southern Section At 18:00, June 6**

Figure 3.31 Temperature Variation At The Northern Cross-Section For June 6, 1998
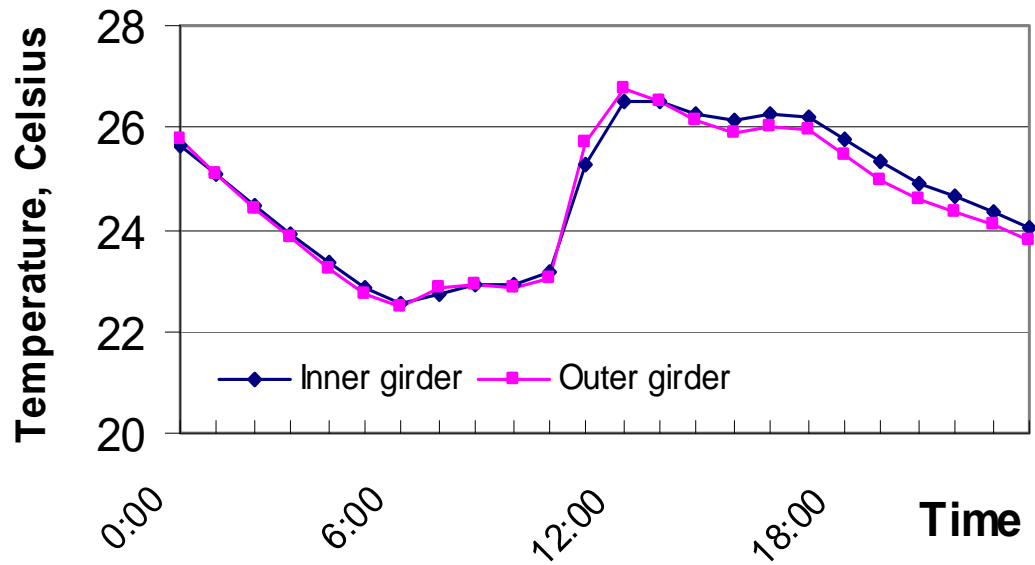

Figure 3.32 Temperature Variation At The Southern Cross-Section For June 6, 1998

Figures 3.33 and 3.34 show recorded temperatures for the exposed girder webs at both cross-sections on June 6. Again, these behaviors are quite different from what has been seen earlier. The curves plotting the recorded quantities closely follow each other throughout the day under study, which sharply contrasts the sometimes large differences observed on the relatively clear days. While a maximum lateral temperature difference of 19.8 Celsius degrees was observed between the exposed webs on March 10, the largest difference seen here is some 1.5 Celsius degrees, at 11:00 at the southern cross-section. This is a whole order of magnitude smaller than the larger difference observed earlier, further illustrating the fact that solar radiation is being prevented from dramatically heating the bridge unevenly.
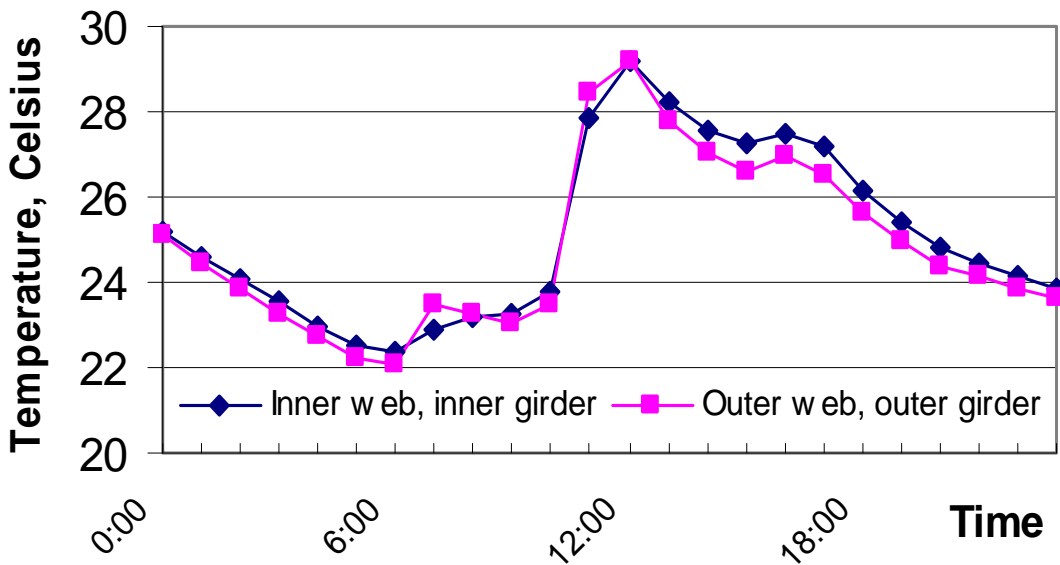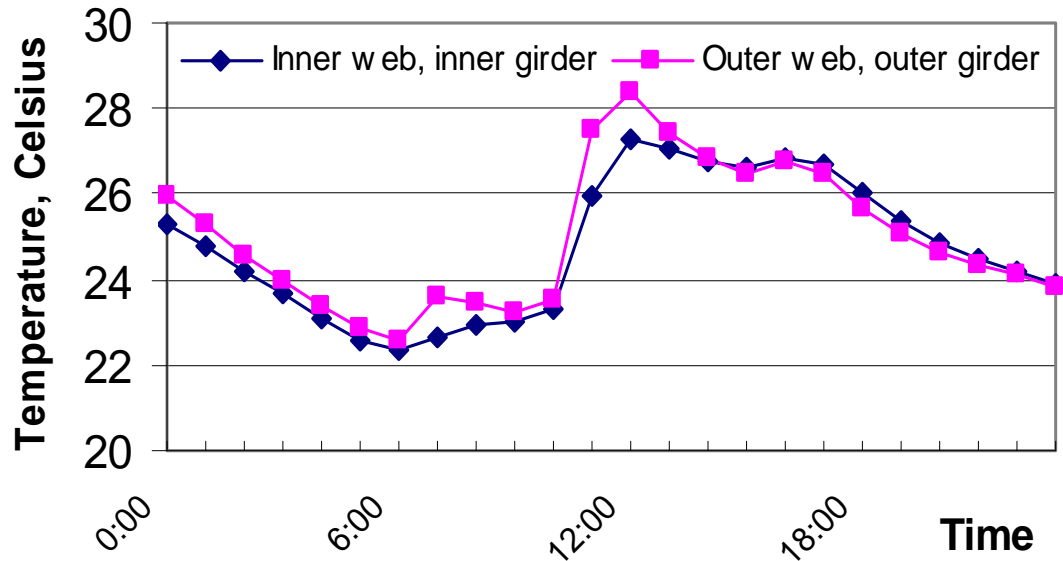

Figure 3.33 Temperature Variation Between Exposed Girder Webs At The Northern Cross-Section For June 6, 1998

Figure 3.34 Temperature Variation Between Exposed Girder Webs At The Southern Cross-Section For June 6, 1998

Next, Figure 3.35 shows the recorded overall mean girder temperatures for June 6. In comparison to what was seen earlier, this graph is remarkable. At several times on the clearer days, mean temperature differences of several degrees were observed between the girders. This graph shows a maximum mean girder temperature difference of only 0.35 Celsius degrees, again, a full order of magnitude smaller than the differences seen before.

Finally, Figure 3.36 shows the recorded temperatures of the outer girder and the slab. It is seen that, regardless of the amount of radiant energy allowed to reach the bridge, the heating and cooling properties of the slab are still significantly different from those of the girders. The fact that the slab takes longer to heat and cool than the steel elements can still be seen here, in that the slab does not reach a well-defined temperature peak, but rather spends several

hours achieving and effectively maintaining maximum temperatures. While this is occurring, the girder has already reached its maximum temperature and has begun its cooling trend into the evening hours. It can thus be concluded that, when substantial cloud cover is the prevailing condition, solar radiation is not a significant factor in the thermal behavior of the bridge. While occasional breaks in the cloud cover can provide an opportunity for radiant energy to strike isolated portions of the bridge, significant temperature differences will not arise in the bridge, and any small differences may be attributed to the bridge's layout and heat-transfer properties. However, the thermal conductivity differences between steel and concrete will still lead to significant temperature differences between the girders and the slab, regardless of the current weather conditions, unless it has been cool for several hours, such as during late-night hours.
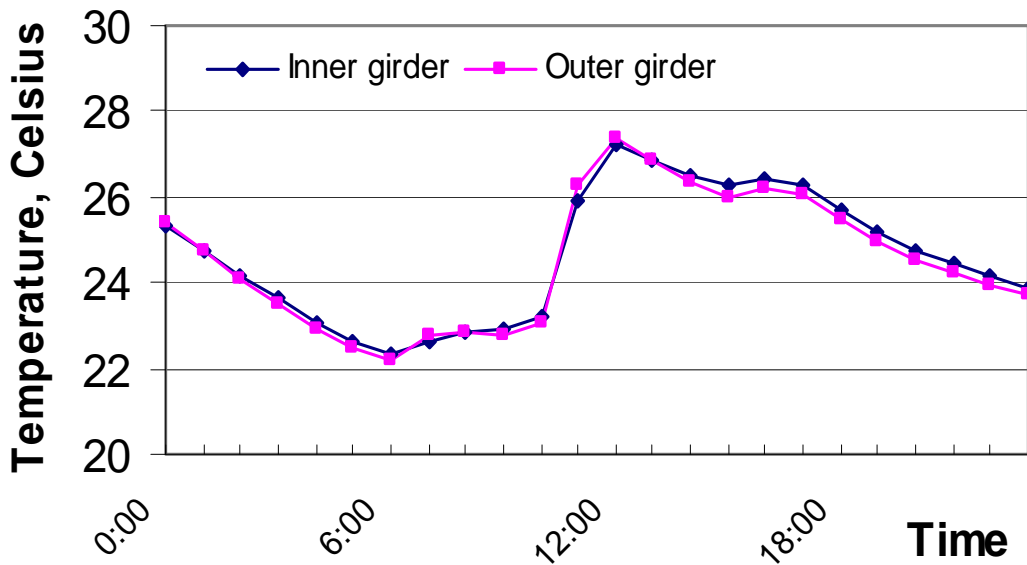

Figure 3.35 Variation Between Mean Girder Temperatures For June 6, 1998
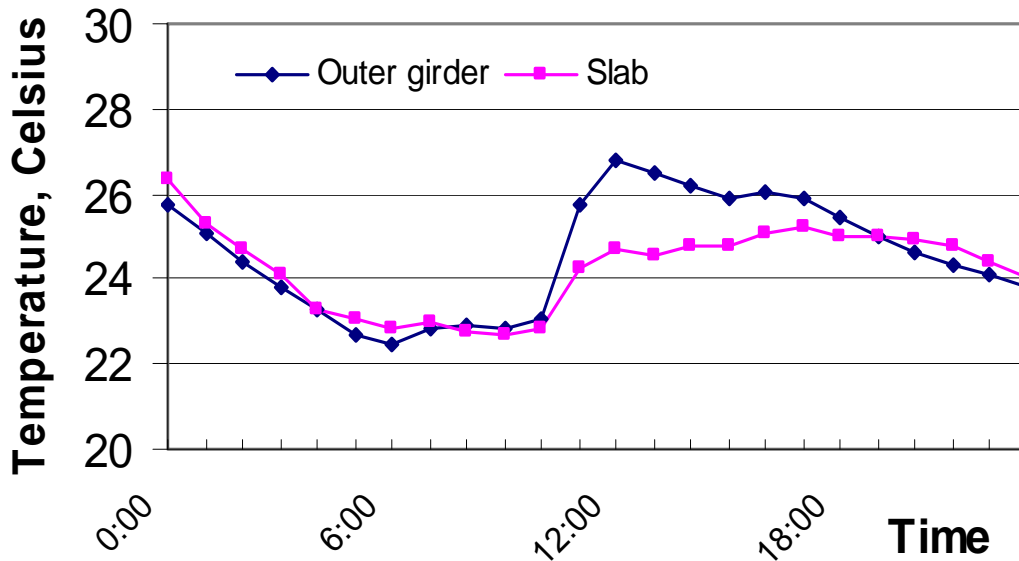
Figure 3.36 Variation Between Slab And Outer Girder Temperatures For June 6, 1998

3.6   Thermal Analysis: Conclusions

The thermal behavior throughout this existing bridge has been studied and described in detail. From this examination, several conclusions may now be drawn. These are listed and described herein.

1. When solar radiation is allowed to occur, the bridge is never at a uniform thermal state throughout the superstructure. This has been shown in some detail. It has been seen that during days of clear skies, there will always be thermal differences and gradients throughout the various elements of the bridge, namely, between the two girders, between the girders and the slab, and along the lengths of the girders.

2. Under a relatively clear sky, the girder receiving the most direct sunlight, particularly in the morning and late-afternoon hours, is often significantly warmer than the other girder, even at the same cross-section. It has been shown that, when the sun is rising or setting, it will transmit particularly intense radiant energy onto one girder, due to the orientation of the bridge. Because of this radiation, the exposed girder will be substantially warmer than the other girder. In particular, it was shown that on the day of the coldest mean bridge temperature recorded, March 10, there existed a lateral temperature difference of nearly 19.8 Celsius degrees across the bridge cross-section. This led to the observation of what the author termed "hot spots," that is, locations in the bridge cross-section which are quite warm relative to other locations. While this phenomenon is not typically accounted for in design, it was somewhat unexpected at the outset of this study, nonetheless. (In fact, it will be shown in Chapter 4 that these lateral temperature differences play a very significant role in inducing lateral bridge translations, which should be considered in bearing design.) It should be recalled, however, that when substantial cloud cover is present, these lateral temperature differences are minimized, as occurred on June 6, 1998.

3. The bridge has always been observed to be at a higher mean temperature than the ambient temperature. While it has been observed that at various times, particularly in the early-morning hours, girder cross-sections often drop below the ambient air temperature, the inclusion of all thermocouple readings into a mean bridge temperature always indicates that the bridge is at a higher mean temperature than the surrounding air. This can reasonably be attributed to the inclusion of slab temperature readings, as the thermal conductivity of concrete is much lower than that of steel, and the slab will thus "store" the thermal energy received for longer periods of time. The higher temperature readings for the slab are enough to boost the mean bridge temperature above that of the air. It was shown that the slab temperature is, at least, nearly equal to the ambient

temperature, and that the slab is, practically speaking, always warmer than the surrounding air.

4. There typically exists a slight lag between the time of maximum air temperature and the time of maximum mean bridge temperature. It was shown that the outer girder and the surrounding air will reach their maximum temperatures at nearly the same time. However, it was also seen that the slab and the outer girder will typically reach their respective maximum temperatures at the same time, and that this time is typically one or two hours after the air has reached its maximum temperature. This is of enough influence to affect the time of maximum mean temperature achievement for the bridge. While this is of no great consequence, it further illustrates the conclusion that the bridge is never at the recorded (or reported, for that matter) air temperature.

5. The AASHTO-specified maximum temperature to be considered in this location appears to be slightly conservative, but quite reasonable. The specified minimum temperature is somewhat more conservative. It was shown that the maximum mean bridge temperature recorded, 44º C, is within 6 Celsius degrees of the prescribed maximum of 50º C. The minimum recorded mean temperature of 4.2º C, however, is 22.2º C warmer than the prescribed minimum of -18º C. While this at first seems overly conservative, it was described that this minimum temperature may in fact be reasonable for other sites included under the climate category of "moderate." Unless further climate refinement is included in a future AASHTO *LRFD Specification*, the current range is adequate and conservative. The review of the AASHTO-specified extreme temperatures using mean bridge temperatures is appropriate because, as described earlier, the AASHTO *Specification* appears to be based upon the assumption that the bridge achieves the extreme temperatures uniformly throughout the structure, even though such a state has been shown to never exist in reality.

Chapter 4

Field Measurement of Girder Translations

Field measurements of girder expansions and contractions will be presented in this chapter. Displacement cycles of single days and long-term durations will be presented and discussed.

4.1   Recording Displacements

The instrumentation installed during two site visits was described in Chapter 2. The bridge was instrumented for longitudinal translations at four points; namely, at each of two bearing plates at both the northern-most ("end") pier and at the next pier to the south ("interior pier"). Only the two bearings at the interior pier were instrumented for transverse displacements, since the bearings at the end pier are guided to prevent transverse displacements. Transverse displacements in this case are normal to the curved longitudinal axis of the bridge, i.e., these displacements are radial translations.

Data Collection and Compilation

As was described in Chapter 2, data was read and recorded for both temperatures and displacements on an hourly basis. The data quickly accumulates at this rate, and requires selective analysis and interpretation in a study such as this. Various problems with the data naturally arise with remote field instrumentation, and particular aspects of this were described in Chapter 2.

All collected data was investigated, and the most informative and illustrative of the translation data will be presented here. Collected and analyzed rotation data for the ends of the girders will be presented and discussed in Chapter 6.

4.2   Daily Displacement Cycles

The observed displacement behavior of the bridge will be described in this section. Comparisons to analytical predictions of displacements will be made in Chapter 6.

4.2.1   Observed Longitudinal Displacements on August 2, 1998

The Emerson Mean Bridge Temperature (hereafter referred to as EMBT) was defined in Chapter 3. This method of calculating a mean bridge temperature is based on equilibrium principles, and accounts for the elastic moduli and cross-sectional areas of concrete and steel in the bridge. It was also noted in Chapter 3 that on August 2 the bridge reached its maximum EMBT of the instrumentation period. It is thus of interest to study the displacement behavior of the bridge on this day. Longitudinal displacements measured on this day will be examined presently.

Shown in Figure 4.1 are measured longitudinal displacements of the inner girder at the end pier for August 2, and Figure 4.2 shows mean inner girder temperatures for the same day. It will be recalled that mean girder temperatures are computed as the arithmetic mean of the reported temperatures of all thermocouples in contact with structural steel. For clarity, all times follow the 24-hour scale introduced in Chapter 3. Also, girder extensions have been taken as positive displacements, while contractions are taken as negative displacements.
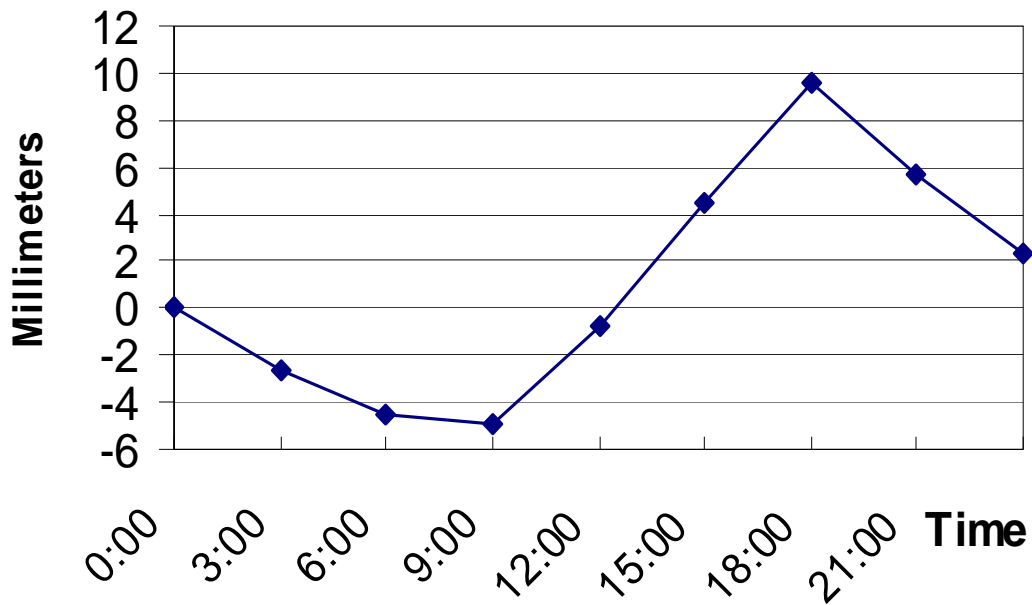
Figure 4.1 Longitudinal Displacements Of The Inner Girder On August 2, 1998
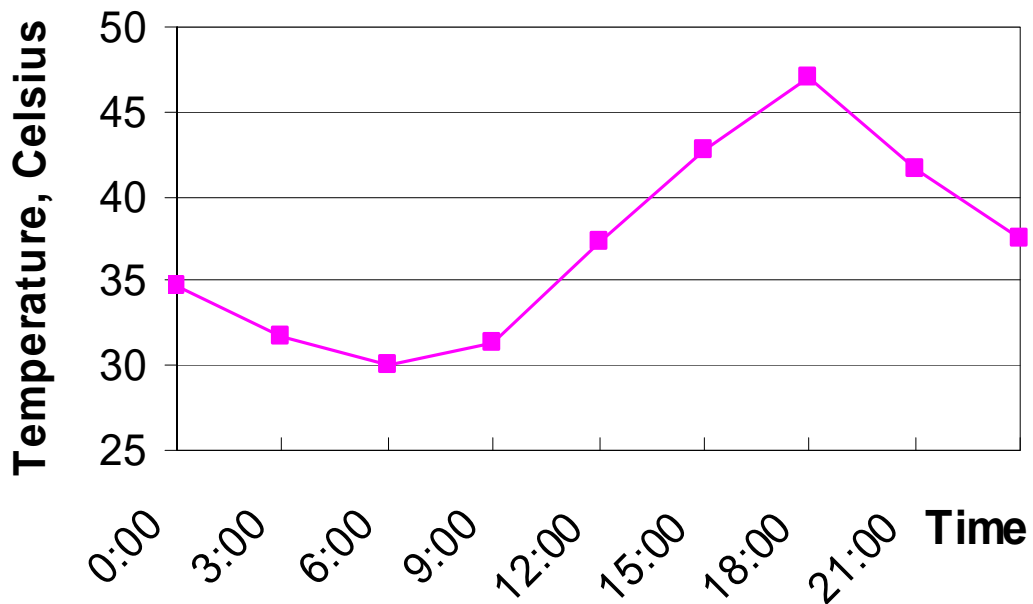

Figure 4.2 Mean Inner Girder Temperatures On August 2, 1998

It was seen in Chapter 3 that the various elements, and the bridge as a whole, achieve their minimum temperatures in the early-morning hours, just before and while the sun is rising. The displacement quantities shown are thus to be expected, as it is seen that the girder contracts through the morning hours, and, upon the influence of warming, begins to expand at 9:00. It is also seen that the girder reaches its maximum extension at 18:00, after which it begins contracting under the influence of decreasing temperatures into the evening hours. The time of maximum girder extension coincides with the maximum girder temperature, as shown in Figure 4.2. Finally, it is seen that the girder reaches a maximum contraction, relative to its position at the start of the day, of approximately 5 millimeters and a maximum extension of nearly 10 millimeters. Because the pot bearings in use at the southern instrumented pier are unguided, transverse displacements are allowed to occur at these locations as well as tangential displacements. Transverse displacements recorded on August 2 will be examined next.

4.2.2   Observed Transverse Displacements on August 2, 1998

Shown in Figure 4.3 are transverse displacements of the inner girder during August 2, and in Figure 4.4 are depicted the mean temperatures of both girders for the same time. In this study, transverse displacements which are radially outward are taken as positive, and inward displacements are taken as negative.

It is clear from Figure 4.3 that, in the early-morning hours, the girder contracts radially inward. This is to be expected, as it has been shown that bridge temperatures decrease through the early-morning hours. Between 6:00 and 9:00, the girder begins its expansion outward, and makes a dramatic outward "sweep" between 9:00 and 12:00. The girder then reaches its maximum radial expansion
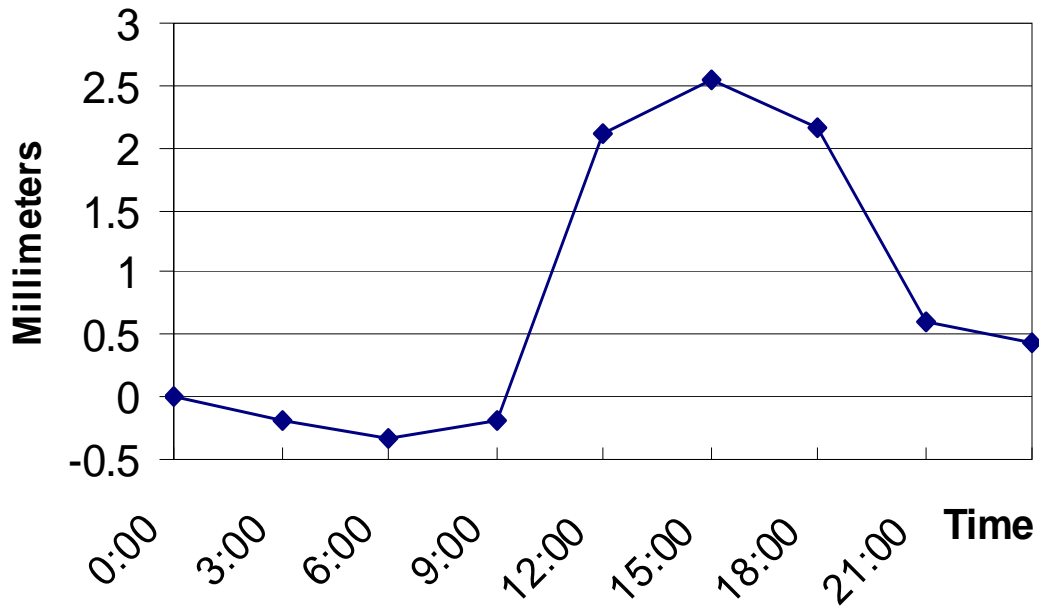
86

Figure 4.3 Transverse Displacements Of The Inner Girder On August 2, 1998
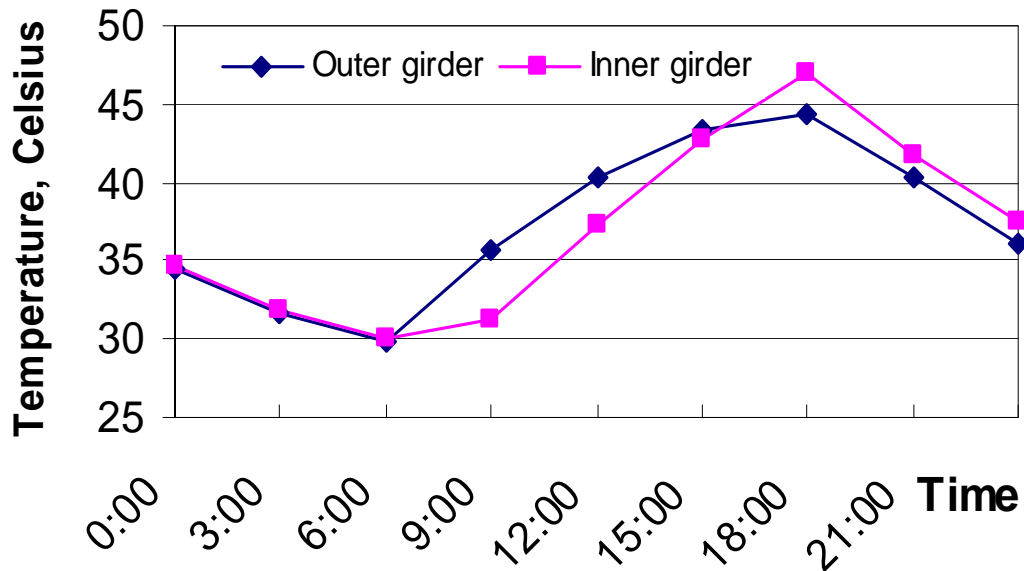

Figure 4.4 Mean Girder Temperatures On August 2, 1998

at 15:00. However, it is clear from Figure 4.4 that the girder's mean temperature does not maximize until 18:00, some three hours later. It is rather surprising that the girder's maximum radial expansion occurs three hours before the maximum temperature is reached, but this occurrence may be attributed to the outer girder's expansion. In Chapter 3, it was shown that, because it is exposed to the east, the outer girder heats sooner in the day than the inner girder, and also reaches its maximum mean temperature earlier. It will also be recalled that there are stiff diaphragms linking the girders at the piers. It is reasonable to conclude that, as the outer girder begins its expansion in the morning hours, it pulls the inner girder outward with it by means of the diaphragm. Later in the day, as the outer girder begins cooling, it begins contracting inward, pushing the inner girder with it. It is possible for the inner girder to achieve its maximum transverse displacements, even as its temperature is still rising. This phenomenon will be seen in future plots of transverse displacements, as well.

In addition to daily displacement cycles, the pot bearings are also expected to withstand accumulated displacements over time as the temperatures change through the seasons. These displacements will be examined next.

4.3   Long-Term Longitudinal Displacements

The study of accumulated longitudinal displacements is restricted to reported displacements of the inner girder at the end pier. Further, this study must be limited to those displacements occurring after the second site visit, as the potentiometer intended to record these displacements was originally wired to a defective multiplexer channel. However, the accumulated displacements after the second site visit are still useful, and insight into the bridge's longitudinal extension behavior will be ascertained from this data.   Further, because displacements in this bridge are governed by linear equations, displacements

occurring prior to the second site visit will be extrapolated from behavior after the second instrumentation period. Findings will then be compared to SAP 2000 analysis results in Chapter 5.

Shown in Figure 4.5 are measurements of the longitudinal displacement of the inner girder between July 3 and July 7. The "zero-displacement" datum is the bridge's position on July 3. Thus all accumulated longitudinal displacements presented in this section are relative to the girder's position on the first day shown here, July 3. The displacements shown in this chart closely follow girder temperature cycles shown in Figure 4.6. In particular, it is seen that the temperatures during the first cycle shown, July 3, plot as a relatively flat curve, indicating slight changes in temperature. The recorded displacements for the same time also plot as a relatively flat curve, indicating a good correspondence between temperature changes and induced displacements. It will also be noted that, immediately upon the warming that ends this cycle of nearly constant temperatures, the potentiometer records girder extensions. This potentiometer responsiveness is actually seen throughout this chart, as the potentiometer records expected changes in displacements practically simultaneously with temperature changes. Finally, it can be seen from the plotted temperatures that temperatures are steadily increasing during this period, and the potentiometer records steadily increasing girder extensions, reaching a maximum value of 12.7 millimeters on July 6. It will be seen in later plots that girder displacements continue to increase during increasing temperatures and decrease under decreasing temperatures.

Figure 4.7 shows accumulated longitudinal displacements for July 15-18, while Figure 4.8 shows mean girder temperatures for the same time. The measurements recorded during this period will be compared to analytical displacement predictions in Chapter 5.
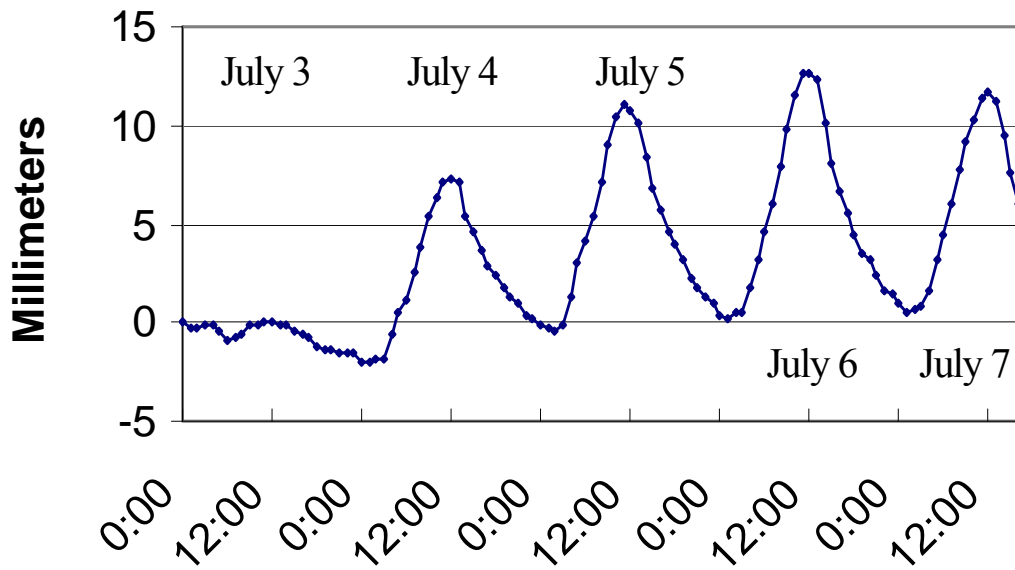
Figure 4.5 Longitudinal Displacements Of The Inner Girder, July 3-7, 1998
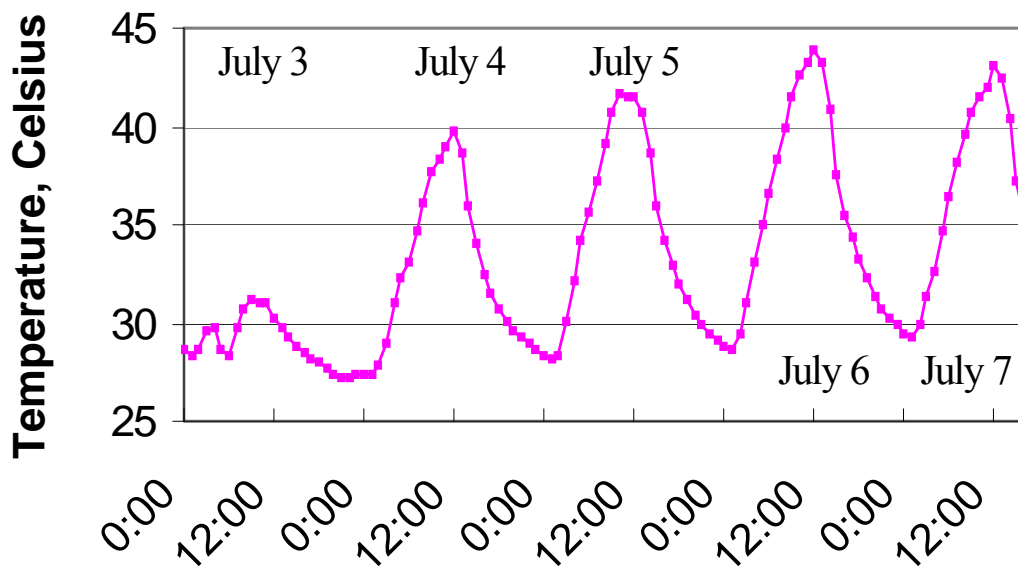

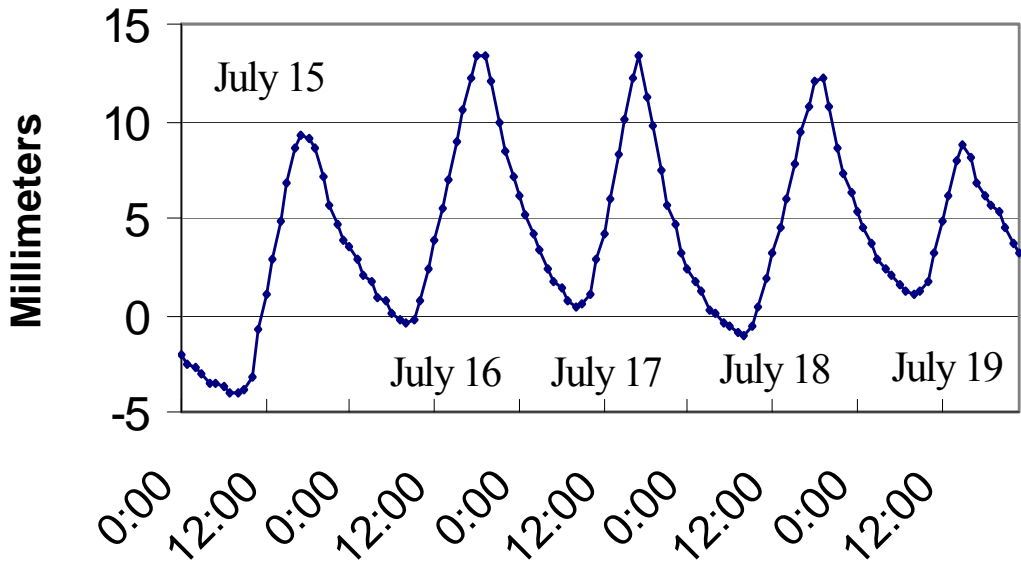**Figure 4.6 Mean Inner Girder Temperatures, July 3-7, 1998**

Figure 4.7 Longitudinal Displacements Of The Inner Girder, July 15-19, 1998
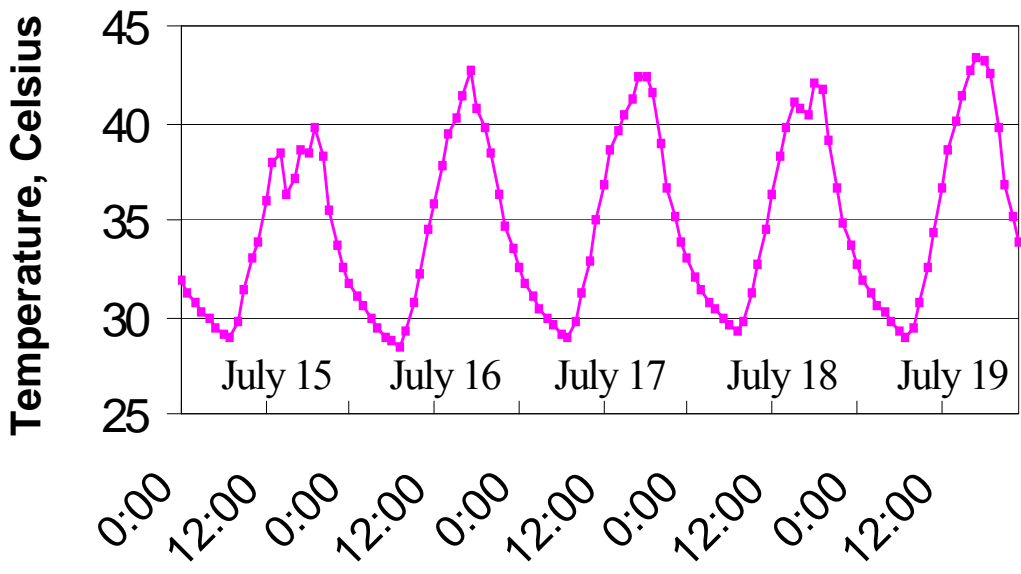

Figure 4.8 Mean Inner Girder Temperatures, July 15-19, 1998

It is seen that the increasing displacements associated with increasing temperatures observed previously for this same time are seen again here. The girder begins this cycle in a position contracted two millimeters from its position at the start of July, as cooler temperatures have occurred just prior to the times plotted here. It is seen again here that the potentiometer is functioning well, recording maximum displacements of 13.4 millimeters relative to July 3. Displacement trends also correlate well with temperature trends shown here.

Shown in Figures 4.9 and 4.10 are accumulated longitudinal displacements and the girder temperatures, respectively, for August 2-7. These graphs are included here to illustrate how positive (extensional) displacements accumulate over time and then decrease, eventually reaching negative values. The girder reaches a maximum displaced position during the first cycle shown of 16.1 millimeters, and a cooling trend then starts. The girder steadily shortens, with its peak extensional displacement decreasing each day. The girder then reaches negative values of displacement at the end of the fourth cycle shown, indicating that, at this time, the girder is slightly shorter than it was on July 3. The girder continues its shortening during the next cycle plotted, reaching a peak extension of only 1.3 millimeters.

It will be recalled from Chapter 3 that the warmest day of the instrumentation period, in terms of EMBT, was August 2. This is the first cycle plotted here, and is the day of maximum girder extension. This is also the maximum girder extension observed thus far. It is also important to keep in mind that these displacements are referenced to the bridge's position on July 3, so that this extension has occurred over one month, not several. Because the only reliable total longitudinal displacements were obtained after July 3, minimum (maximum contraction) displacement records were not obtained. However, as will be shown shortly, it is still possible to extrapolate backward in time to garner an idea of
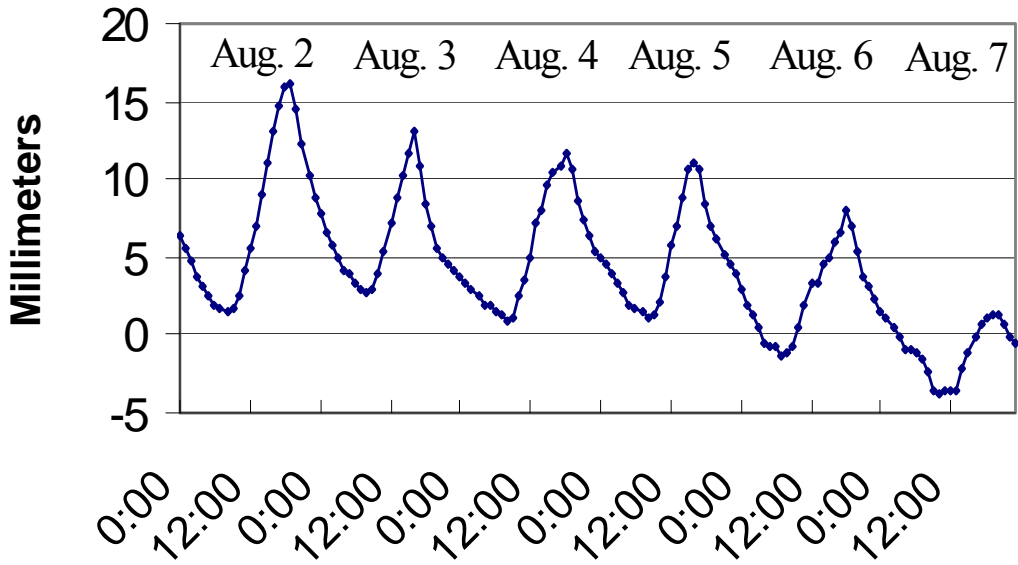
Figure 4.9 Longitudinal Displacements Of The Inner Girder, August 2-7, 1998
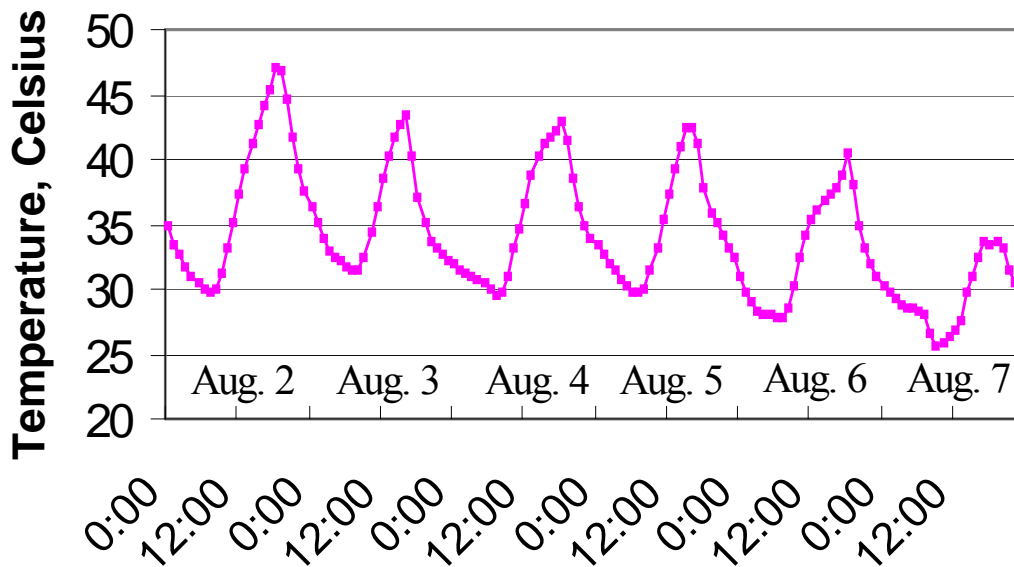

Figure 4.10 Mean Inner Girder Temperatures, August 2-7, 1998

what displacements would have recorded had the potentiometer been functioning properly for the duration of the study.

Finally, Figure 4.11 shows accumulated longitudinal displacements for October 8-14, while Figure 4.12 shows the girder temperatures for the same time period. It is clear from this plot that decreasing temperatures have led to the girder spending most of the time shown here in a negative (compressed) position, relative to its position on July 3, with positive displacements only occurring during peak temperatures. This is to be expected, as this plot is for a period in October after temperatures have dropped somewhat, and this conclusion is confirmed upon comparison of the temperatures shown here with the temperatures shown in plots for July and August. It is also important to note that the girder is returning to its original (July 3) position over time, and compressing further during times of low temperature. It is clear from this plot that, at times of high temperature, the girder spends much of the plotted time near its original (zero displacement) position, and, during times of low temperature, the girder is in a compressed state. This is to be expected, as temperatures are seen to be lower than they were in July.

4.3.1   Summary of Long-Term Longitudinal Displacements

It has been shown that the potentiometer measuring longitudinal displacements of the inner girder at the end pier measured appreciable accumulation of longitudinal displacements. It was seen that the recorded displacements mimicked temperature cycles well and was able to record significant ranges of displacements. It was also seen that positive girder displacements (extensions) accumulated through July and August as temperatures rose, and displacements reached negative values (contracted states of the girder) as temperatures cooled.
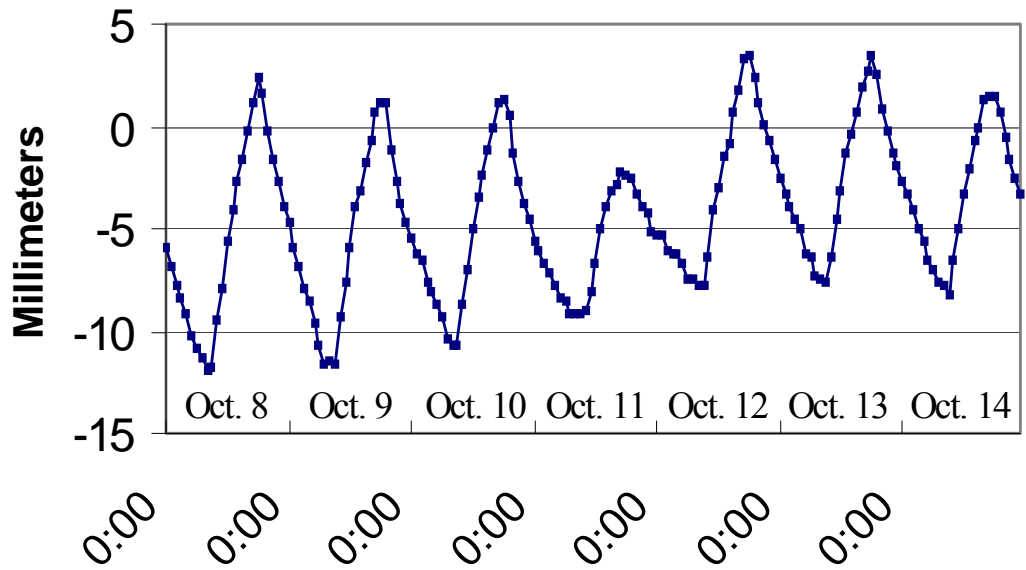
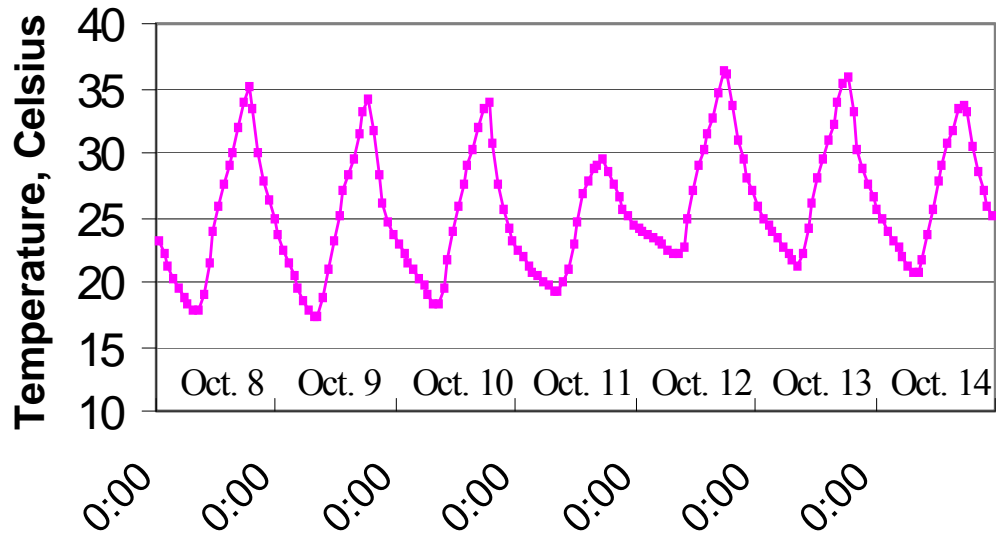**Figure 4.11 Longitudinal Displacements Of The Inner Girder, October 8-14, 1998**

Figure 4.12 Mean Inner Girder Temperatures, October 8-14, 1998

However, it is of the utmost importance in this study to examine extreme displacements and displacement ranges, as well. Because this study concerns long-term displacements and rotations as they occur at the bearings, a prime concern is the maximum absolute displacements which are observed to occur.

Because the potentiometer used to measure longitudinal translations was wired to a defective multiplexer channel prior to the second site visit, some extrapolation was necessary to determine translations which should have occurred prior to the second site visit. It was shown in Figure 4.5 that, immediately after the second site visit, during the first several days of July, the potentiometer used to record these displacements appeared to function very well, with every nuance of the temperature cycles reflected in the displacement curve. Using the values in this plot, a measured longitudinal displacement of 0.94 millimeters per degree Celsius change of the mean inner girder temperature was calculated. This was computed as the mean of the value $\Delta_{Disp}/\Delta_{Temp}$ where the changes in displacement and temperature are the differences between the extreme values of the respective quantities for each day. These values were calculated for the first seven days after the second site visit. Values are tabulated in Table 4.1, and the mean value of 0.94 mm/°C was used in the predictions.

Table 4.1 Values Used To Estimate Longitudinal Displacements Prior To The Second Site Visit

Date	$\Delta_{Disp.}$	$\Delta_{Temp.}$	$\Delta_{Disp.}/\Delta_{Temp.}$
July 3	10.38 mm	12.51 ℃	0.83 mm/℃
July 4	11.69 mm	13.14 ℃	0.89 mm/℃
July 5	13.37 mm	15.19 ℃	0.88 mm/℃
July 6	12.61 mm	13.56 ℃	0.93 mm/℃
July 7	13.34 mm	11.81 ℃	1.13 mm/℃
July 8	13.82 mm	14.20 ℃	0.97 mm/℃
July 9	12.84 mm	13.46 ℃	0.95 mm/℃

Using this factor, the temperature records for each month were examined, maximum and minimum temperatures were located, and the factor 0.94 mm/°C was multiplied by the differences between the maximum and minimum temperatures and the temperature at the outset of valid longitudinal displacement measurements. The mean inner girder temperature at the start of valid data collection was the temperature datum used. For example, suppose that, in a given month, the maximum temperature the inner girder reached was 40°C, and the minimum was 20°C. The mean inner girder temperature at the start of valid displacement measurements was 28.7°C. The maximum displacement that could be expected during the month, relative to the girder's position at the start of valid measurements, is 0.94(40-28.7)=10.6 millimeters. Also, the minimum displacement that could be expected, relative to the girder's position at the start of the valid data, is 0.94(20-28.7)=-8.2 millimeters. In this manner, expected longitudinal displacements have been extrapolated to include times under which the instrumentation failed. These values have been calculated under the assumption that the potentiometer would function in the early months of

instrumentation as well as it did immediately after the second site visit. Of course, the potentiometer collects residue with time and could not be expected to function this well over long periods of time, and friction in the bearings is unpredictable as well, but these displacements are those which could be expected under ideal conditions. Results are shown in Table 4.2. The estimation was performed for the months February-June, with reliable measurements listed for other months. It will be recalled from Chapter 2 that the potentiometer measuring these deformations became "stuck" in November, thus, the tabulated values are not reliable measurements of the extreme displacements experienced during that month.

Table 4.2 Extreme Longitudinal Displacements With Respect to July 3.

Month	Maximum Temperature	Minimum Temperature	Maximum Displacement	Minimum Displacement
February	25.3 °C	3.9 °C	-3.2 mm[*]	-23.3 mm[*]
March	33.5 °C	3.8 °C	4.5 mm[*]	-23.4 mm[*]
April	37.7 °C	13.3 °C	8.5 mm[*]	-14.5 mm[*]
May	44.4 °C	19.5 °C	14.8 mm[*]	-8.6 mm[*]
June	44.3 °C	21.8 °C	14.7 mm[*]	-6.5 mm[*]
July	46.0 °C	26.9 °C	16.3 mm	-1.7 mm
August	47.0 °C	24.6 °C	17.2 mm	-3.9 mm
September	42.2 °C	23.3 °C	12.7 mm	-5.1 mm
October	39.1 °C	12.1 °C	9.8 mm	-15.6 mm
November	38.9 °C	11.3 °C	-3.5 mm	-10.3 mm

*Extrapolated from valid data.

The displacements increase to a peak in August as temperatures are higher than they are in July, and displacements decrease into the autumn months, as temperatures cool.

In order to validate this method of extrapolating displacements from valid data, longitudinal displacements for the first four days of August were computed based on this method, and are plotted in Figure 4.13, along with measured longitudinal displacements. The datum is the bridge's position at 0:00 on August 1. In this curve, the smooth line is the estimation, while the line with markers is the measurement. It is clear from this plot that the method of extrapolating displacements is reasonable. No such method would yield results which exactly match measured displacements, but these estimated displacements are reasonably accurate, and lend credibility to the values presented in Table 4.2. Measurements of long-term transverse displacements will be presented next.
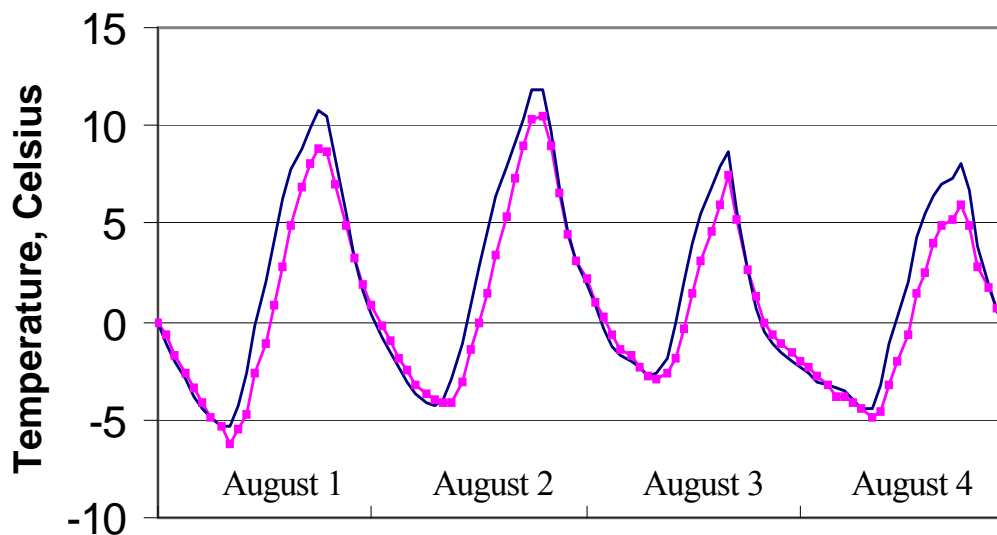
Figure 4.13 Measured And Estimated Longitudinal Displacements Of The Inner Girder, August 1-4, 1998

4.4   Long-Term Transverse Displacements

The potentiometer measuring lateral displacements of the inner girder behaved well throughout the duration of this study. It almost always recorded smooth, sinusoidal displacement patterns, in sharp contrast to the malfunctioning potentiometers. Displacement differences between the measured and predicted values are inevitably present, but the cyclic nature of the measured displacements is what could reasonably be expected to occur under thermal loading. In order to determine long-term recorded displacements, spreadsheets were used which would read the current potentiometer voltage, subtract the initial potentiometer voltage from the current voltage, and multiply this quantity by the potentiometer calibration. The resulting quantity is then the current displacement with respect to the potentiometer's initial position. The "initial" potentiometer voltage used was the value at the end of the first week of instrumentation, i.e., the voltage at the end of February 7, 1998. Several plots will now be examined, in order to gain insight into the girder's accumulated transverse displacements over time.

Shown in Figures 4.14 and 4.15 are the accumulated transverse displacements for March 24-28 and the mean inner girder temperatures for the same time period. Upon examination of this graph, it appears that the girder "locks up" during the early hours of March 27, and "snaps free" during March 28. It can be seen that the girder's displacement cycles continue to follow a sinusoidal curve, with maximum peak displacements decreasing during the second and third cycles as maximum peak temperatures decrease, as well. However, it is seen that during March 28 the minimum peak displacement is substantially greater (in absolute value) than the minimum for the previous day. This is unexpected, as the minimum temperatures on March 28 are slightly higher than they are on March 27. This indicates that minimum displacements are not being allowed to occur freely during the third cycle. The girder then makes a two-millimeter "sweep"

outward as temperatures increase on the next cycle and displacements are then relatively free to occur.

It is also interesting to note that the girder spends almost all of the plotted cycles at negative displacements, indicating that it has moved radially inward relative to its position during the first site visit. This is in agreement with the fact that the coldest day of the data collection period, in terms of EMBT, was March 10, less than two weeks before the period shown (see Chapter 3). The relatively low temperatures experienced at the bridge site during March led to the bridge maintaining positions near that at the time of instrumentation during daily high temperatures and moving inward at times of low temperatures, as shown here.
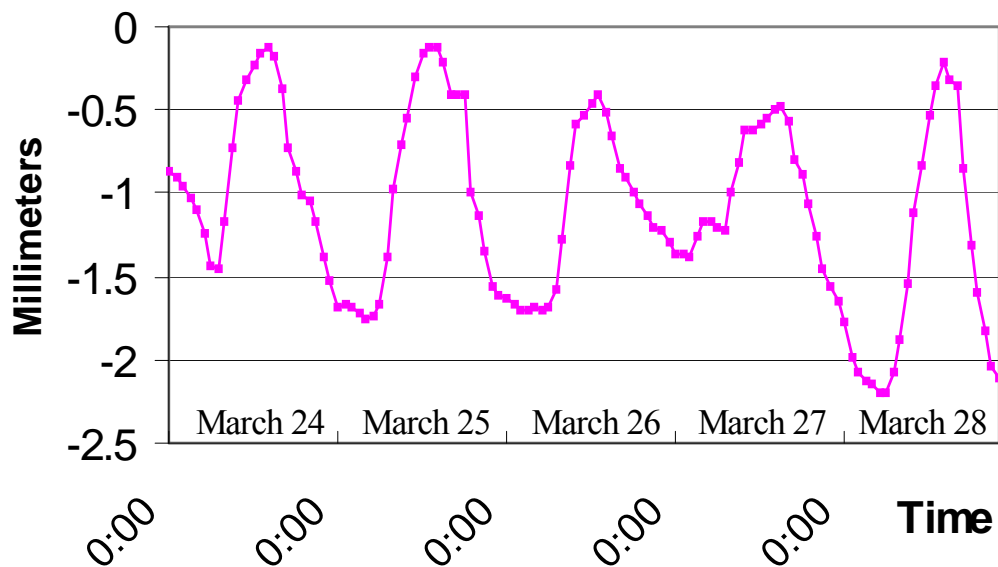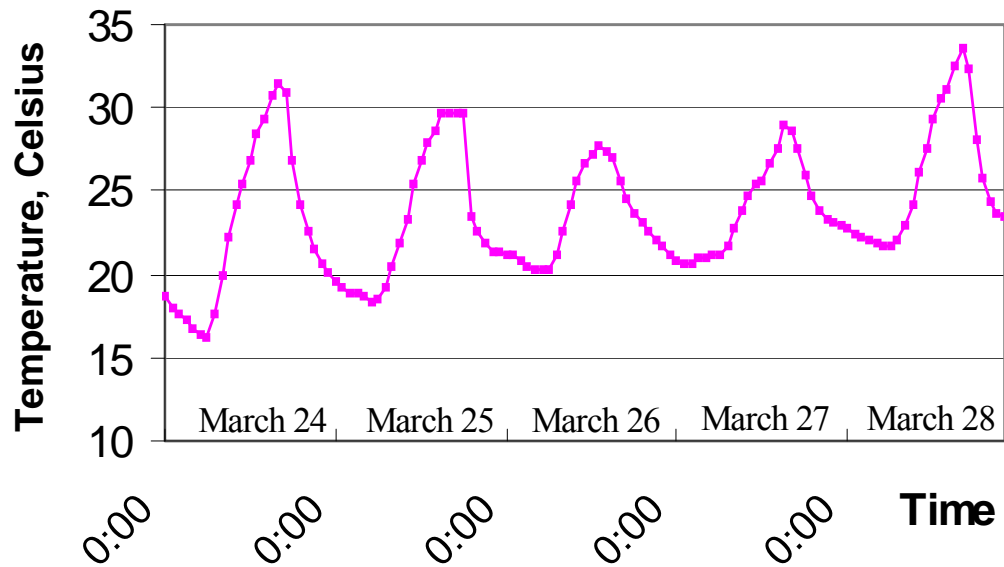

Figure 4.14 Transverse Displacements Of The Inner Girder, March 24-28, 1998

Figure 4.15 Mean Inner Girder Temperatures, March 24-28, 1998

Figures 4.16 and 4.17 show accumulated displacement cycles for May 11-14 and the inner girder temperatures for the same time period. This plot illustrates three characteristics of interest. First, it is again seen that peak maximum displacements usually precede peak high temperatures, as has been seen before. Next, it is seen that the girder again appears to be impeded when it is contracting laterally during times of low temperature. This occurs at the beginning of the first cycle shown and during the times of low temperature of the second cycle. It is seen during these two cycles that the girder is contracting laterally and suddenly stops, even as temperatures continue to decrease. However, this does not occur during the second two cycles shown. It appears that the girder was allowed to move freely during these days, and minimum displacements were achieved practically simultaneously with minimum temperatures.

Finally, these plots show that the girder's lateral position in space is steadily increasing in an outward direction with respect to its initial position. This is concluded from the fact that the girder is spending most of the time shown at a position of positive displacement, and only returns to negative values during times of overnight low temperatures. This is to be expected, as temperatures increase significantly between February and May. Relatively warmer temperatures lead the girder to spend more time in an expanded position relative to its initial position.

Figures 4.18 and 4.19 show total displacements and girder temperatures for June 8-14. This plot is included here to illustrate what displacements may be measured when there appear to be no restrictions on the girder's movement, and the potentiometer is functioning well. This graph shows the largest displacement "sweeps" seen thus far, as there is a maximum range of nearly 3 millimeters recorded during the sixth cycle shown. Maximum displacement peaks are again seen to slightly precede high temperature peaks, while minimum displacement peaks are nearly synchronous with minimum temperatures. It is also seen again that the girder is spending more time in an expanded position, with negative displacements occurring only during low temperature periods.
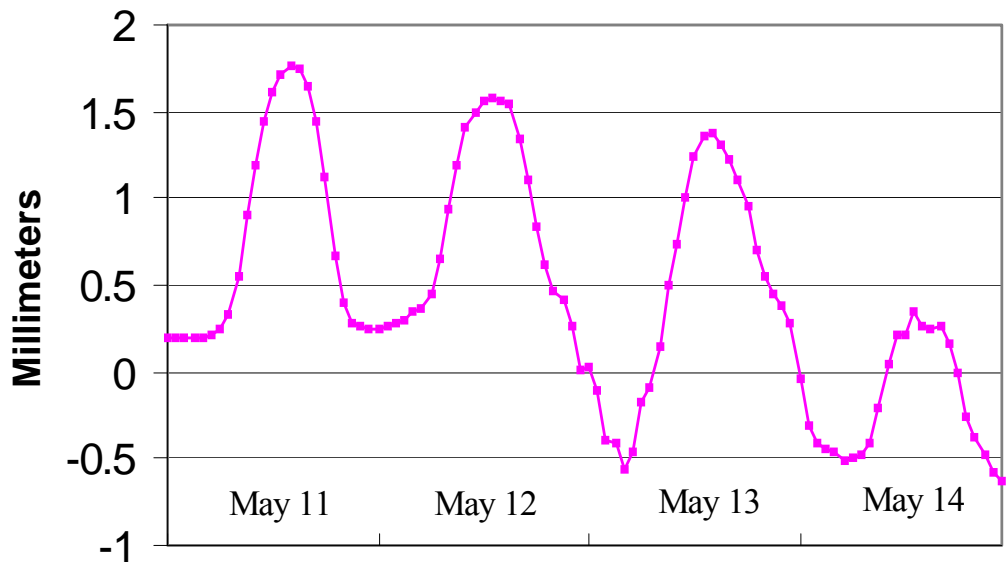
Figure 4.16 Transverse Displacements Of The Inner Girder, May 11-14, 1998
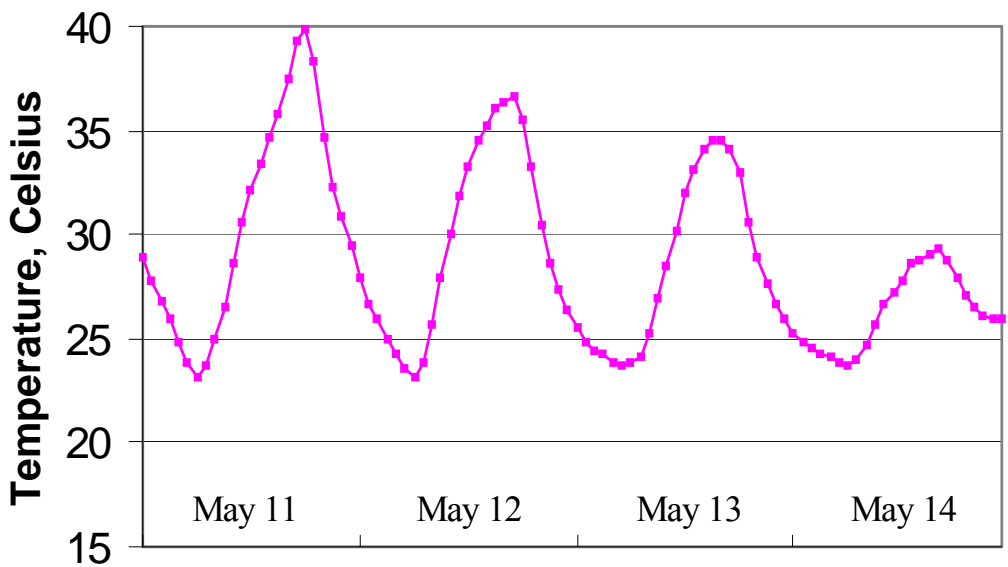

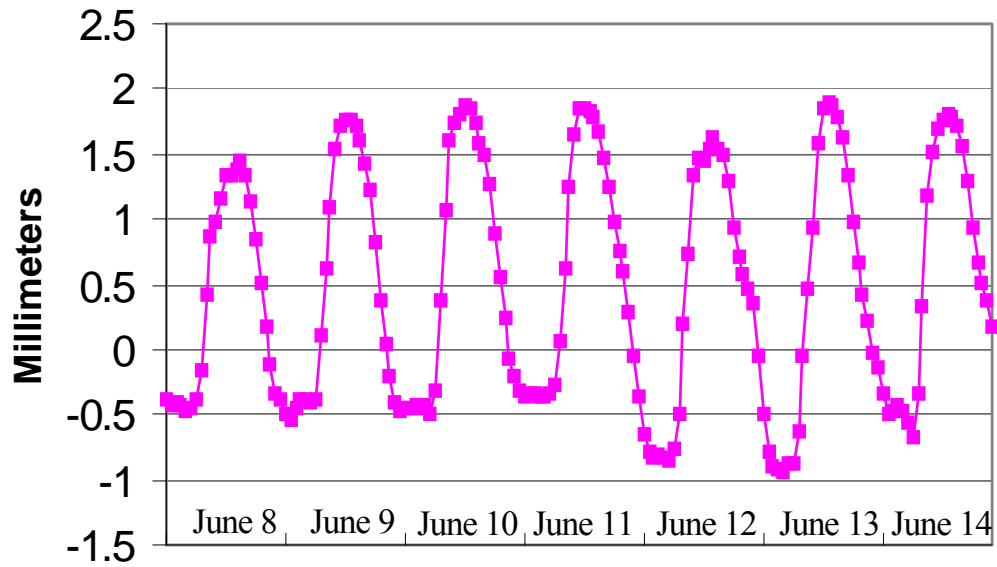**Figure 4.17 Mean Inner Girder Temperatures, May 11-14, 1998**

Figure 4.18 Transverse Displacements Of The Inner Girder, June 8-14, 1998
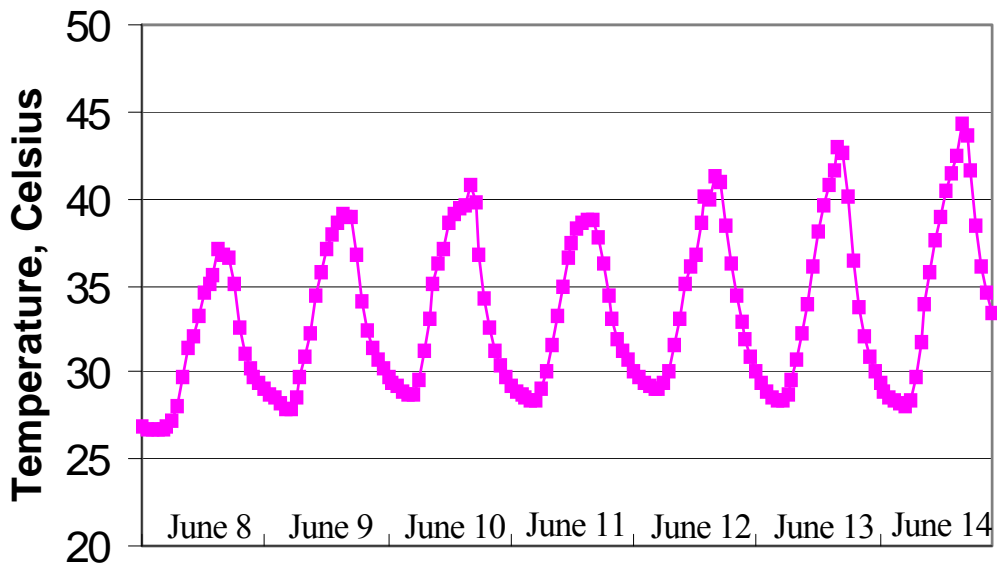

Figure 4.19 Mean Inner Girder Temperatures, June 8-14, 1998

Shown in Figures 4.20 and 4.21 are accumulated transverse displacements and girder temperatures for July 22-24. This is included here to indicate that, over this time period, the temperatures are sufficiently warmer than the temperatures at the time of instrumentation that the girder is now accumulating significantly larger displacements in the outward direction than it has at any time thus far. It is seen that, during the third cycle shown, the girder reaches a maximum peak displacement of nearly 5.6 millimeters after expanding from a minimum peak displacement of some 2.5 millimeters on the previous cycle. It also appears that there is some degree of "locking" of the bridge's movement in this direction during the second cycle shown. Cursory examination of this chart shows that the peak maximum displacement during the third cycle shown is approximately 0.6 millimeter larger than the previous peak, even though high temperatures are nearly the same for the two cycles. It seems that, during the third cycle, the girder's movement is relatively unrestricted relative to its motions during the previous cycle, and the girder thus attains slightly larger peak displacements. This plot shows that this phenomenon is not limited to cool or moderate temperatures, but also occurs during relatively warm periods.

Figures 4.22 and 4.23 illustrate the accumulated transverse displacements and girder temperature cycles for September 15-17. While the behaviors shown in this plot have been seen before, it is interesting to note that temperatures are slightly cooler than their values shown in Figure 4.19 for July 22-24, and, as a result, displacement magnitudes are starting to decrease. This indicates that the girder is beginning to move back to a position near its position at the time of instrumentation. All displacements are still in an outward radial position relative to the girder's initial position, but these displacements are decreasing, and

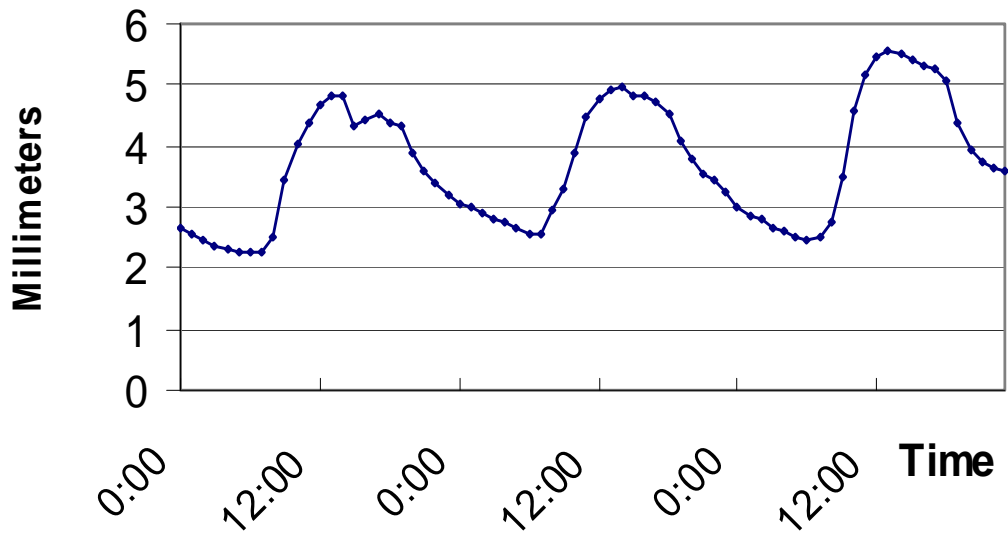**Figure 4.20 Transverse Displacements Of The Inner Girder, July 22-24, 1998**
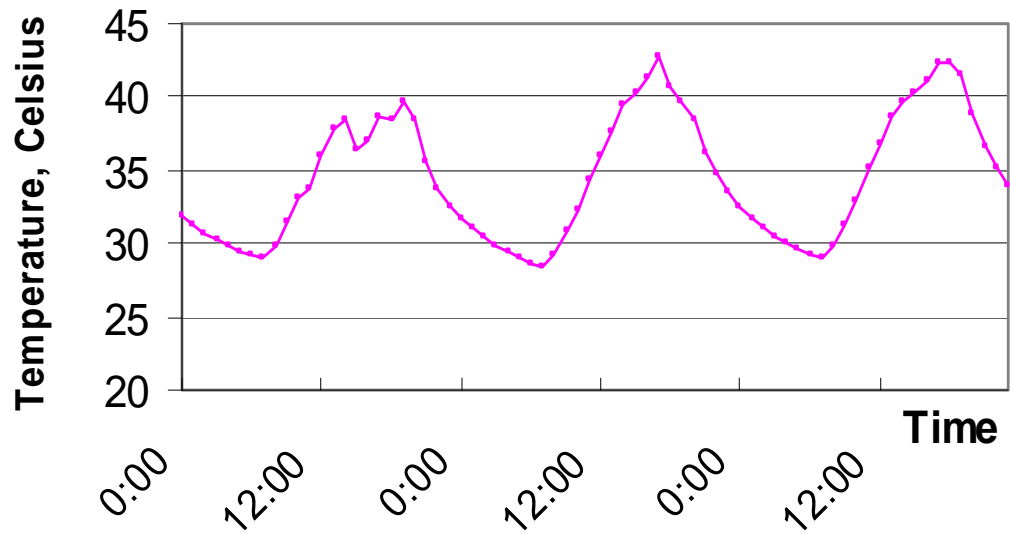

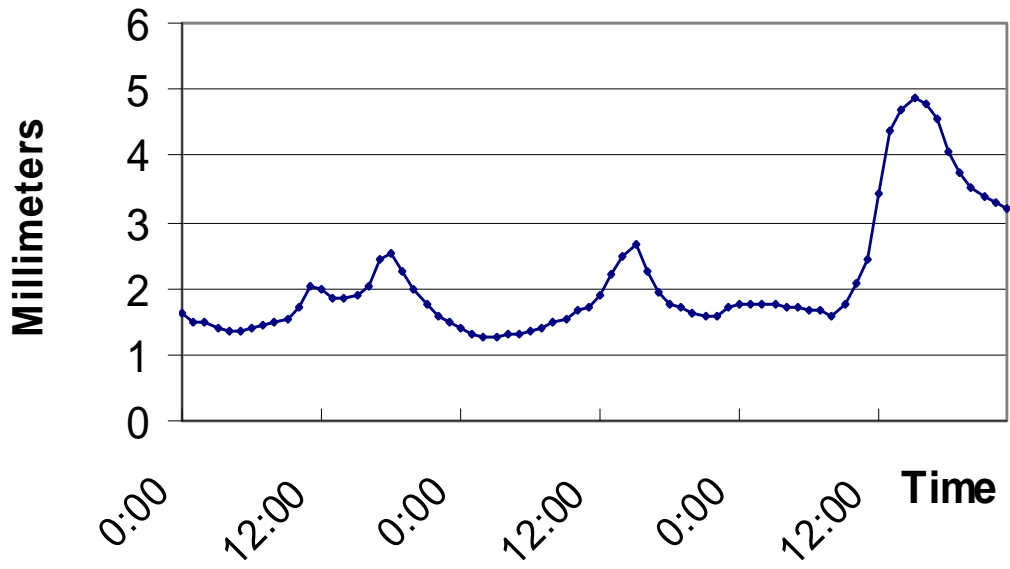**Figure 4.21 Mean Inner Girder Temperatures, July 22-24, 1998**

107

Figure 4.22 Transverse Displacements Of The Inner Girder, September 15-17, 1998
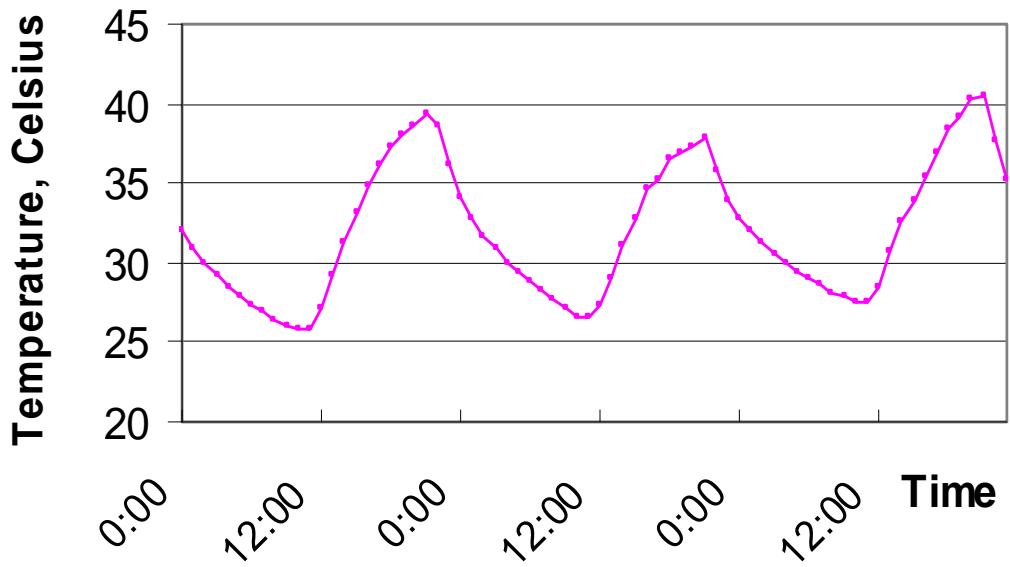

Figure 4.23 Mean Inner Girder Temperatures, September 15-17, 1998

minimum displacements are seen to be as small as 1.3 millimeters during the period shown. It is seen that the same "locking" phenomenon seen several times before occurs again during the first and second cycles shown in Figure 4.20. When displacements become uninhibited during the third cycle shown, the girder reaches a maximum displacement some 2 millimeters larger than its peak during the second cycle, even though the high temperature during the third cycle is less than three Celsius degrees warmer than the high during the second cycle.

4.4.1   Summary of Observed Transverse Displacements

Having examined cumulative transverse displacements for a period of several months following the time of instrumentation, some conclusions may now be drawn on the observed transverse displacement behavior of the bridge.

First, it has been shown that, near the time of displacement instrumentation, the total displacements are seen to oscillate about the initial position of the bridge, and displacements are quite small. This is explained by consideration of the fact that the daily temperature cycles do not vary greatly on a day-to-day basis, and it takes some time for thermal cycles to change appreciably from those at the time of instrumentation. Because these thermal cycles are what induce girder translations, the girder also takes a significant amount of time to "move away" from its initial position.

Second, it has been seen that the girder often appears to encounter frictional forces, restraining it from moving completely freely. When the girder overcomes these constraints, recorded displacements show a "slip," during which time the girder will move significantly larger amounts than it had been moving prior to overcoming the friction. Perhaps the best example of this was seen to occur in the plot of the girder's behavior for the period March 24-28. On this graph, it was apparent that the girder was struggling to achieve its minimum displacement, i.e.,

its position of greatest contraction relative to its position during the instrumentation installation. When the girder was finally allowed to move more freely, it made a relatively large sweep in position, during the fifth cycle shown. This leads to the conclusion that, even when sliding surfaces are used in conjunction with the pot bearings, there is still some amount of friction present in the girder-bearing system. However, the possibility that the sweeping motion of the potentiometer shaft was impeded in some way at various times during the study cannot be discounted. As described earlier, dust and moisture appear to be the causes of the malfunctioning of the potentiometers in use at the outer girder, and it is possible that the potentiometers which function reasonably well may encounter the same difficulties at times. This possibility is difficult to confirm or refute, however, and would have to be examined under more controlled conditions than this study permits. However, even though it is impossible to discern whether the observed inhibitions on recorded displacements were due to friction in the system or problems with the potentiometers, it has been seen that the "locking" behavior will be overcome with time. At all times there appeared to be restrictions on the reported displacement peaks, these restrictions were soon overcome and the displacements were then allowed to occur more freely.

Next, it was seen that the potentiometer responded rather quickly to significant temperature increases, and mimicked relatively flat temperature cycles well. It was also able to record relatively large "sweeps" in displacements when there appeared to be no inhibitions present in the system.

It was also seen that, as the bridge enters the warmer late spring and summer months, its accumulated transverse displacement steadily increases outward from its original position. This was ascertained from the fact that plots presented for these times show girder displacements at increasingly positive values, with negative values occurring only during overnight low temperatures. This will also be seen in Table 4.3. The girder's position was seen to oscillate about its initial

position in the cooler months, but, as the temperatures warmed, the cumulative displacements were seen to increase several millimeters radially outward, and the girder did not typically return to its initial position during periods of low temperature. This is to be expected, as warmer temperatures lead to larger transverse displacements, while the low temperatures in the warmer months are not as low as those in February, thus allowing the bridge to contract to a position still outward from its initial location. Conversely, it was seen that, as temperatures began to decrease in September, cumulative displacements started to decrease in magnitude, as the girder began to move back toward its initial position. It was seen in Figure 4.22 that minimum displacements returned to values near two millimeters outward from the original position of the bridge, thus indicating that outward displacements were decreasing.

Finally, it was shown that, at several times, the girder's peak maximum displacement was achieved at times prior to the time of peak high temperature. This was not always the case, but it is an interesting occurrence, nonetheless. As described earlier, this seems to indicate that as the outer girder's temperature increases in the mid-morning hours, it expands outward, pulling the inner girder with it. The inner girder thus shows significant displacements, even as the temperature is still increasing. Under the influence of the location of the afternoon sun and the layout of the bridge, as described in Chapter 3, the inner girder, at times, continued to translate radially outward, but often reached its peak displacement before high temperatures peaked. The lack of additional outward movement frequently observed may be attributed to the frictional restraining forces described earlier, and to the fact that the outer girder begins cooling and contracting inward before the inner girder does. It was hypothesized earlier that the inner girder may thus restrain additional outward displacement of the inner girder and possibly begin to force it inward, even as the inner girder is still warming. Because cumulative displacements are of importance, monthly

maximum and minimum displacements are tabulated in Table 4.3. Maximum and minimum temperatures shown are those of the girder mean temperature.

Table 4.3 Monthly Extreme Temperatures And Transverse Displacements With Respect To July 3.

Month	Maximum Temperature	Minimum Temperature	Maximum Displacement	Minimum Displacement
February	25.3° C	3.9° C	0.4 mm	-1.0 mm
March	33.5º C	3.8º C	2.3 mm	-2.2 mm
April	37.7º C	13.3º C	2.6 mm	-1.9 mm
May	44.4º C	19.5º C	1.8 mm	-2.0 mm
June	44.3º C	21.8º C	3.3 mm	-1.5 mm
July	46.0º C	26.9º C	5.6 mm	-0.5 mm
August	47.0º C	24.6º C	6.4 mm	-0.1 mm
September	42.2º C	23.3º C	5.2 mm	0.3 mm
October	39.1º C	12.1º C	6.3 mm	0.8 mm
November	30.7 ºC	11.3 ºC	4.7 mm	0.4 mm
December	25.6 ºC	9.3 ºC	1.7 mm	-0.3 mm

It should be noted that the minimum tabulated displacement for August, -0.1 mm, was an inward "slip" in the displacement data. The nearest minimum displacement which followed displacement trends was 0.6 mm. Also, it should be noted that the relatively large outward displacements for October occurred during a relatively warm period at the beginning of the month. As seen in Figure 4.22, typical displacement values during this period, as temperatures are cooling, are somewhat smaller than these values.

4.5 Long-Term Bridge Positions

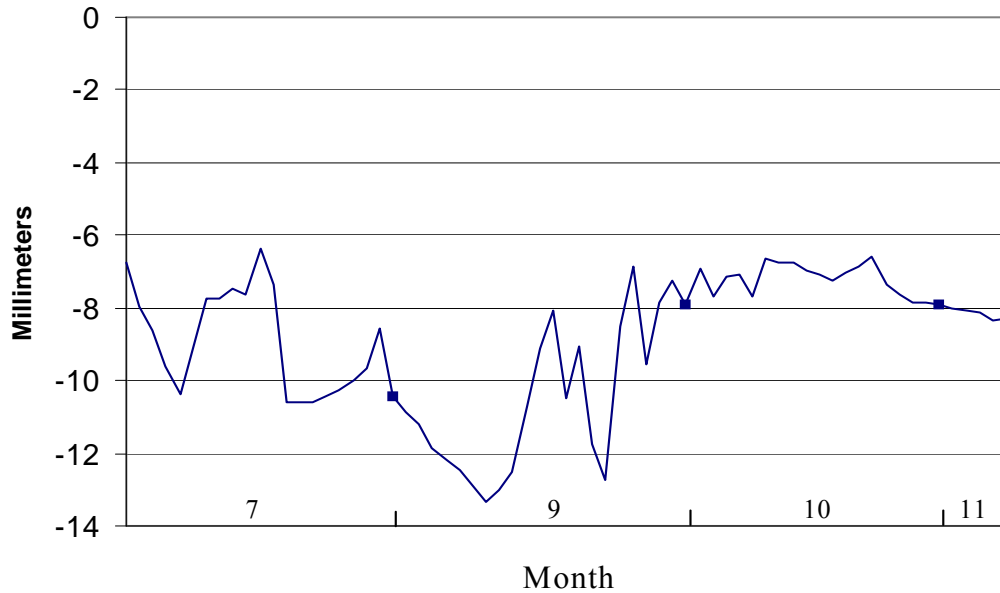### 4.5.1 Girder Positions At A Constant Temperature

Regardless of the temperature at the time of the setting of the bridge bearings, the bridge position should be constant over time at a given temperature. This is what would occur if the system were frictionless. However, it has been shown that this is not a perfect system. Friction is inevitably present in the bearings, and measured displacements typically do not exactly match theoretical values. Also, it is impossible to ascertain at any given time whether the mismatch is due to potentiometer error, friction in the bearings, or a combination of both.

Nonetheless, it is of interest to examine bridge positions at a given temperature over time to determine whether the bridge position is in fact nearly constant at a given temperature. Shown in Figure 4.24 is a plot of the inner girder's position with respect to transverse displacements at a mean girder temperature range of 19.5-20.5°C. The one-degree range was used because girder mean temperatures are typically not going to reach precise values of desired temperatures. The numbers on the horizontal axis refer to months of the year, with February taken as "2." The small boxes on the chart indicate the start of the next month in the sequence. These displacements are taken relative to the girder's position at the end of the first week of instrumentation, February 7, 1998. It is immediately obvious that there is some degree of scatter in the system and that the girder's position laterally is not in fact constant. In fact, there is a range in its position of approximately six millimeters. As the total range of recorded transverse displacements was nearly nine millimeters over the entire range of temperatures during the instrumentation, this is a relatively large range of bridge positions at a constant temperature.

Shown in Figure 4.25 is a plot of the inner girder's position with respect to longitudinal displacements at the same temperature, 20°C. These positions are relative to the girder's position at the start of valid longitudinal displacements, July 3. Numbers on the horizontal axis again refer to months and the small symbols on the chart indicate the start of the next month in the sequence. It is seen again here that there is a broad range of girder positions at a constant temperature.   The range of girder positions shown here is nearly seven millimeters. While this is a smaller percentage of the total range of longitudinal girder positions recorded than the range of transverse positions shown in Figure 4.24, this is still significant.   This is further indication that the system is not perfect, and that the girders will not necessarily return to a constant position over time at a given temperature.
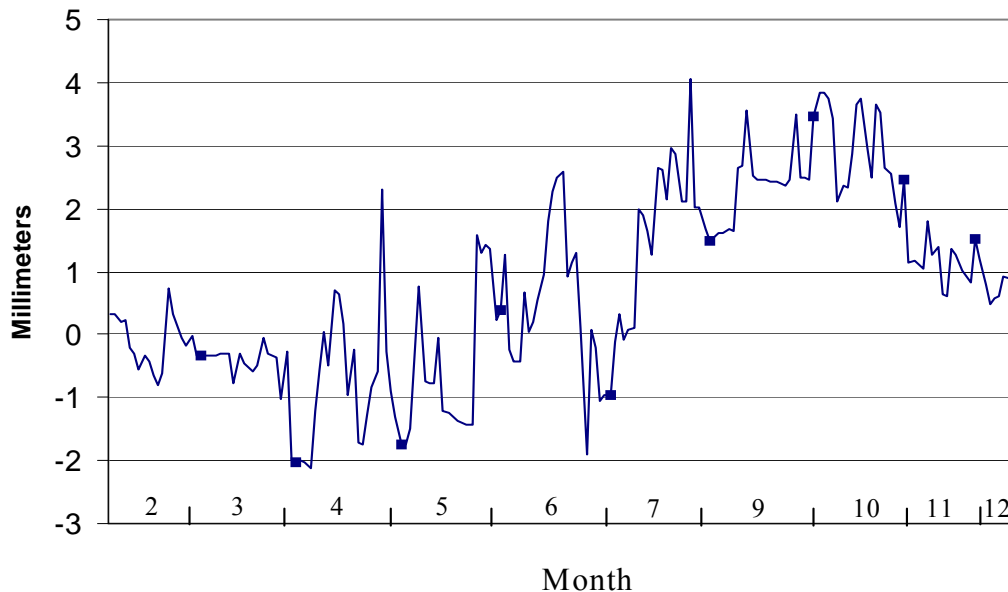
Figure 4.24 Transverse Girder Displacements At A Mean Temperature of 19.5-20.5º C, Relative To The Girder's Initial Position

Figure 4.25 Longitudinal Girder Displacements At A Mean Temperature Of 19.5-20.5 C, Relative To The Girder's Position On July 3

4.5.2 Displacement Histories

It is also of interest to determine whether the girders will "return" to their relative initial positions over time. If the instrumentation indicates that the girder displacements continually increase (or decrease) it is clear that there is a problem with the instrumentation. Otherwise, the girders would eventually slide off the bearings.

Shown in Figure 4.26 is a plot of the history of transverse displacements of the inner girder and in Figure 4.27 are shown the mean inner girder temperatures for the same period. It is clearly seen in this plot that girder displacements increase through the warmer months of the year, and then decrease into the cooler
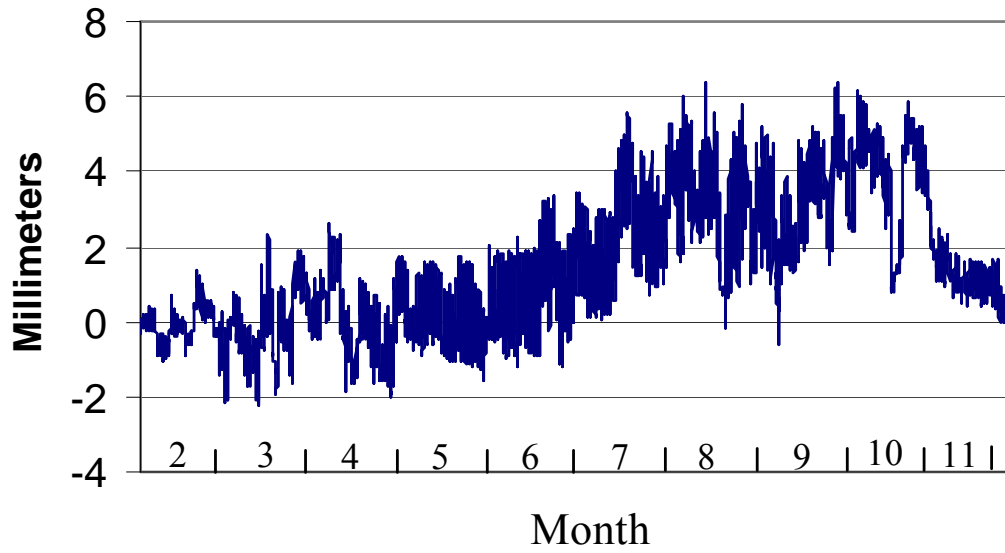
Figure 4.26 Transverse Displacement History
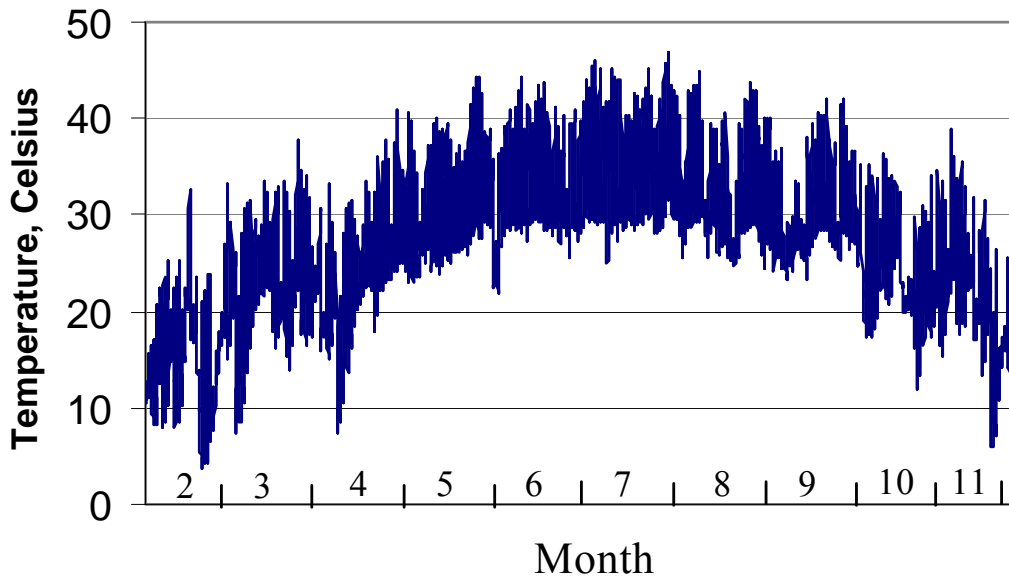
Figure 4.27 Inner Girder Mean Temperature (Determined By Thermocouples In Contact With Structural Steel) History

months, eventually returning to values near that at the time of initial instrumentation. The numbers on the horizontal axis again refer to months. It is also interesting to note that it appears that the girder takes a period of several months to attain appreciable values of displacement. This was seen earlier, when it was shown that, for a period of time following the instrumentation installation, the girder tends to oscillate laterally about its initial position. Finally, it is seen that girder mean temperatures have been cooling for a significant period of time before the girder begins its return to its original position, but that the girder does in fact return.

Shown in Figure 4.28 is the total longitudinal displacement history of the inner girder at the end pier and in Figure 4.29 are shown the mean inner girder temperatures for the same period. This curve extends from the start of July to early November, as it was described in Chapter 2 that the potentiometer used to make these measurements became "stuck" in November. Nevertheless, the curves shown here show a very good correlation between displacement and temperature trends, and show that, with respect to longitudinal displacements, the girder returns to its original position over time, as well. In fact, it can be seen that, before the potentiometer failed, the girder had already reached negative values of displacement, indicating that the girder was compressed relative to its state in July. This is naturally to be expected, as temperatures are significantly cooler in November than they are in July.

Finally, it was desired to ascertain whether there appears to be any clear correlation between transverse and longitudinal displacements of the girder. To this end, plotted in Figure 4.30 are displacement histories in both directions from July to November, when the longitudinally-oriented potentiometer failed. Although both quantities increase in warmer months and decrease in cooler months, there appears to be no correlation between the quantities. It is clear,

however, that both quantities increase in warmer months and decrease in cooler months.
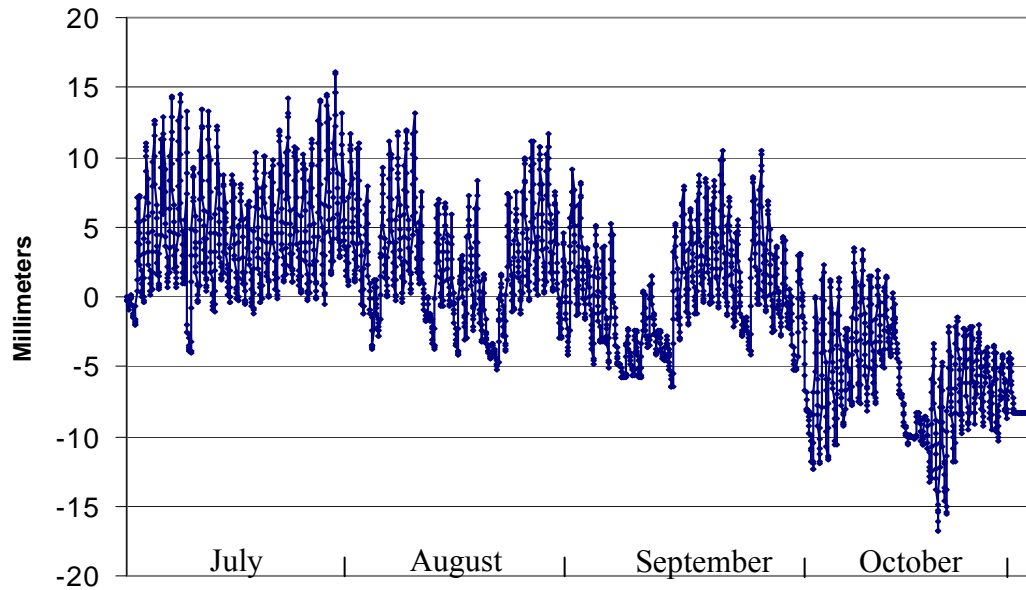
Figure 4.28 Longitudinal Displacement History Of The Inner Girder, July-November, 1998
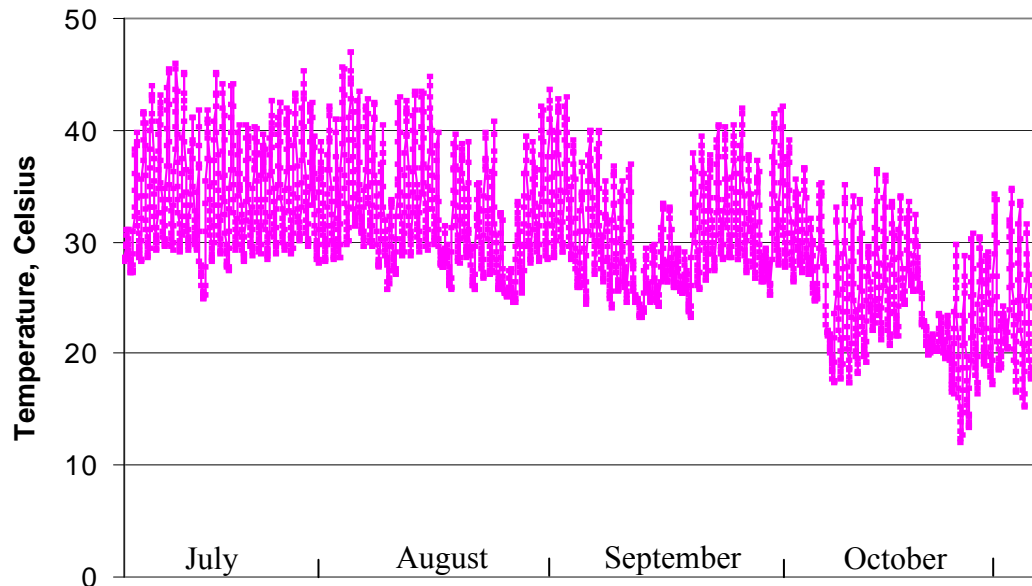
Figure 4.29 Inner Girder Mean Temperature History (Determined By Thermocouples In Contact With Structural Steel), July-November, 1998

118

Figure 4.30 Longitudinal And Transverse Displacement Histories Of The Inner Girder, July-November, 1998

Chapter 5

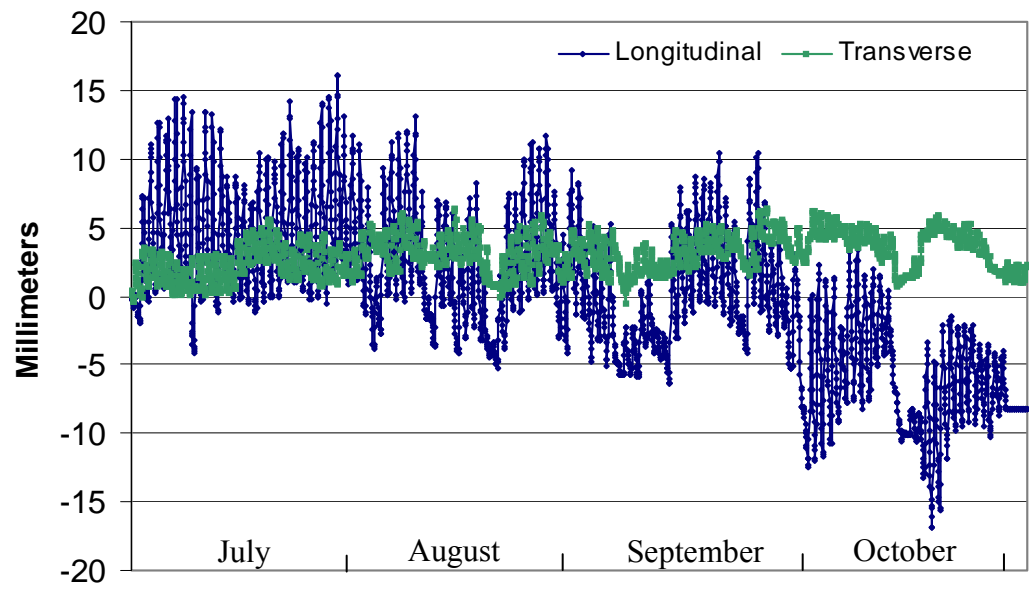# Finite Element Analysis of Thermally-Induced Deformations

5.1   The Finite Element Model

A finite element model of the bridge was developed for this study. The model
was developed with the intention of comparing measured thermally-induced
displacements and rotations with theoretical values.   The measured bridge
temperatures were used in the finite element analysis to compute theoretical
deformations of the bridge.

As described earlier, the bridge consists of two trapezoidal steel box girders,
topped with a slab 240 millimeters thick. The bridge comprises three spans, of
lengths 87.2, 56.7, and 54.9 meters. The bridge is curved in plan and is supported
by concrete piers of varying heights. The bridge has diaphragms between the
girders at each support. The diaphragms are different at the two instrumented
piers. The end pier has a truss diaphragm consisting of double-angle members.
The interior pier has a steel plate diaphragm linking the girders. Pot bearings are
in use at both instrumented piers. As described in Chapter 1, pot bearings may be
used with guide bars to dictate in which direction the bearing will allow
translation. The interior pier has no such guide bars, that is, movements in any
horizontal direction are allowed at this support. The end pier, however, has guide
bars on the bearings which will allow motion only in the tangential direction.
That is, local longitudinal displacements are allowed, but transverse, radial
displacements are prevented by the bars at this support. Of course, vertical

motions are prevented at all supports. A detailed description of the bridge superstructure, along with diagrams, is provided in Chapter 1.

The bridge was modeled using the proprietary finite element program SAP 2000 Nonlinear, version 7.00. The entire superstructure was modeled with shell elements, which incorporate plate bending and shell membrane stiffness and displacement characteristics. The element is a four-node element with user-specified thickness. The bridge was divided into segments 0.9 meter in arc length for the model. The webs and bottom flange plates of both girders were divided into two elements in each 0.9 meter length, that is, each web and bottom flange is two shell elements deep or wide, respectively. This provides aspect ratios close to unity throughout the girder web models. Flange thickness changes between positive and negative moment regions were modeled, but top flange width changes were neglected. Also, slab overhangs and cast-in-place barriers were not included. The top flanges were also divided into two elements in each 0.9 meter length. In all, there are 10 shells comprising each girder in each 0.9 meter length. All girder elements were assigned typical steel properties, namely, an elastic modulus of 200 GPa, a coefficient of thermal expansion equal to 1.17×10^{-5} /°C, and a Possion's ratio of 0.3. The concrete deck was included in the finite element model, as well. A concrete strength of 41.3 MPa was assumed. The modular ratio of steel to concrete may thus be taken as 6, and the thickness of the deck was divided by a modular ratio of 6, in order to use steel shells for it as well. The elements comprising the deck span between the top flanges of each girder and between the girders, connecting their adjacent top flanges. Half of the bridge cross-section, as modeled, is shown in Figure 5.1. Symmetry applies to the other half of the section.
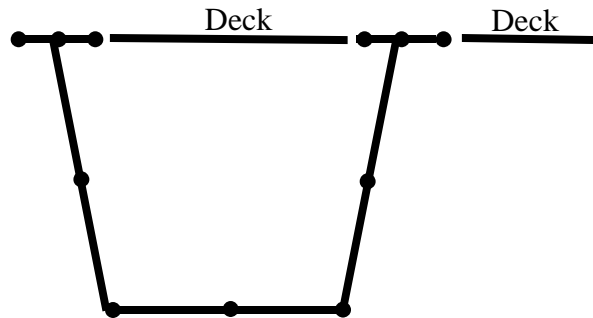
Figure 5.1 Half Of Bridge Cross-Section As Modeled, Showing Joints And Shells

In all, over 5,000 shell elements comprise the finite element model. The diaphragms at the supports were incorporated into the model by using rigid diaphragm constraints adjacent to each support point in the model. SAP 2000 Nonlinear does not allow the user to introduce diaphragm constraints at support points, so the diaphragms were placed at adjacent joints in the model, 0.9 meter away from the supported joints, which will introduce negligible error. These diaphragm constraints effectively force the included joints to displace equal amounts, by use of additional boundary conditions in the analysis. A cross-section of the bridge, as modeled for the analysis, is shown in Figure 5.2. It should be noted that SAP 2000 does not graphically represent diaphragm constraints as "elements," but instead as joints of different colors in the graphical module. Even though the diaphragm constraints can not be seen in this figure, they are in fact in place.

The correct modeling of support conditions in the model was essential. The northern instrumented pier has bearings which are guided to allow translation into the span only. This was accounted for in the finite element model by preventing

translation transverse to the bridge at this support, while allowing translations to occur in the local tangential direction. The southern instrumented bearings allow translation in all horizontal directions. This was accounted for in the model by providing true roller supports at this location, which allow translations in all directions. The next support, which is not instrumented in this study, is fixed against translations in all directions, to match the existing field condition. Finally, the fourth support, again not instrumented for this study, allows translation in any direction, and was modeled in the same way as the inner instrumented pier. Rotations are allowed in all directions at all supports.
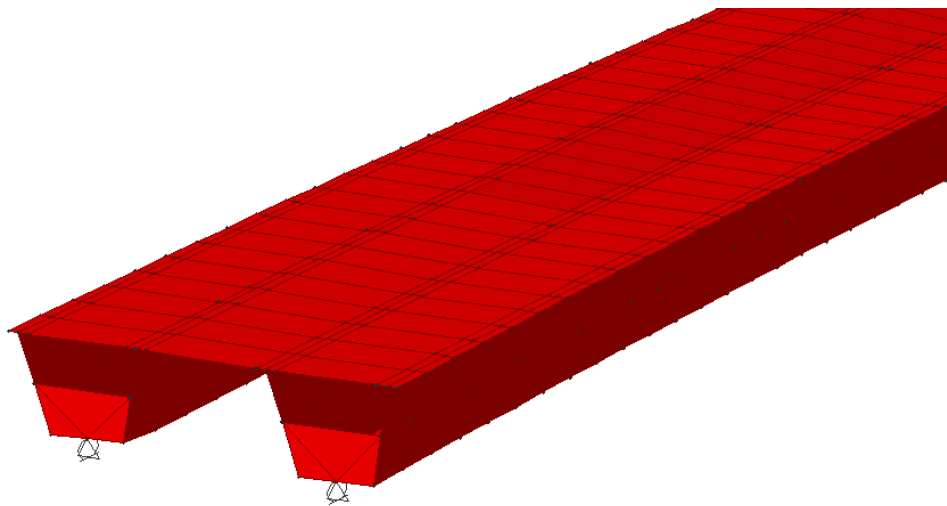
Figure 5.2 Screen Capture Of A Portion Of The SAP 2000 Model Of The Bridge

5.2   Thermal Deformation Analysis with SAP 2000 Nonlinear

The finite element model of the bridge consists of over 5,000 shell elements. SAP 2000 Nonlinear requires, for thermal displacement analyses, either the input of a stress-free reference temperature for an element or the acceptance of a default reference temperature of 0º Celsius. Thus, the calculation of thermally-induced displacements in SAP 2000 Nonlinear is much like a potential energy calculation, in which the gravitational potential energy of a body is referred to some chosen datum. As a matter of convenience, the reference temperature for all elements in this study was taken as the default value of 0º Celsius. It is essential to note here that relative temperatures are used in the analysis. That is, when a period of time is chosen for displacement and rotation analysis, the bridge temperatures at the start of the time under analysis must be subtracted from the temperatures at each period used in the analysis to calculate the relative temperatures for use in the analysis.

5.2.1   Computation and Tabulation of Predicted Deformations

The procedure used to compute theoretical thermally-induced deformations will be described here. For a given analysis, the starting temperature values of the elements comprising the girders and slab are all taken as the default value of 0º Celsius. The days analyzed were then divided into intervals suitable to provide a reasonably accurate estimate of the bridge's deformation behavior. It was found that three-hour temperature intervals provided reasonable accuracy. Also, in a time-history analysis such as this, it is important to judiciously select intervals of time used, so that accurate behavior representations are gathered, without excessive analysis "runs." If it were desired to perform the analysis at one-hour

intervals, 24 "runs" would be required for each day studied, which would require a prohibitive amount of time and bookkeeping.

The instrumentation recorded 37 bridge temperatures along with the local air temperature at each time. Because the temperature of each element at each time step was not obtained, an approximation of the thermal loading on the bridge was necessary in the analysis. A detailed temperature representation was developed and is discussed below.

Shown in Figure 5.3 are the distributions of temperature throughout the southern instrumented bridge cross-section at 8:00, March 10. Figure 5.4 depicts the thermal distribution throughout the northern instrumented cross-section at the same time. It is clear that there is a wide range of temperatures
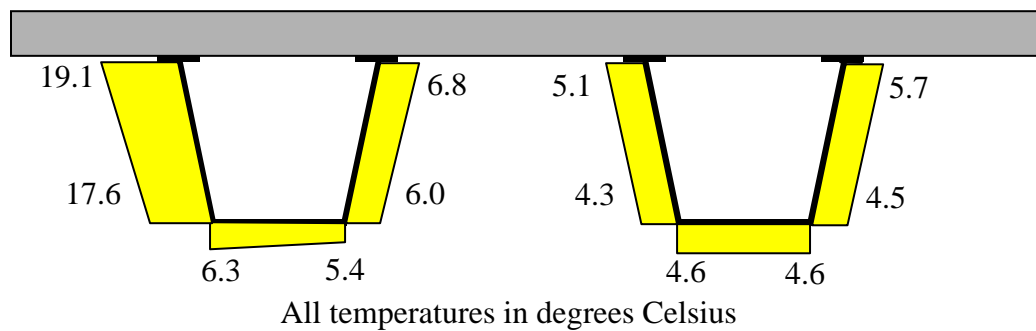
Figure 5.3 Temperature Distribution At The Southern Cross-Section, 8:00, March 10.

17.6   6.2   5.1   4.6

17.2   5.6   4.4   5.1

5.9   5.1   4.3   4.5

All temperatures in degrees Celsius
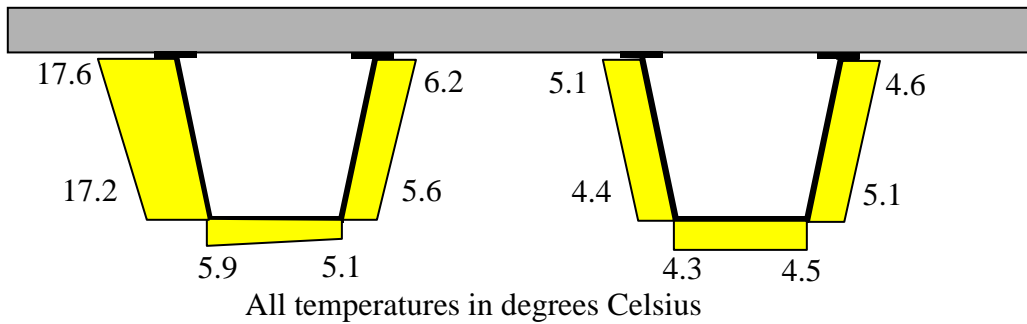
Figure 5.4 Temperature Distribution At The Northern Cross-Section, 8:00, March 10.

across the cross-section which should be accounted for in the analysis. The analysis was thus carried out using three temperatures at each time step. The mean temperature of the outer girder was determined by averaging the recorded temperatures of each thermocouple in contact with structural steel at both cross-sections of the outer girder. This mean temperature was applied to each element comprising the outer girder. The same was done for the inner girder and slab. The mean temperatures calculated from the values shown in Figures 5.3 and 5.4 are shown in Figure 5.5 (slab temperatures are not shown, for clarity).   The differences between these mean temperatures at each time step and their respective values at the previous time step are applied to the bridge model and deformations are computed. This procedure is carried out for the duration of the time under analysis. The deformations computed at each time step are added to those previously computed to define the bridge's position over time. In equation form, this may be written as:

$$\Sigma\Delta_i = \Delta_i + \Sigma\Delta_{i-1}$$

This was found to be a very effective way of using SAP 2000 to perform time history analyses of thermally-induced deformations.

Mean Girder Temperature:
9.9 ℃

Mean Girder Temperature:
4.7 ℃
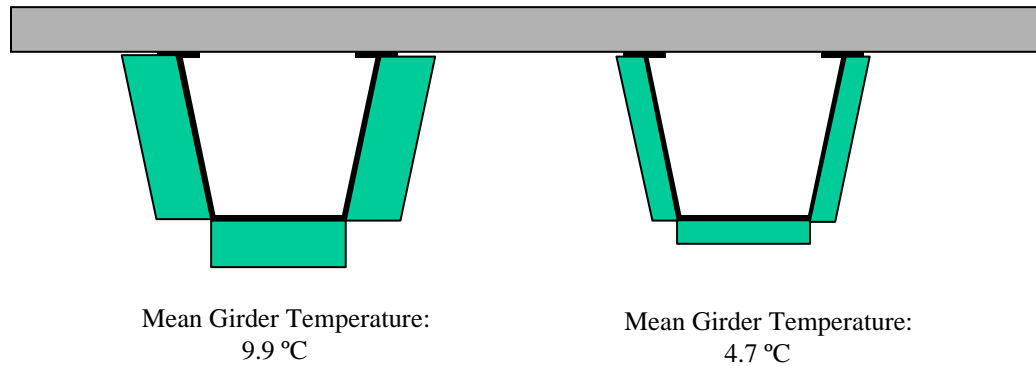
Figure 5.5 Mean Girder Temperatures As Computed From Figures 5.3 And 5.4

5.3   Theoretical Daily Displacements

Predicted daily cycles of thermally-induced deformations are described in this section. Comparisons will be made with measured displacements, which were presented in Chapter 4.

5.3.1.1 Longitudinal Displacements on August 2, 1998

As was described in Chapter 3, the bridge achieved its maximum Emerson Mean Bridge Temperature on August 2. It is of interest to examine the predicted displacements during this day, and to compare these displacements with those measured by the instrumentation and presented in Chapter 4.

Shown in Figure 5.6 is a plot of recorded and predicted longitudinal displacements of the inner girder at the end pier for August 2. Figure 5.7 shows mean inner girder temperatures for the same time period. The analysis and data interpretation was performed at three-hour intervals, as described earlier, and this

plot shows displacements from 0:00 to 24:00. All displacements are relative to the position of the bridge at midnight. The predicted displacements shown were computed by using three mean temperature differences at each time step-namely, those of the inner girder, the outer girder, and the slab, as described in Section 5.2.1.

The measured and theoretical curves have the same trends and displacement magnitudes. For purposes of this thesis, longitudinal girder contractions have been taken as negative girder displacements, while longitudinal girder extensions have been taken as positive quantities. It can then be seen that the bridge and the model of the bridge both reach their maximum expansions at 18:00. After this maximum is reached, both quantities begin to decrease into the evening hours.

It can also be seen that there are some differences between the predicted and the measured displacement values. The difference in values varies in magnitude over the day, with the quantities closer to each other in the early morning and late evening hours of the day. There are several possible reasons for the observed differences, as described below.

The pot bearings are not frictionless supports. Friction in the bearings will reduce induced displacements. The bearings were modeled as frictionless rollers, which is not exactly correct, since friction is inevitably present at the supports. This friction inevitably stiffens the structure, and predicted displacements will generally be larger than measured quantities. These restraining frictional forces will, however, induce pier deflections, which will be considered in Chapter 7.

A photograph of an expansion joint over the end pier is shown in Figure 5.8. It can be seen here that a significant amount of residue and litter have clogged the joint. This debris will add some amount of longitudinal stiffness to the bridge system, although the added stiffness is difficult to quantify. This may in fact be a very small stiffness contribution, but it is still a possible explanation of the observed differences. Also, the clogged expansion joint will stiffen the system
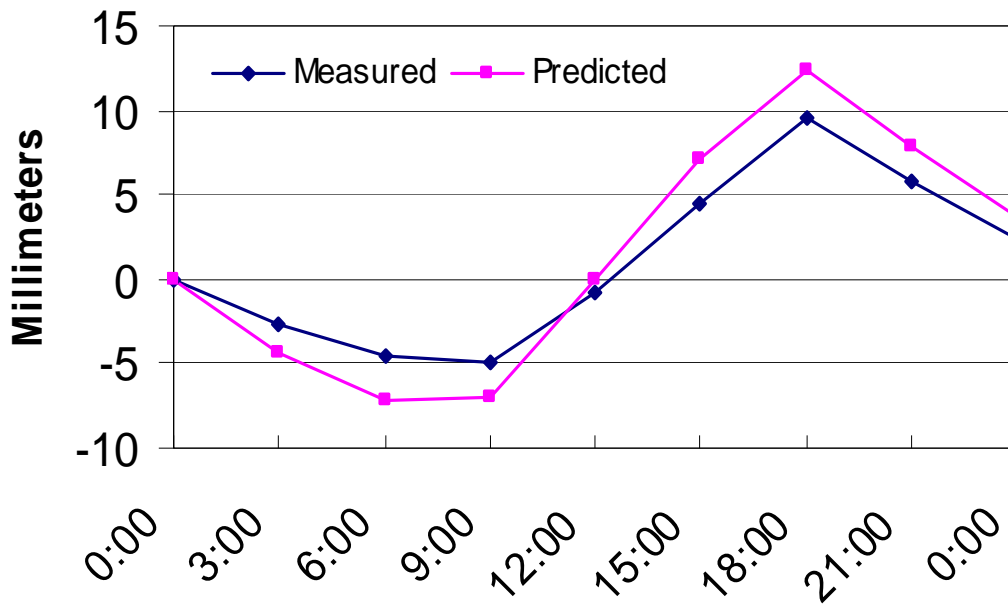
Figure 5.6 Measured And Theoretical Longitudinal Displacements Of The Inner Girder, August 2, 1998
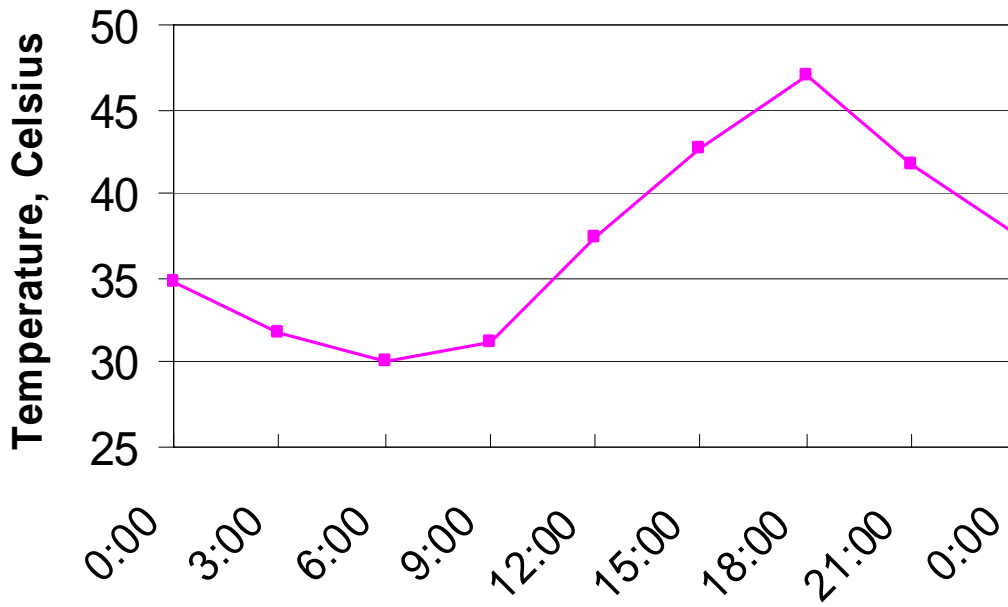

Figure 5.7 Mean Inner Girder Temperatures, August 2, 1998

with respect to positive (extensional) longitudinal displacements, and not negative displacements. This is in agreement with the observation that maximum differences between measured and theoretical longitudinal displacements typically occur during the hottest times of the day (this will be seen in future plots), when the bridge's longitudinal displacements are expansions, not contractions.

5.3.1.2 Longitudinal Displacements on October 24, 1998

It was also desired to examine the measured and predicted longitudinal displacements of the inner girder for a day during which there was a substantial range of recorded temperatures. While this was seen to occur several times throughout the duration of this study, it was also desired to investigate the behavior of the potentiometers some time after the second instrumentation period. The displacements of October 24 were thus analyzed.

Shown in Figure 5.9 is a plot of predicted and measured longitudinal displacements of the inner girder at the end pier for October 24, while Figure 5.10 shows the inner girder temperatures for the day. It is seen that both curves show the girder contracting through the morning hours as temperatures are falling. At 09:00, both curves give nearly identical values of displacement, and the girder then starts to expand under warming. It is then seen that both curves give the maximum girder extension as occurring at 18:00, which is not surprising, in light of the thermal trends illustrated in Chapter 3. The maximum predicted displacement is 16.8 millimeters and the maximum measured displacement is only 8.7 millimeters. This is a difference of 48% of the predicted value. The maximum such difference in the plot of longitudinal displacement at this location for August 2 was 40% of the theoretical longitudinal displacement. It is clear then, that there are often significant differences between theoretical and measured

displacements. As mentioned in Chapter 4, it is impossible to know with certainty whether these differences at any given time are due to potentiometer error or due to friction in the system.

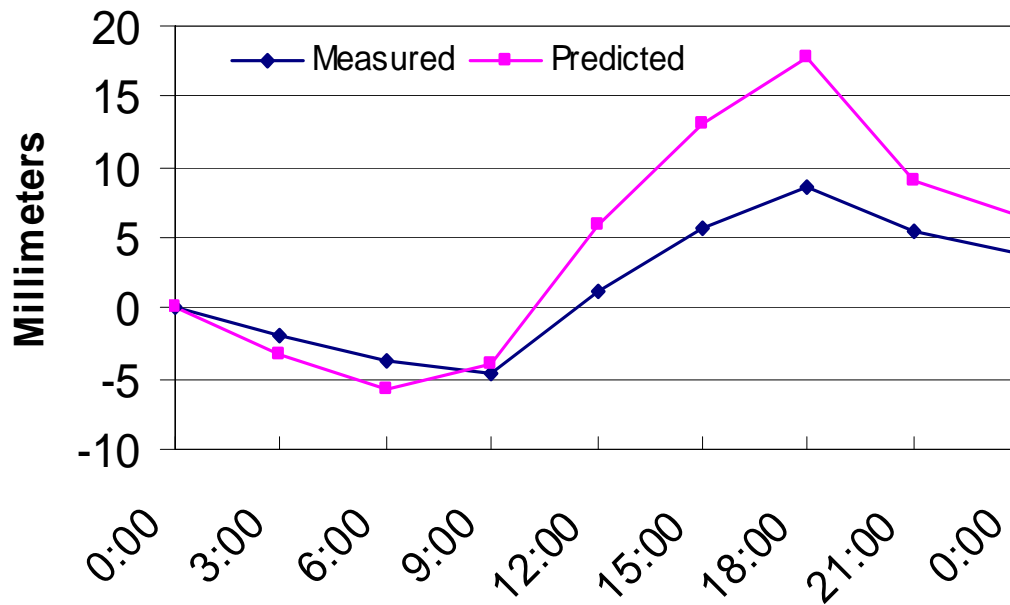**Figure 5.8 Photograph Of Expansion Joint Over The End Instrumented Pier**

Figure 5.9 Measured And Theoretical Displacements Of The Inner Girder, October 24, 1998
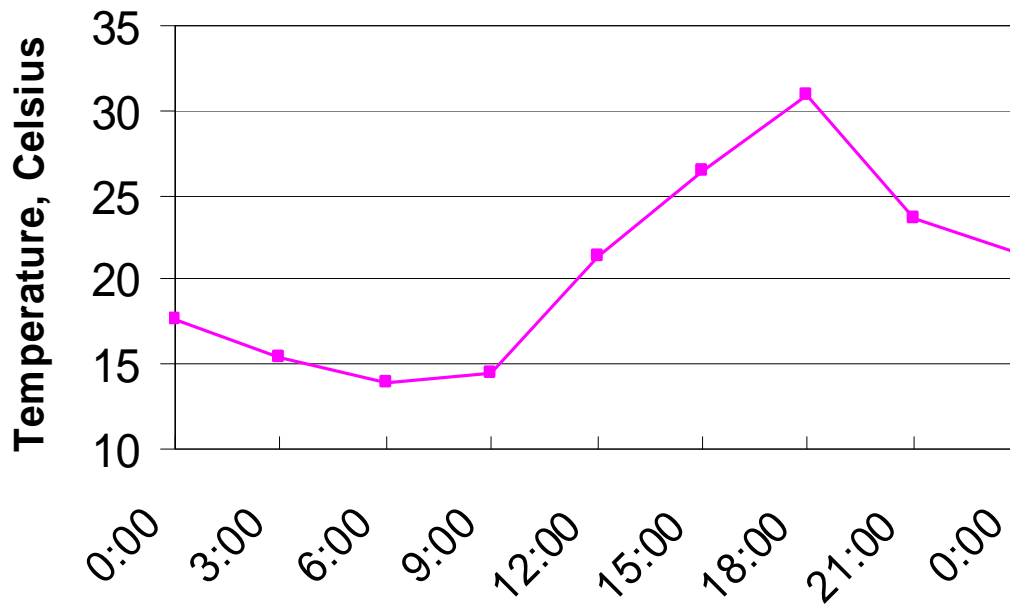
Figure 5.10 Mean Inner Girder Temperatures, October 24, 1998

5.3.2   Transverse Displacements: Observed and Predicted

The use of three temperatures to predict longitudinal displacements instead of a single bridge temperature was described earlier. This approach was also used in the computation and presentation of predicted transverse displacements, as presented in this section.

5.3.2.1   August 2, 1998

Shown in Figure 5.11 are plots of recorded and predicted transverse displacements of the inner girder during August 2. Shown in Figure 5.12 are plots of mean inner girder temperatures. As in Chapter 4, positive displacements are taken here as radially outward. Negative transverse displacements are radially inward. It can be seen immediately from the plots of displacements that the curves have the same general shape, but that a "lag" of one time step exists between the times of maximum predicted displacements and maximum recorded displacements. This lag is typical in the measured transverse displacements. It will also be noticed in this plot that it takes several hours from the start of the cycle for the measured transverse displacements to reach positive values. But it is important to recall that three mean temperatures were used in the finite element analysis. It was shown in Chapter 3 that there are often significant temperature differences within the cross-section of the bridge. The temperature representation used in the analysis may thus miss localized lateral temperature gradients within each girder, causing the time differences exhibited here. For example, it is seen in Figures 5.3 and 5.4 that there are localized "hot spots," as described in Chapter 3. These localized high temperatures will increase the mean girder temperatures used in the analysis, causing the theoretical maximum displacements to precede the measured values.

Figure 5.11 Measured And Theoretical Transverse Displacements Of The Inner Girder, August 2, 1998
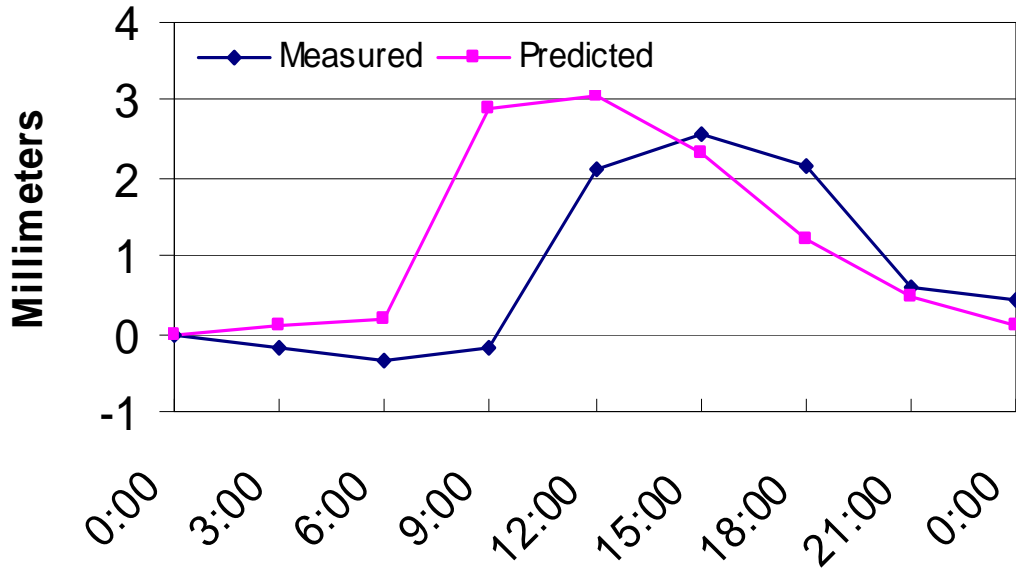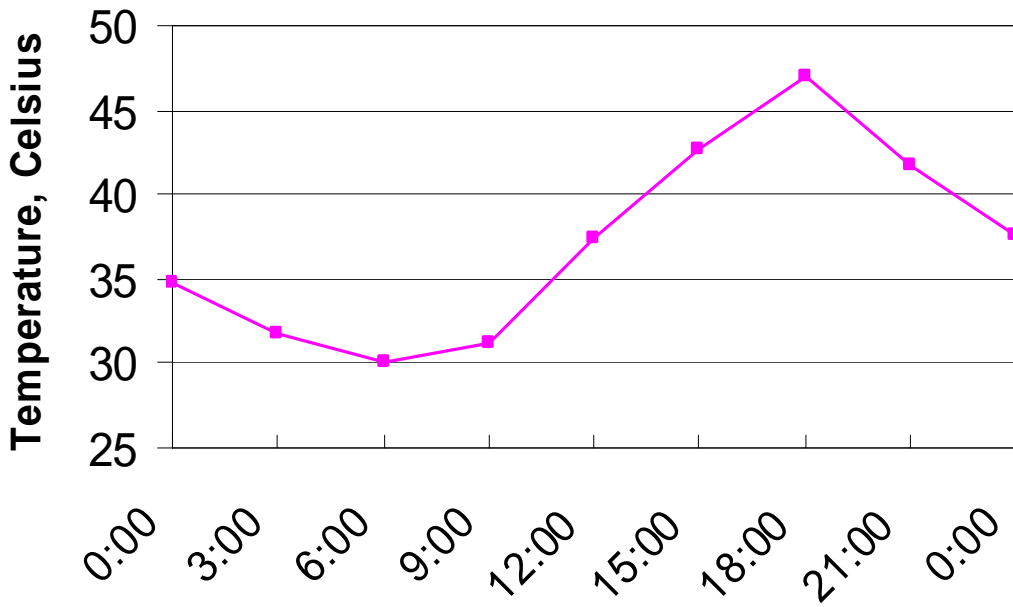

Figure 5.12 Mean Inner Girder Temperatures, August 2, 1998

It is also clear from Figure 5.11 that the measured displacements are again not as large as predicted displacements. This was also seen in the plots of longitudinal displacements, and the reasons for the differences between measured and predicted values may again be attributed to the factors mentioned earlier in this section. There will inevitably be some amount of friction in the bearings, which are assumed to be frictionless in the finite element model. It was also explained earlier, and applies to these plots as well, that the potentiometers, over time, collect moisture and dust which adds friction to their shafts, thus inhibiting full measurement of displacements. These factors will inevitably lead to differences between recorded and predicted displacements.

5.3.2.2   October 24, 1998

Shown in Figures 5.13 and 5.14 are plots similar to those shown for August 2. Figure 5.13 shows curves of predicted and measured transverse displacements for October 24, while Figure 5.14 depicts the mean girder temperatures for the same day. The same trends observed in the plots for August 2 are immediately observed again here. It is again seen that the maximum measured displacement lags behind the maximum predicted displacement, however, in this case, the lag consists of only one time step. It is interesting to note the sudden dramatic "jump" in the curve of predicted displacements. Included in Figure 5.14 is a plot of mean outer girder temperatures for October 24. It will be noticed that there is also a relatively large increase in the outer girder's mean temperature, and this "jump" occurs at 9:00, coinciding exactly with the large increase in transverse displacements. This lends credence the earlier-presented hypothesis that, because the finite element model uses mean girder temperatures in the analysis, temperature differences within each girder may be missed in the analysis. When
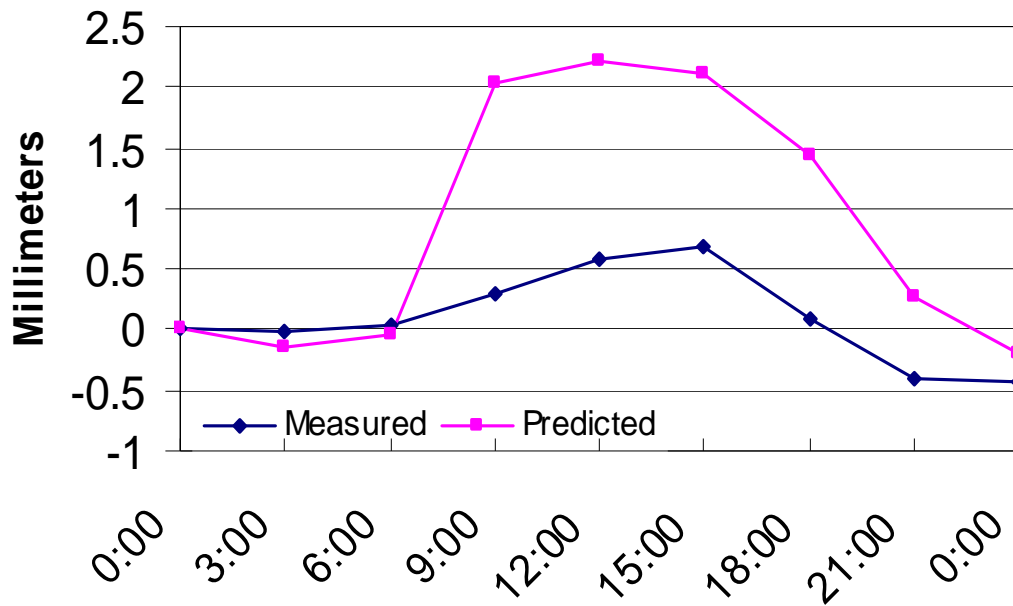
Figure 5.13 Measured And Theoretical Transverse Displacements Of The Inner Girder, October 24, 1998
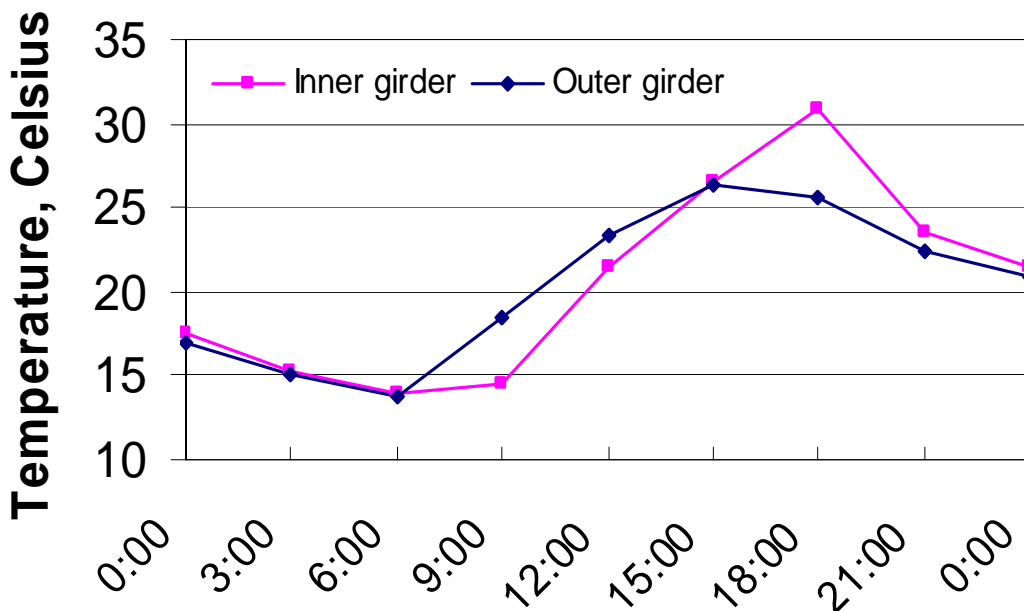
Figure 5.14 Mean Girder Temperatures, October 24, 1998

there are significant lateral temperature differences input as thermal loading, such as in this case, significant lateral translations can occur suddenly, as seen here. That this behavior is not observed in the measured displacements and only appears in the predicted displacements may be attributed to the causes described earlier (friction in the bridge bearings and the potentiometers).

It is obvious upon inspection of Figure 5.13 that the differences between measured and predicted displacements are larger than they were in the plots for displacements on August 2. On August 2, the maximum recorded displacement was 2.6 mm, while the maximum predicted displacement was 5.2 mm. This is a difference of 50% of the predicted value. However, the maximum recorded displacement on October 24 was 0.7 mm, while the maximum predicted displacement was 2.2 mm, for a difference of 68% of the predicted value. It is obvious, then, that substantial differences between measured and theoretical displacements also occur with respect to transverse displacements. It is also again impossible to ascertain at any particular time whether the differences are due to potentiometer malfunction, friction in the system, or a combination of these two factors. However, while the percentages of error are large, magnitudes are small. When considering that the instrumented portion of the bridge has an expansion length of some 143 meters, errors of 2-3 mm may be considered small.

Because translations of this bridge are cyclic in nature, it will be informative to examine displacement cycles as they occur over periods of several days. This will be done presently.

5.4 Longer Displacement Cycles: Theoretical and Measured

It has been seen in the examination of single-day displacement cycles that the bridge, under cooling, will contract in both its longitudinal and transverse directions in the early-morning hours and expand in both directions as it warms in

137

the mid-morning and afternoon hours. It was also seen that, as temperatures cool into the evening, the bridge again contracts at the end of the day. The bridge thus oscillates in position over time, though not about a fixed point, as temperatures do not typically return to a constant value. In this section, displacement cycles in both directions are examined for the four-day period July 15-18, 1998. The starting time for this analysis is midnight on July 15 and the ending time is midnight on July 19. This range of time provides detailed insight into the displacement trends of the bridge over several days' time.

5.4.1 Longitudinal Displacements for July 15-18, 1998

Shown in Figure 5.15 is a plot of predicted and measured longitudinal displacements for the period under investigation, and shown in Figure 5.16 are the mean inner girder temperatures for the same time. Longitudinal displacements shown are those occurring in the inner girder at the end pier. The reference temperatures used in computing the predicted values are those at midnight on July 15, while the reference bridge position used to tabulate measured displacements is that at midnight on July 15. As before, positive longitudinal displacements are extensions, while negative displacements are girder contractions, and the analysis was performed at three-hour intervals.

It is immediately obvious that the displacement trends are similar to those observed previously for single-day cycles. It is seen that maximum measured girder displacements occur at the same time as theoretical maximum displacements, and minimum recorded displacements occur within one time step of the predicted minimum displacements. It is also seen that, once the displacements reach positive values (extensions) on July 15, they don't return to zero or negative values during the period of investigation. This indicates a warming trend, and this conclusion is validated upon inspection of Figure 5.16. It

138

is seen in this plot that indeed, girder temperatures are on a rising trend during this period of investigation.

Figure 5.15 Measured And Theoretical Displacements Of The Inner Girder, July 15-18, 1998
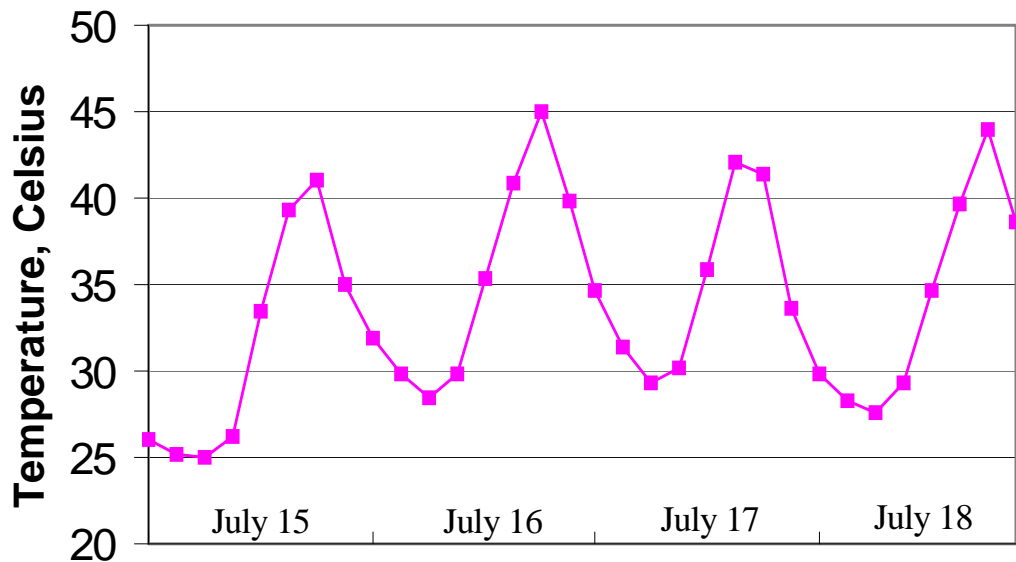
Figure 5.16 Mean Inner Girder Temperatures, July 15-18, 1998

It is also seen that significant differences between theoretical and measured displacements exist, as was seen in single-day plots before. The largest such difference occurs at the time of maximum displacement on July 16, the second peak shown here. At this time, the theoretical longitudinal displacement is 27.1 mm, while the recorded displacement is 15.4 mm. This is a difference of 43% of the predicted value. As was shown in Chapter 1, when the bridge is prevented from moving freely under thermal differences, stresses will arise in the bridge. These will be examined in Chapter 7. Finally, it is seen that, with the exception of the first three time steps in this analysis (the morning hours of July 15), there is always some difference between the theoretical and measured displacements. This seems to be unavoidable, as it has been seen in previous plots and will be obvious again in future plots.

5.4.2   Transverse Displacements for July 15-18, 1998

Shown in Figure 5.17 are theoretical and measured transverse displacements for July 15-18. Figure 5.16 is repeated here for convenience, and depicts mean inner girder temperatures for the same time frame. It is again seen here that the measured displacements lag behind predicted displacements. Reasons for this lag were offered in Section 5.3. It was noted there that the use of mean temperatures in the analysis often does not account for substantial thermal variations within each girder, and that some temperatures within the girders which are substantially higher than others will elevate the overall mean girder temperatures used in the analysis, possibly misrepresenting overall girder behavior.
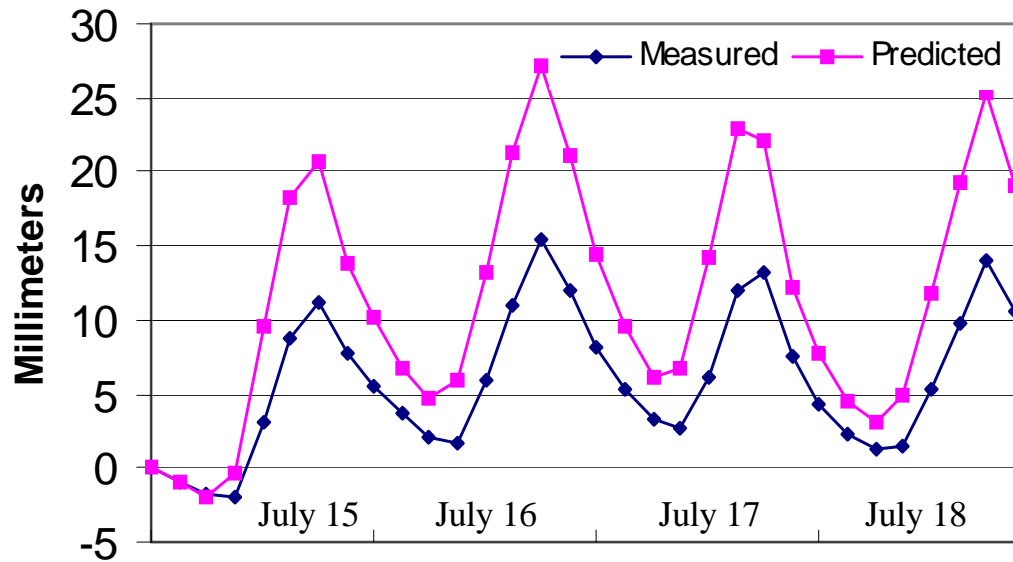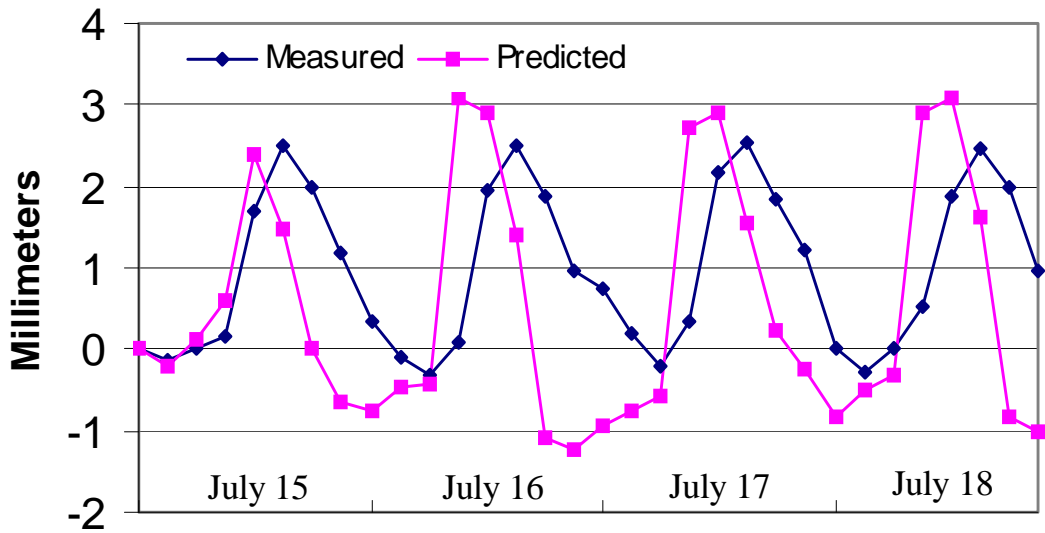
Figure 5.17 Measured And Theoretical Transverse Displacements Of The Inner Girder, July 15-18, 1998
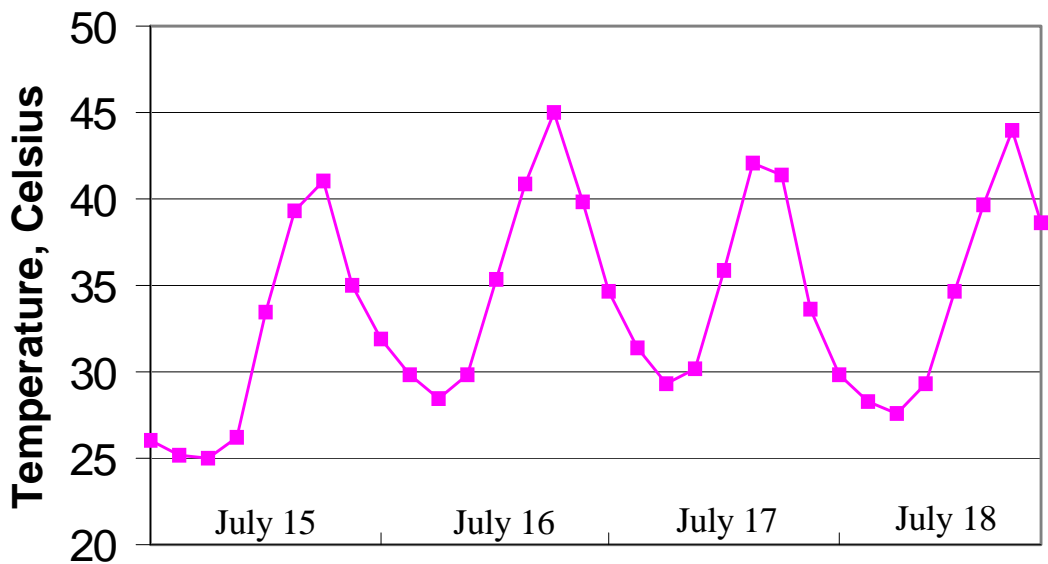
Figure 5.18 Mean Inner Girder Temperatures, July 15-18, 1998

It is also seen that, similar to the predicted behavior for October 24, there is a sharp "jump" in the positive transverse displacement each morning. It was shown earlier that this is due to the warming of the outer girder. As the outer girder warms, it expands outward, and because of the diaphragm, which is assumed rigid in the model, the inner girder is pulled outward with it. It will also be observed from this four-day plot that, unlike the plot of longitudinal displacements, negative transverse displacements (inward) do occur during this period. Thus, with respect to transverse displacement, the bridge comes closer to oscillating about its initial position than it does with regard to longitudinal displacements.

Finally, it is seen again here that there are differences between measured and predicted displacements at all times other than during the first three time steps in the analysis. As described earlier, these displacement differences appear to be inevitable.

As with any permanent bridge structure, the bearings in use will have to withstand long-term displacements, as well as small cycles examined thus far. Because of this longevity requirement, it is very important to examine long-term displacements occurring in the structure. Measured long-term displacements were described in Chapter 4. Comparisons may now be made between measured and theoretical values. This will be done in the next section for displacements in both directions.

5.5 Long-Term Displacements: Measured vs. Theoretical

The finite element model used to compute theoretical displacements and rotations has been described previously. The piecewise method of analysis used in this study has been described, as well. The author also used the model to determine theoretical ranges of displacement at monthly intervals for comparison to the values presented in Tables 4.1 and 4.2. To do this, the temperature

extremes used for longitudinal displacements were the Emerson Mean Bridge Temperatures (EMBT). These were used instead of mean inner girder temperatures, because, as was shown in Chapter 3, girder and slab extreme temperatures do not occur simultaneously. The EMBT, on the other hand, is a reasonable single temperature to be used in the analysis. The minimum EMBT for each month is subtracted from the maximum, thus defining the monthly range of EMBTs. This result was applied to all the elements in the bridge model and the theoretical displacements were computed. The resulting displacements are the theoretical range of displacements for each month. Because thermal gradients across the width of the cross-section produce larger transverse displacements than uniform temperature changes, maximum gradients were used for the computation of these displacements. Extreme differences in mean girder temperatures (considering the temperatures at both cross-sections) were located for each month. The differences were applied to all elements of the model. The resulting transverse displacements are absolute maximum monthly displacement ranges. Maximum ranges are tabulated in Table 5.1 for longitudinal displacements and in Table 5.2 for transverse displacements.

In addition to monthly ranges of displacements, maximum displacements for the entire instrumentation period are also of importance. The theoretical computation of the longitudinal displacements was performed in an identical manner to those computed for monthly ranges. The minimum EMBT for the entire period of study was subtracted from the maximum EMBT, and the result was applied to all the elements in the model.

Table 5.1 Measured And Theoretical Longitudinal Displacement Ranges

Month	Recorded Range	Predicted Range	% Difference
February	23.1 mm	32.6 mm	29.1
March	26.8 mm	44.9 mm	40.3
April	21.9 mm	42.1 mm	48.0
May	22.4 mm	36.9 mm	39.3
June	20.3 mm	33.9 mm	40.1
July	18.8 mm	31.3 mm	39.9
August	21.3 mm	33.3 mm	36.0
September	16.9 mm	27.5 mm	38.5
October	23.7 mm	40.7 mm	41.8

Table 5.2 Measured And Theoretical Transverse Displacement Ranges

Month	Recorded Range	Predicted Range	% Difference
February	1.4 mm	8.1 mm	82.7
March	4.5 mm	10.5 mm	57.1
April	4.5 mm	9.6 mm	52.1
May	3.8 mm	8.5 mm	55.3
June	4.8 mm	8.0 mm	40.0
July	6.1 mm	7.2 mm	15.3
August	6.5 mm	7.7 mm	15.6
September	4.9 mm	6.2 mm	21.0
October	7.1 mm	9.5 mm	34.8
November	4.3 mm	8.2 mm	47.6
December	2.0 mm	5.8 mm	65.6

The resulting longitudinal displacements are the absolute maximum theoretical displacements which are predicted to occur under the observed thermal conditions in the bridge. The thermal variations across the cross-section of the bridge were again used to compute theoretical transverse displacement ranges. Because the maximum girder temperatures do not occur at the same time and there are significant thermal gradients across the cross-section of the bridge when the inner girder reaches its maximum temperatures, this is a viable approach. The resulting transverse displacement is the absolute maximum transverse displacement predicted for the bridge under the observed thermal conditions. The maximum recorded range of displacements in each direction was determined by subtracting the minimum recorded displacements in each direction from the maximum recorded displacements in the same direction. Monthly maxima and minima have been reported earlier, and the maximum ranges for the entire instrumentation period were determined by subtracting the minimum values in each table from the maximum values in the same table. The result is the absolute maximum range of recorded displacements in the real structure. Results are shown below in Table 5.3.

Table 5.3 Maximum Recorded And Predicted Displacement Ranges During The Study

Direction	Measured Range	Predicted Range	% Difference
Longitudinal	40.6 mm	62.1 mm	34.6
Transverse	8.6 mm	15.9 mm	45.9

For illustrative purposes, maximum ranges of EMBT, ambient temperatures, and mean inner girder temperatures (again calculated from all thermocouples in contact with structural steel in the inner girder) are tabulated in Table 5.4.

Finally, the maximum predicted displacements of the finite element bridge model, based on the use of a uniform temperature rise in the structure equal to the range of ambient temperatures recorded, are shown in Table 5.5. These displacements are what a design engineer would calculate based on recorded air temperatures at the bridge site. Note that the use of a uniform temperature rise underestimates transverse displacements significantly.

Table 5.4 Maximum And Minimum Recorded Various Temperatures

	Ambient	Emerson Mean	Mean Inner Girder
Minimum	2.5º C	44.0º C	3.8º C
Maximum	39.8º C	4.2º C	47.0º C

Table 5.5 Predicted Displacements Under Uniform Temperature Rise Dictated By Ambient Temperatures

Longitudinal	59.4 mm
Transverse	0.6 mm

5.6   Orientation of Sliding Guides in Pot Bearings

It was described in Chapter 1 that polytetraflourethylene (PTFE) surfaces are often used in conjunction with standard pot bearings to allow girder translations to occur at the supports. It was also noted there that guides are sometimes used in conjunction with the PTFE surfaces to dictate in which direction the girders are allowed to move at the supports. To the practicing engineer designing a curved bridge such as this one, the question of the proper orientation of guides used at the bearings is a formidable one, as it has been noted earlier (Roeder and Stanton), that curved bridges move both tangentially as well as radially. An incorrect

orientation of guides will inevitably lead to stress buildups within the bearings, as free translations will be prevented by the guides.

The question of guide orientation was explored in this study. Specifically, the four-day period analyzed earlier for displacements, July 15-18, was analyzed to determine whether the bridge moved in a manner which could be defined in geometric terms. The analysis procedure was described earlier, and it will be recalled that three mean temperatures are used at each time step; namely, those of the outer girder, the inner girder, and the slab.

It will be recalled that the bearings at the end pier was installed with guides which prevent translation in the radial direction. Also, it was noted earlier that the bearings at the inner instrumented pier are free of such guides and translations are allowed in any direction in the horizontal plane. Finally, it will be recalled that the bearings at the next pier beyond the inner instrumented pier are fixed, i.e., no girder translations are allowed at this support. In order to ascertain in which direction(s) the bridge girders tend to move, a vector was defined from the inner girder's fixed bearing to the inner girder's instrumented bearing at the inner pier. Only the inner girder's motions are considered here, as reliable displacement measurements were not obtained at the outer girder. The vector was first defined based on the undeformed geometry of the bridge. The vector was then updated at each time step in the analysis of July 15-18, incorporating predicted translations in both directions into the new vector components. The vectors from the fixed bearing to the "free" bearing were tabulated in a spreadsheet to include each time step. Next, the updated vectors at each time step were used with the original vector to define the angle changes between the original vector and the updated vectors. This angle change is given by the trigonometric formula that states that the cosine of the angle between two vectors is given by the ratio of the inner product of the vectors to the product of the magnitudes of the vectors. This calculation was carried out at each time step, incorporating theoretical

displacements at each step. It was discovered that the theoretical displacements of the inner girder are along the chord from the fixed bearing to the unguided bearing. That is, if an imaginary line is drawn from the fixed bearing to the unguided bearing, the girder's predicted displacements are along this line at each time step. This conclusion is corroborated by Roeder (1998), who notes that if the bridge is treated as a single line element with uniform temperature and fixity at one location, the girder movement at moveable supports will be along the chord from the fixed support.

While Roeder's statement is validated by theoretical calculations for this bridge, it was also desired to determine whether this in fact occurs in the real structure. To this end, another vector was defined from the fixed support to the unguided support, this time incorporating measured displacements. The same procedure outlined in the previous paragraph was again followed, for the same duration of time. It was discovered that measured displacements are also on the chord from the fixed bearing to the unguided bearing. The angle between the original vector and the updated vector was computed to be zero at each time step, indicating that the vector between the two bearings does not change direction.

While this is an interesting result, it should not be taken as definitive. As Roeder points out, several factors prevent curved bridges from moving strictly along the chord from the fixed bearing to the unguided bearing. Because the bearings are supported on piers which have their own flexibilities (more on this in Chapter 7), the piers themselves may deflect, thus interrupting the "chord-oriented" movement. Also, it was noted that calculations for the measured displacements were performed only for the inner girder. In real curved bridges such as this, there are always at least two girders in use, and the connectivity of the girders will influence movements. Finally, it has been shown that motions were inhibited somewhat in the bridge during this study. Because the measured displacements, relative to the overall bridge dimensions, are small, they do not

greatly affect the components of the vector described from the "fixed" bearing to the "free" bearing. It may thus be considered rather fortuitous that these calculations indicate motion along the chord from the fixed bearing to the unguided bearing. As Roeder further notes, these factors make it difficult to attain a perfect orientation of guides in real structures. If guides are used, they must be relatively strong or the pier must be flexible to avoid all damage which may occur from imperfect guide orientations. Because of these aspects of real bridge structures which deviate from idealized models used to obtain results such as those revealed above, Roeder notes that there is wisdom in using unguided bearings such as those in use in this bridge. For these reasons, the calculation results presented herein showing bridge motion along the chord should not be taken as a definitive rule on guide orientation.

5.7   Summary and Conclusions

The following conclusions may now be drawn about the theoretical and measured thermally-induced displacements of the bridge.

1. Girder translation trends in both directions follow temperature trends and theoretical displacement trends. It has been shown that measured displacement cycles closely mimic temperature cycles, with extensions occurring at times of high temperatures and contractions developing during times of low temperatures. It was also shown that cycles of measured displacements follow cycles of theoretical displacements well. There are, however, lags the between times of maximum predicted transverse displacements and the occurrence of maximum measured displacements. Possible reasons for this were given earlier, as it was hypothesized that, because the temperature representation in the finite element analysis must be simplified somewhat, the analysis may miss localized temperature gradients within the girders. It was described how local high

temperatures may artificially raise girder temperatures used in the analysis, producing the time differences observed.

2. Displacements in both directions do not reach maximum values predicted by theory. The differences between measured and predicted values of girder translations are typically on the order of 30-50% of the theoretical values. The prevention of free expansions of the girders will lead to stress buildup within the structure. This will be examined in Chapter 7. Several partial explanations for the differences have been roferred, including: the presence of friction in the bearings instead of the assumed frictionless conditions, the clogging of the expansion joint over the end pier, and the accumulation of residue of the potentiometer shafts over time, inhibiting free extensions of the potentiometer shafts. Pier deflections, which may accommodate induced translations, will be described in Chapter 7. Pier deflections may in fact be a significant factor in the translation behavior of the girders, as girder translations observed and computed thus far are relative to the pier caps.

3. The potentiometers recorded appreciable ranges of displacement, though the ranges were not as large as theory predicts. It was shown that the potentiometer measuring transverse displacements of the inner girder was able to record appreciable ranges of displacement with time, and the potentiometer measuring longitudinal displacements at the end pier was able to record ranges after the second instrumentation. From the values reported by the longitudinally-oriented potentiometer, the author was able to extrapolate back in time to ascertain expected ranges of recorded displacements at the end pier. These ranges, however, were seen to be smaller than theoretical displacement ranges.

4. Theoretical and measured displacements of the unguided bearing were seen to occur along the chord from the fixed bearing to the unguided bearing. It was shown in the analysis of the period July 15-18 that theoretical displacements occur along the chord, as do measured displacements for the same time period. It

was noted, however, that several factors can change this occurrence from occurring reliably enough to orient guides in this direction. As Roeder (1998) points out, there is wisdom in using unguided bearings at such locations, as imperfections in the orientation of guided bearings will lead to stresses which will require strong guides and flexible piers to prevent damage to the structure.

Chapter 6

Rotation Measurement and Analysis

The instrumentation used to measure girder translations was described in Chapter 2, and measurements were compared to analysis results in Chapter 4. While the placement of potentiometers to measure girder rotations at the bearings was also mentioned, a detailed description of rotation calculations based upon the potentiometer readings was omitted. A description of these calculations will be presented now. Also in this chapter, girder rotation measurements will be described, both on scales of several days and on a long-term basis. Measured rotations will also be compared with finite element predictions.

6.1   Instrumentation to Measure Rotations

It was mentioned in Chapter 2 that four vertically-oriented potentiometers were positioned at each of the four instrumented bearings to measure and record girder rotations.   This is achieved by measuring the extension of each potentiometer relative to the extensions of the others at the same location over time. The relative positions of the potentiometers, along with their locations in the horizontal plane, define the current plane of the top bearing plate, and, because the bearing is firmly connected to the bottom of the girder, the plane of the girder's bottom flange at the instrumentation location is defined, as well.

However, it was also desired to ascertain rotation magnitudes in the two principal directions, that is, how much the girders rotate about the longitudinal and transverse axes of the bridge. Because the bridge cannot be expected to heat

and cool uniformly across its width, and because the bridge is curved in plan, the girders could not be expected to rotate solely about the bridge's transverse axis, and rotations about the bridge's longitudinal axis could be significant. Figure 6.2, on page 154, illustrates this concept. It should be noted that the bottom bearing plates do not undergo rotation, as they are firmly attached to the piers.

Longitudinal and transverse rotations were separated in the following manner. Because the bearing plates are relatively stocky (~50 mm thick) and have small plan dimensions (~1065 mm), they were assumed to be rigid out of their plane. Four points were then defined, with one point at each mid-point of an imaginary line extending between adjacent potentiometers. These points are as shown in Figure 6.1 below.
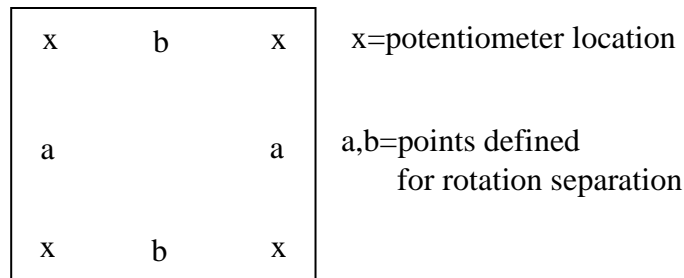
Figure 6.1 Potentiometer Layout And Defined Points For Separating Rotations Into Two Directions

In this figure, the "a" and "b" signs represent the points described above, which are defined at the mid-points of lines connecting adjacent potentiometers. The elevations of these points at each data collection time are taken to be halfway between the elevations of the adjacent potentiometers-that is, the elevation difference from one potentiometer to an adjacent potentiometer is assumed to vary linearly because of the assumed bearing plate rigidity.
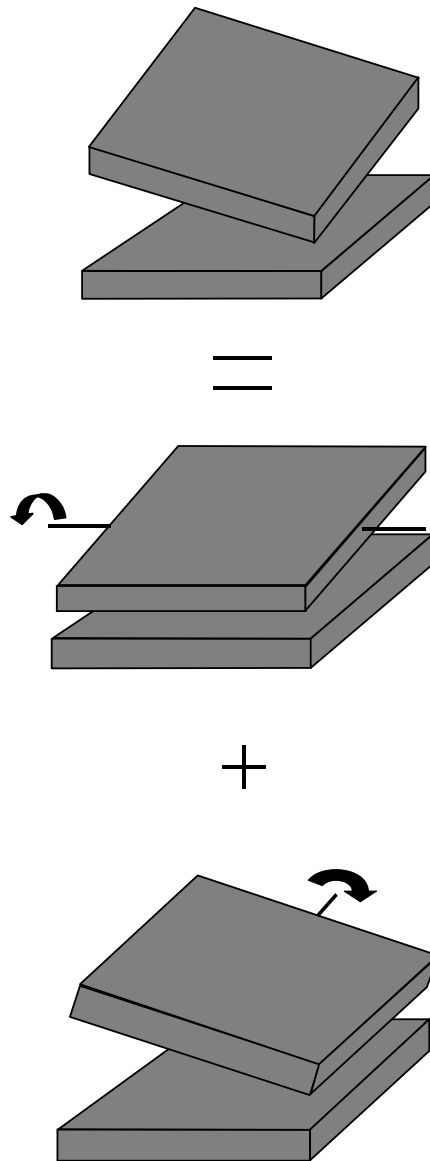
Figure 6. 2 Rotations At Any Time May Be Separated Into Components

Because the positions of the potentiometers are known, the distances between the defined points are known. The difference in the calculated elevations of the defined points is then divided by the distance between the points, and the rotation is obtained. An example will clarify this concept. Suppose the bearing plate depicted in Figure 6.3 is instrumented with four potentiometers and the distances between them are as shown (the numbers indicate potentiometer numbers, used here for convenience):
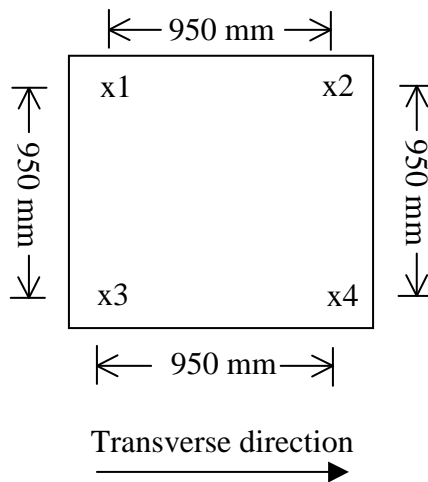
Figure 6.3 Diagram Of Potentiometer Locations Used In Example

Further, suppose that the relative elevations of the potentiometers are as follows: x1, 1 mm; x2, 3 mm; x3, -2 mm; x4, 4 mm. The elevation halfway between potentiometers x1 and x3 is then: (1+(-2))/2=-0.5 mm. The elevation halfway between potentiometers x2 and x4 is: (3+4)/2=3.5 mm. The longitudinal rotation, or rotation about the transverse axis, is then: (3.5-(-0.5)) mm/950 mm=0.0042 radian. The elevation halfway between potentiometers x1 and x2 is: (1+3)/2=2 mm. The elevation halfway between potentiometers x3 and x4 is: (-2+4)=1 mm. The transverse rotation, or the rotation about the longitudinal axis,

155

is then computed to be: (2-1) mm/950 mm=0.0011 radian. It is seen, then, that the instrumentation scheme used is an effective and simple way of calculating girder rotations and determining how much rotation occurs in each principal direction. This separation of rotation directions also allows for easy comparison to SAP 2000 output, as SAP 2000 reports joint rotations about three local axes.

6.2   Girder Rotations: Measured and Predicted

The same finite element model described in Chapter 5 was used to predicted rotational deformations. The period July 15-18, examined for displacements, will be studied for rotational output, as well. Long-term rotational deformations will then be examined.

6.2.1   Rotation Analysis: July 15-18, 1998

The analysis of the period July 15-18 was described in Chapter 5. Specifically, it was described how the analysis of this time was carried out in three-hour intervals, with the thermal loading at each interval taken as the thermal changes of the girders and slab since the previous time step. After all time steps are analyzed, displacements and rotations are then summed, with the resulting deformations at each time step providing a time-history of predicted displacements and rotations.

6.2.1.1 Transverse Rotations

Shown in Figure 6.4 are predicted and measured transverse rotations of the outer girder at the northern pier for July 15-18, and in Figure 6.5 are shown the mean outer girder temperatures for the same period.   The mean girder

temperatures were again calculated as the average of all thermocouples in contact with structural steel, at both cross-sections instrumented. It is important to note here that positive transverse rotations are taken to be a twisting of the girders inward toward the center of curvature of the bridge. This is the convention for transverse rotations at both supports.

It is immediately clear that measured rotations are smaller than theory predicts. The validity of the model is again displayed in the fact that the measured and predicted rotations both reach their extreme values at the same times, but it is clear that the finite element model predicts larger transverse rotations than are measured. It is also seen in Figure 6.4 that the measured rotations of the bridge do not often reach negative values, or, if they do, these values are very small and quickly return to positive rotation values. This indicates that the girders evidently do not twist outward, even though the finite element model predicts the occurrence of these rotations. Finally, it is clear that, even though there are differences between measured and predicted values of transverse rotation, peak values of both quantities are very small. It was described in Chapter 1 that the pot bearings typically have rotation capacities of 0.04 radian. It is clear from Figure 6.4 that predicted transverse rotations at this location (the outer girder at the end pier), reached peak values during this period of approximately 0.0015 radian, one order of magnitude less than the capacity of the bearing. It is also clear that peak measured transverse rotations were approximately 0.0005 radian, two full orders of magnitude less than the pot bearing capacity.
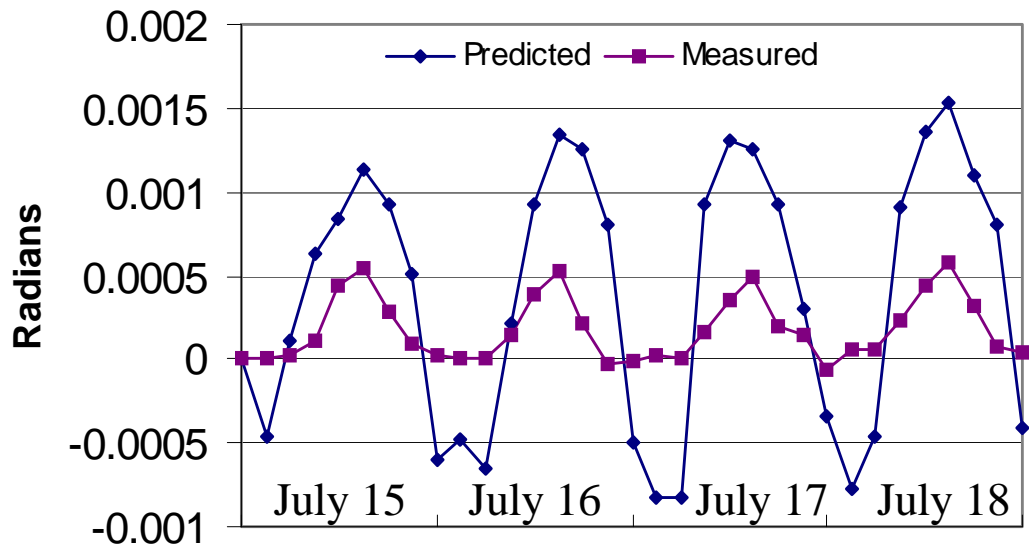
Figure 6.4 Measured And Theoretical Transverse Rotations Of The Outer Girder At The Northern Pier, July 15-18, 1998
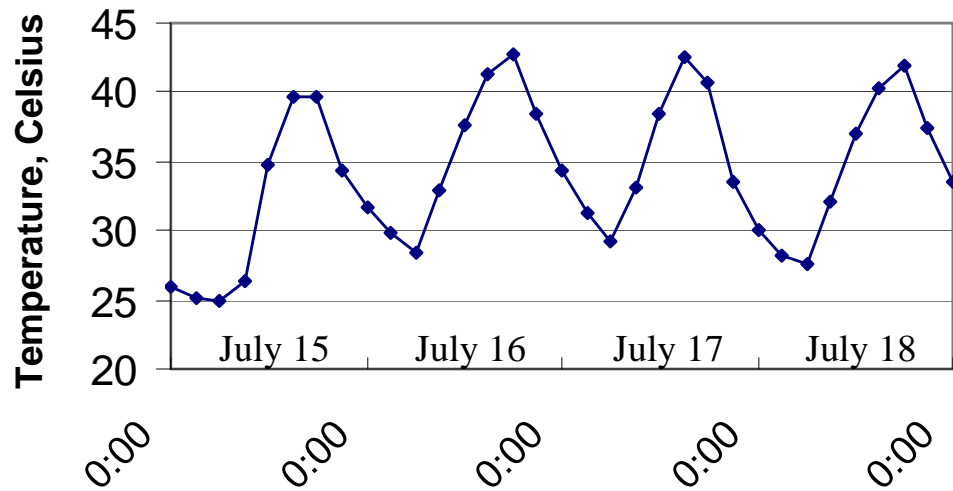
Figure 6.5 Mean Outer Girder Temperatures, July 15-18, 1998

Similar behavior is seen in Figure 6.6, which is a plot of the same quantities for the inner girder at the northern pier. It can be seen that predicted rotations at this location are smaller than at the outer girder. This is to be expected, as the inner girder, with its shorter length, is stiffer than the outer girder. It is also clear from Figure 6.6 that measured rotations of the inner girder are slightly larger than those of the outer girder, indicating that the potentiometers at the inner girder are probably functioning better than at the outer girder. This has been seen before, as it was shown in Chapter 4 that displacement measurements of the outer girder suffered throughout the course of this study. It is important to note that both measured and predicted transverse rotations of the inner girder are also many times smaller than the capacity of the bearings.
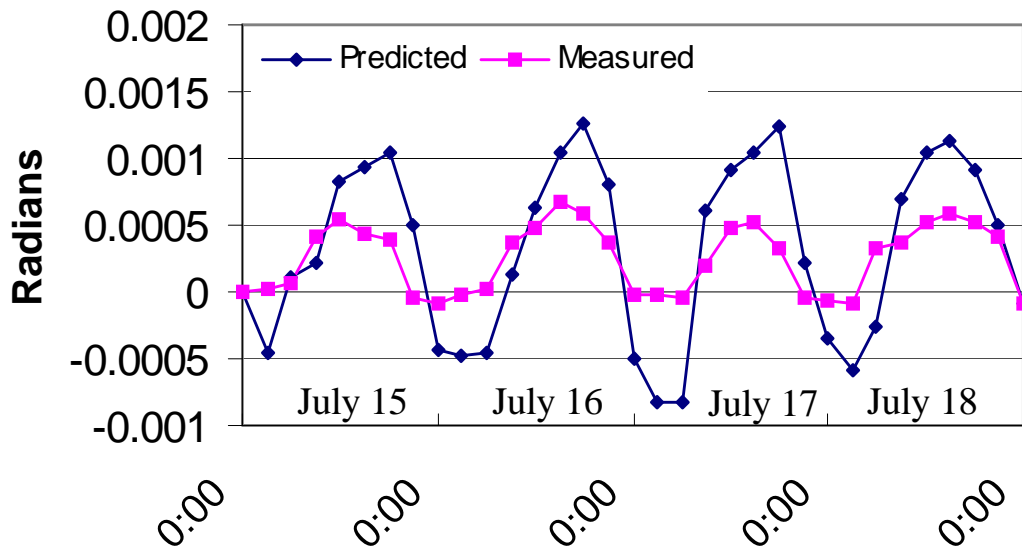
Figure 6.6 Transverse Rotations Of The Inner Girder At The Northern Pier, July 15-18, 1998

6.2.1.2 Longitudinal Rotations

Shown in Figure 6.7 are predicted and measured longitudinal rotations of the outer girder at the northern pier for the same period. In this study, positive longitudinal rotations are taken such that, under positive longitudinal rotation, the bottom flanges of the girders are in compression, while the top flanges and slab are in tension. It is seen that measured longitudinal rotations at this location are actually larger than predicted values. These differences are probably due to potentiometer error. The bottom flange plates are thick near the supports, and internal diaphragms are present, as well, which would preclude localized large rotations. The bearing plates, as described earlier, are stocky, as well. Even still, the differences seen here are physically very small and of minor consequence.
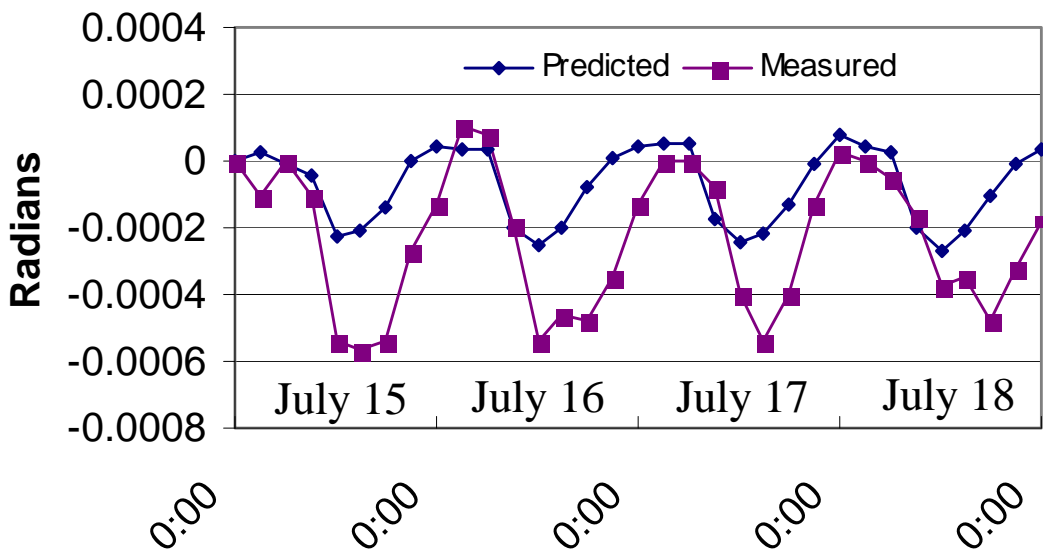

Figure 6.7 Longitudinal Rotation Of The Outer Girder At The Northern Pier, July 15-18, 1998

Figure 6.8 is a similar plot; shown are predicted and measured longitudinal rotations of the inner girder at the northern pier for the same period. It is clear

that measured rotations at this location again correlate relatively well with predicted values. What is surprising is the fact that there are larger longitudinal rotations, predicted and measured, at this location than there are at the outer girder for the same time. Intuitively, it seems that the outer girder, with its longer length and thus smaller stiffness, should encounter larger rotations. However, it will be recalled from Chapter 3 that there are often significant temperature differences between the slab and girders. These temperature differences, occurring through the depth of the bridge section, are what cause longitudinal rotations to occur. Further, it will be noted from Figure 6.8 that the largest (absolute) rotations are seen to occur at the 18:00 time step for each day in this analysis. It was shown in Chapter 3 that the inner girder's maximum temperatures typically occur around this time, and that this time is the time of the maximum differences between slab and inner girder temperatures. Finally, it will be recalled that negative longitudinal rotations induce tension in the girder's bottom flange, i.e., the bottom flange is stretched. It thus makes sense that the largest absolute rotations shown in Figure 6.8 are negative, as the girder was shown in Chapter 3 to be significantly warmer than the slab during these late-afternoon hours, and will elongate more than the slab will, inducing the negative rotations seen here.
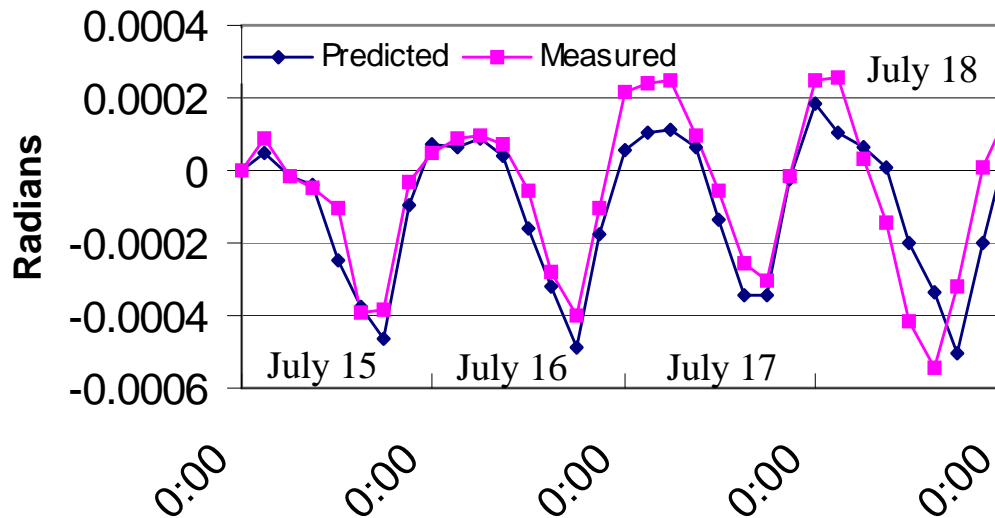
Figure 6.8 Longitudinal Rotations Of The Inner Girder At The Northern Pier, July 15-18, 1998

6.3   Rotation Histories

As displacement histories were examined, rotation histories will be examined presently. For brevity, only the first weeks of each month are shown, and only the months March-October are included. It will be seen that this is sufficient to determine long-term rotational behaviors at the bearings. Shown in Figure 6.9 are transverse rotations at the northern pier. It is clear from this plot that, at this location, both girders spend the cooler months twisted inward and spend the warmer months twisted outward. It is also clear that the girders return to positions near their original configurations over time. Finally, it is also clear that the magnitude of transverse rotations induced at the northern pier is very small throughout the instrumentation period.
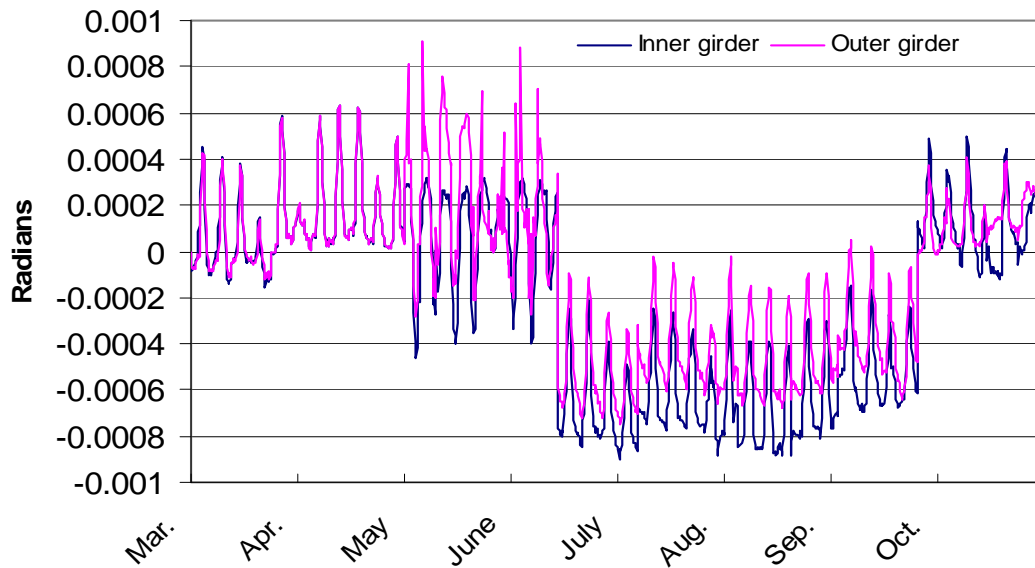
Figure 6.9 Transverse Rotation History At The Northern Pier

Shown in Figure 6.10 are longitudinal rotations at the northern pier for the same period. This plot is somewhat more ambiguous than the previous plot. It is seen that, in the early months of the instrumentation, the girders undergo nearly the same rotations. In the warmer months, however, the rotations appear to "mirror" each other about the zero axis. It is clear again, however, that the thermally-induced rotations at this pier in the longitudinal direction were much smaller than the bearing capacities over the entire duration of the study.

Shown in Figure 6.11 is the transverse rotation history at the southern pier. It is seen that, as with the northern pier, the girders spend the cooler months twisted inward and the cooler months twisted outward. Again, they are also seen to return to their original positions, and induced rotations are again very much smaller than the bearing capacities.
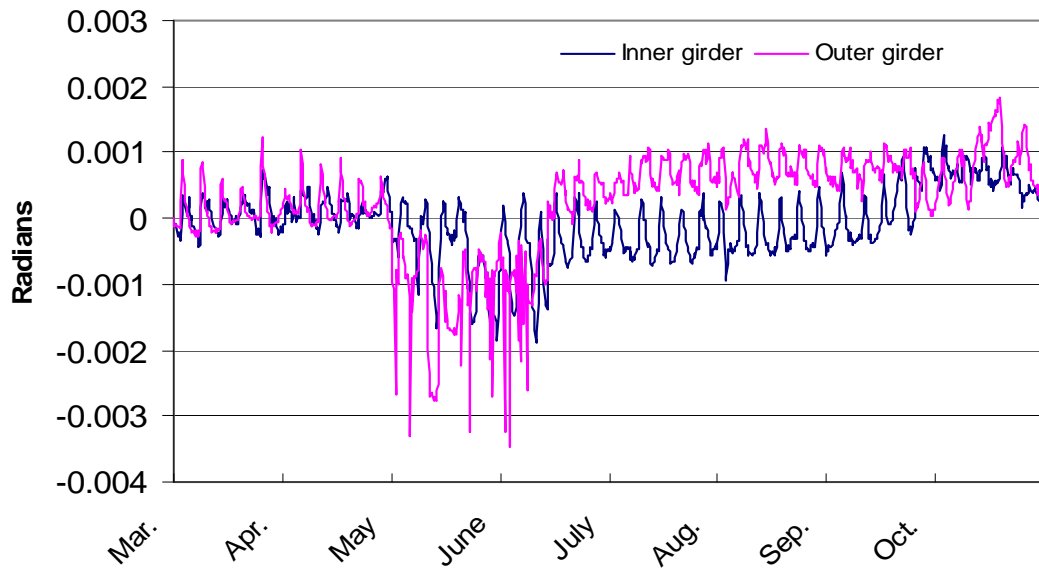
Figure 6.10 Longitudinal Rotation History At The Northern Pier
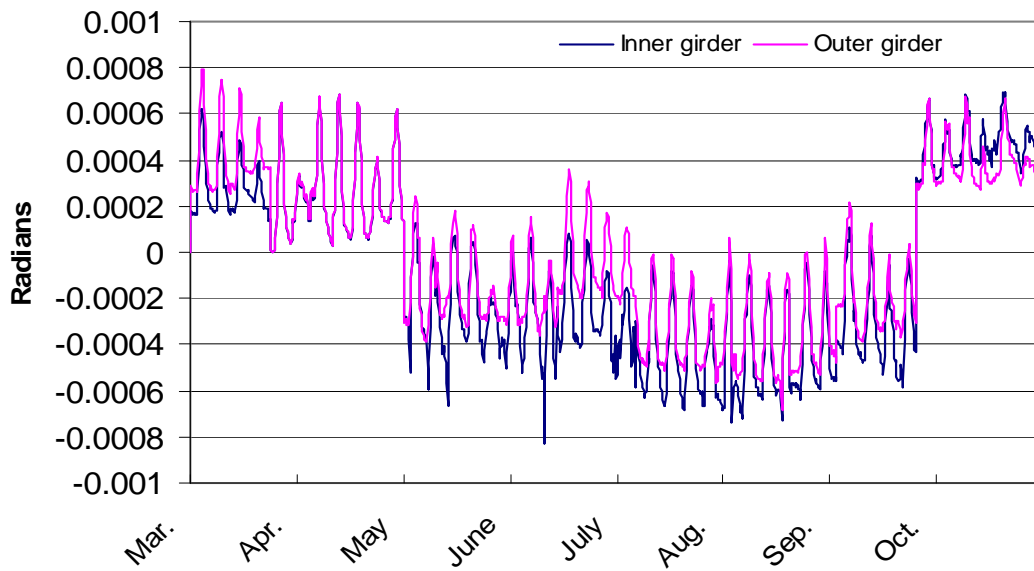
Figure 6.11 Transverse Rotation History At The Southern Pier

Finally, Figure 6.12 shows the longitudinal rotation history at the southern pier. As with the longitudinal rotation history at the northern pier, this plot is more ambiguous than the transverse rotation history plots. However, it is clear that both girders rotate near their original positions and that induced rotations are again much smaller than the capacities of the bearings.
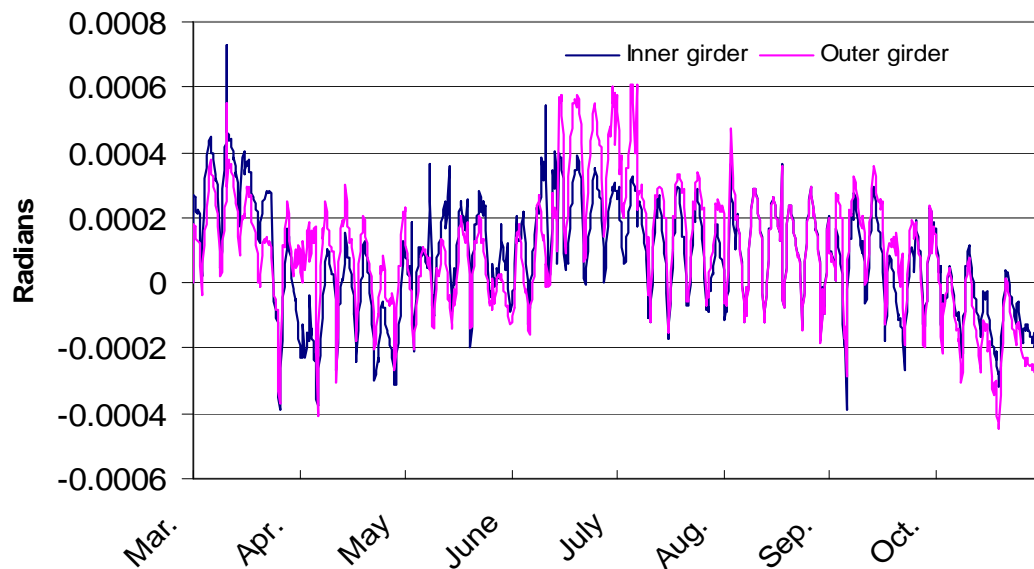
Figure 6.12 Longitudinal Rotation History At The Southern Pier

Maximum rotations in both directions at each pier, and the vector combination of each, are listed in Table 6.1. The combination of the rotations in orthogonal directions as a vector is somewhat conservative, as it is unlikely that maximum rotations in the orthogonal directions will occur simultaneously. These are the maximum recorded rotations during this study.

Table 6.1 Absolute Maximum Recorded Rotations And Their Vector Combination Magnitudes

Northern Pier			Southern Pier		
Longitudinal	Transverse	Combined	Longitudinal	Transverse	Combined
0.00345 rad	0.0009 rad	0.0036 rad	0.0007 rad	0.0008 rad	0.0011 rad

6.4   Summary and Conclusions

Having examined both daily and long-term rotations at the bearings in both principal directions, conclusions may now be drawn regarding the rotational behavior of the girders at the bearings.

1. As expected, rotations do in fact occur in both principal directions at the bearings. It was described that with the instrumentation used in this study, rotations about the two principal horizontal axes of the bridge could be separated at each measurement time. It was shown that rotations do occur in both of these directions, and that there is no apparent "preferred" direction of rotation of the girders.

2. In general, measured rotations are somewhat smaller than predicted values. It has been seen during the investigation of rotational behavior from July 15-18 that measured rotations tend to be smaller than finite element predictions would account for. It was discovered, however, that longitudinal rotations of the inner girder at the end pier were measured to be larger in magnitude that theory predicts, but the physical differences between the two quantities were still quire small and may be caused by potentiometer error.

3. Both daily cycles of rotation and long-term rotations are substantially smaller than the pot bearings in use will allow. This has been shown in some detail. It was described in Chapter 1 that pot bearings typically allow for girder rotations up to 0.04 radian in magnitude. It has also been seen that, even through the largest temperature changes of the year, from February to August, this limit is not nearly approached at any of the bearings in use in this bridge.

Chapter 7

Finite Element Stress Predictions

It was shown in Chapter 5 that, while longitudinal displacement cycles in this bridge follow those predicted by a finite element model of the bridge, the measured displacements are typically not as large in magnitude as those predicted by the model. While the differences between measured and predicted transverse displacements are not very large, there is typically a lag between the times of peak displacements predicted by the model and peak measured displacements. Finally, it was also seen in Chapter 6 that, while rotation cycles generally correlate well with predicted cycles, rotation magnitudes can often be larger or smaller than predicted magnitudes.

It was also shown in Chapter 1 that if thermally-induced displacements and rotations are not allowed to occur freely, stresses will develop. The bridge under study was not instrumented for strain measurements which could be used to measure stresses during the period of study. The SAP 2000 program allows the input of prescribed displacements as well as thermal changes over time. SAP 2000 then outputs stresses at each joint of each shell element. Stress predictions can be obtained, however, stress measurements are not available for comparison. SAP 2000 was used in this manner to gain insight into what magnitudes of stresses could be developed in this bridge when measured displacements and rotations do not match predicted values. These findings are presented in this chapter.

It should first be noted that stress results presented herein are approximate. There are several unknown factors which influence these predictions. It has been

shown that measured deformations often do not match theoretical values, but the causes of these differences cannot be known exactly. In addition to friction in the bearings, potentiometer error is a possible cause of the differences. The measurements may thus not always be exact. The thermal changes imposed upon the analytical model are also approximate. The exact temperature distribution throughout the structure is impossible to ascertain with the instrumentation used, so changes in mean temperatures of the elements were used in the analysis, which is an approximate procedure. It will be recalled that mean respective girder temperatures were calculated at each cross-section, and both cross-sections were included in determining mean girder temperatures. These mean temperatures were applied over the entire length of the bridge, which is not exactly correct. Finally, pier deflections may accommodate thermally-induced bridge deformations, thus relieving stress buildup within the structure.

The first portion of this chapter is devoted to a study of the worst-case stress conditions which may be expected to occur in the structure. In this analysis, the piers are considered rigid, so that inhibited deformations must cause stress buildup within the bridge superstructure. Temperature changes and displacement differences are input to the SAP 2000 bridge model, with girder and slab stresses obtained as output. In the second portion of the chapter, pier deflections as monitored in the existing structure will be examined.

7.1   The Use of Enforced Displacements to Obtain Stress Output

The user can prescribe displacements into SAP 2000 input files as well as temperature changes to determine stresses within the structure. The use of this option will be illustrated here with a simple example.

Consider a uniform bar fixed at one end, as shown in Figure 7.1a. Suppose it is subjected to a uniform temperature increase ΔT. Elastic theory indicates that

the bar would stretch an amount $\Delta L = \alpha L \Delta T$, where L is the original length of the bar, and α is the coefficient of thermal expansion of the bar's constituent material.
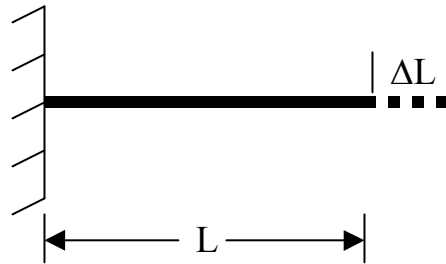
Figure 7.1a. Free expansion of a bar under uniform temperature rise.

Now consider the same bar, subjected to the same rise in temperature, but restrained so that it can only expand an amount $\Delta < \Delta L$, as shown in Figure 7.1b. Elastic theory dictates that the bar will develop a compressive stress equal to:

$$\sigma = \frac{E}{L}(\Delta - \Delta L).$$
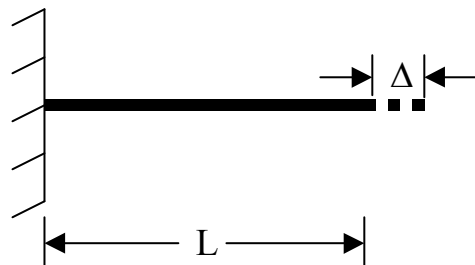
Figure 7.1b Bar under thermal expansion $\Delta < \Delta L$

Restraining displacements allows the computation of stresses within the bridge under the measured temperatures and displacements. The procedure used to calculate thermally-induced displacements was described in Chapter 5. One

additional step is necessary to obtain stress predictions. As with any structural analysis program, correct modeling of boundary conditions is essential for the correct analysis of the structure. Boundary conditions used in the displacement analyses were described in Chapter 5. These boundary conditions must be modified to obtain stress computations, however. In order to prescribe displacements in SAP 2000, the joint in question must be restrained against displacements in the direction of prescribed displacement. For example, a prescribed joint displacement at a roller support is achieved by changing the roller support to a pin support. The reaction forces caused by the prescribed displacements are computed, and the boundary conditions are then restored back to their correct values. The procedure is outlined below.

1. Perform the analysis under thermal loading, as described in Chapter 5. That is, the only loads present are the three mean temperature differences calculated for each time step. Again, these temperature differences are those calculated for each girder and for the slab. The temperature change of each respective element is applied over the length of the element. This analysis yields theoretical displacements. This is shown in Figure 7.1a.

2. Calculate the differences between measured and theoretical displacements, as illustrated in Figure 7.1b.

3. Change the boundary conditions to prevent displacements at the joints considered. Perform the analysis again, with the displacement differences calculated in step 2 as the only load. These differences must be prescribed in the opposite direction to which they actually occur. This analysis yields reaction forces developed in the structure under the prescribed displacements. This is shown in Figure 7.2, where the reaction is denoted by "R."
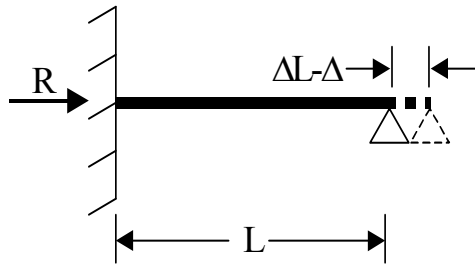
Figure 7.2 Bar Under Modified Boundary Conditions And Prescribed Displacement

4. Restore the boundary conditions to their correct configurations. Superimpose the reaction forces calculated in step 3 with the thermal loading used in step 1 as the load on the structure, as shown in Figure 7.3. Perform the analysis again. This analysis yields the desired shell stresses at the joints.
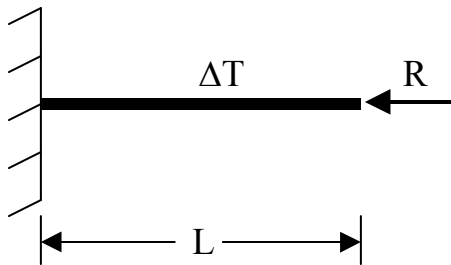
Figure 7.3 Bar Under Thermal Loading With Reaction Force Superimposed

7.2   Selection of Analysis Cases

Because the data collected during this study is quite voluminous, it is important to judiciously select conditions to be used in the analysis of predicted stresses in the bridge. It was desired to gain insight into the "worst-case" stress conditions which may arise.

It is important to note that, because the analysis of induced deformations is performed in a piecewise fashion, the displacement differences to be used in the stress analysis are those arising between two consecutive time steps in the analysis. For example, if a longitudinal displacement of 2 millimeters is predicted between two time steps and the measured displacement between the same steps is only 1 millimeter, the 1 millimeter difference is used in the analysis.

Inspection of Figure 5.15, the curves of measured and theoretical longitudinal displacements of the inner girder at the northern pier, show that typical differences between measured and theoretical girder extensions at individual time steps are between four and five millimeters. For the sake of conservatism, a difference of five millimeters was used in the stress analysis at the end pier. As described in Chapter 2, the potentiometer measuring longitudinal displacements at the inner pier typically yielded larger differences from theoretical values, so a longitudinal displacement difference of six millimeters was used at this support. This is conservative, as the bridge's expansion length at this pier is smaller than it is at the end pier. Also, as reliable longitudinal displacements of the outer girder were never obtained, it was assumed that the same differences occurring at the inner girder were also applicable to the outer girder. This may or not be what actually occurs in the structure, but there is no way of validating or invalidating this assumption. Thus, longitudinal displacements of five millimeters were imposed upon both girders at the end pier, and displacements of six millimeters

were imposed upon both girders at the inner pier. The far end bearing was not restrained.

Transverse displacement differences were neglected in the analysis. Inspection of plots presented in Chapter 5 of these displacements shows that differences between measured and theoretical values of transverse displacements are typically small, and that measured girder translations typically "catch up" with theoretical values. That is, peak theoretical displacements are larger than measured values, but the measured displacements often reach values near the theoretical peaks within one additional time step. Also, because the bridge spans are relatively long, the bridge is somewhat flexible with respect to lateral translations. In fact, preliminary transverse displacement restraint analyses revealed that induced stresses are substantially smaller than stresses caused by longitudinal displacement restraint. Also, because the thermally-induced rotations in the structure were shown in Chapter 6 to be significantly smaller than the bearings will allow, rotational differences were neglected in all the analyses.

It is necessary to superimpose thermal loading on the structure to gain accurate output of induced stresses. Because there are always thermal differences throughout the structure, it was necessary to use a single bridge temperature in the stress analysis so that the magnitudes of induced stresses could be compared meaningfully. For this purpose, a change in the bridge temperature (all elements were included) of 40°C was used in all the analyses. This is a reasonable approximation of the entire temperature range the bridge may be expected to undergo during a year.

In order to gain insight into the stresses induced, a separate analysis was performed to determine the stresses which arise under thermal loading only, with the "real" boundary conditions. If the bridge were straight, stresses would not arise under the boundary conditions used, as the same temperature change was applied to all the elements in the model. Because the bridge is curved, however,

and guided to prevent transverse displacements at the end pier, stresses will arise. These stresses were computed for comparison to stresses arising under the restrained longitudinal displacement analysis.

Finally, the stresses examined were limited to those occurring in the bottom flange of the inner girder and in the slab. Bottom flange stresses are examined to determine whether the possibility of flange buckling could result, while slab stresses are examined to study the possibility of slab cracking under tension.

7.3   Predicted Stress Values Under Longitudinal Restraint

As stated above, even in the absence of imposed restraints, this bridge will still develop stresses under "free" thermal expansion. It will be recalled that the supports at the end instrumented pier are guided to prevent translation in the transverse direction, and thus induce stresses within the structure. In fact, if these restraints are not provided within the structure, the bridge becomes unstable with respect to rotation about a vertical axis. This is the case even under uniform temperature changes through the structure. Because of the presence of stresses within the girders at all times, stresses induced by enforced displacements (restraint of free deformation) only become relevant when compared to stresses arising under thermal loading in the absence of enforced restraints. That is, stresses induced by displacement restraint are only meaningful when compared to stresses arising under the friction-free boundary conditions.

7.3.1   Bottom Flange Stresses

In this section, tensile stresses are taken as positive, and compressive stresses are negative. Also, the guided instrumented bearing will be referred to as "Bearing 1," the free instrumented bearing will be referred to as "Bearing 2," the

fixed bearing will be referred to as "Bearing 3," and the last free bearing (not instrumented) will be referred to as "Bearing 4." Shown in Figure 7.4 are bottom flange stresses along the girder length for the case of unrestrained thermal expansion. These stresses are taken along the centerline of the bottom flange of the inner girder. It is clear that the flange is in a state of tension throughout the length of the bridge, and that the tensile stresses are small. It is also clear that the presence of Bearing 3 leads to a stress concentration, as it absorbs the reaction due to the thermal strain accumulated along the length of the structure. Finally, it is seen that the stresses at the ends of the girder are very close to zero. This is to be expected, as there is no load other than the temperature change present. Locations of the bearings are shown.
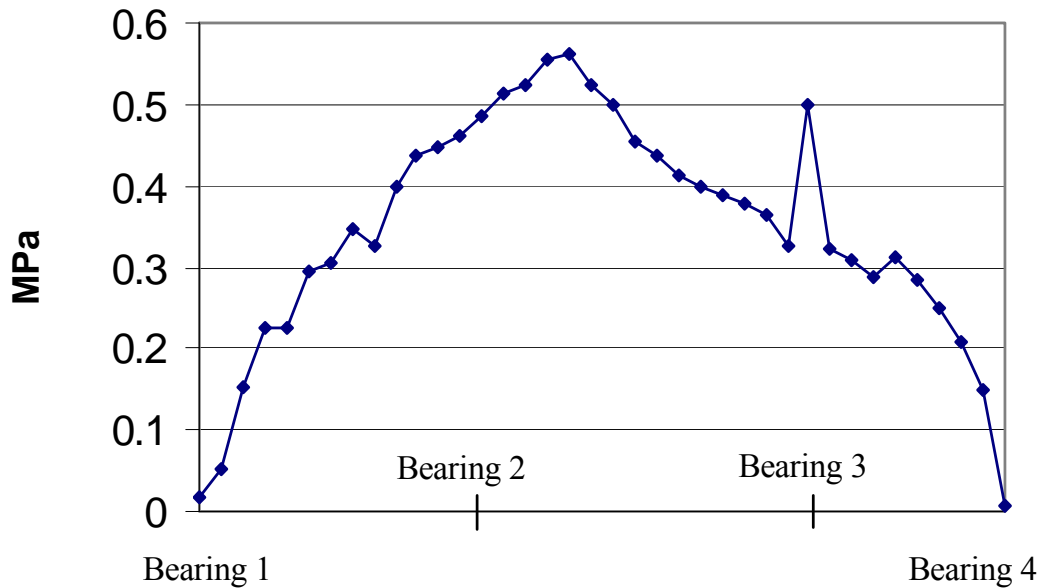
Figure 7.4 Inner Girder Bottom Flange Stresses Under No Restraint

Shown in Figure 7.5 are bottom flange stresses caused by the longitudinal displacement restraints at Bearings 1 and 2, as shown in the figure. Bearing locations are again shown. As expected, regions of the girder under displacement restraint are under compression. It is clear that there are stress concentrations at the "free" bearings, in addition to the reactive stress Bearing 3. This is because these bearings are where the displacement restraints are imposed upon the structure.
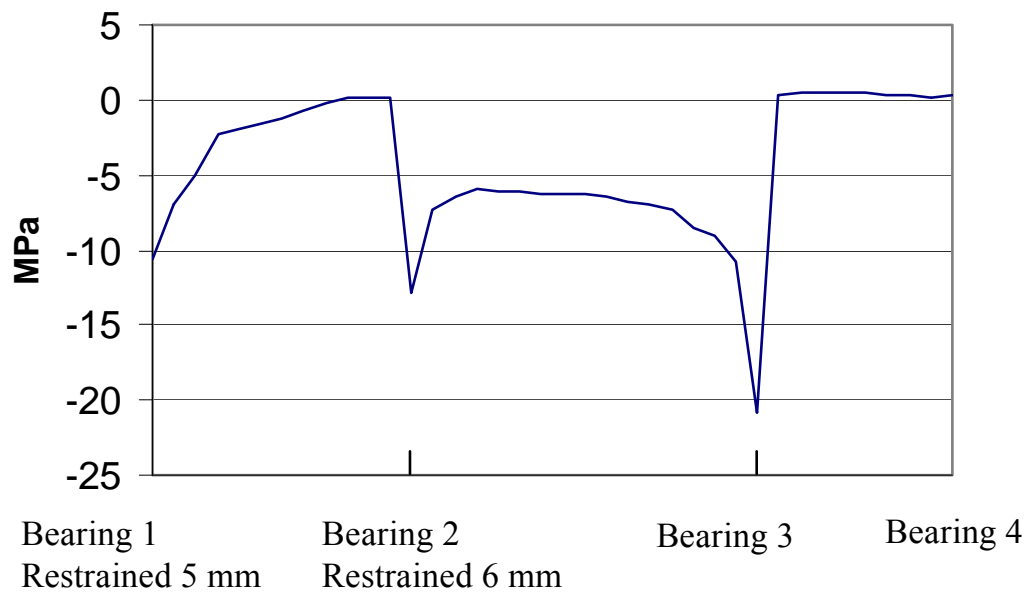
Figure 7.5 Girder Bottom Flange Stresses Under Longitudinal Restraint

It is also clear that the stress concentration at the Bearing 2 is larger than that at the end bearing. This is due to two factors. First, as described earlier, a larger longitudinal displacement was imposed at this bearing than at Bearing 1. Second, the girder's expansion length at Bearing 2 is significantly smaller than at Bearing 3, making the girder stiffer at this location with respect to longitudinal

displacements. Thus, a prescribed displacement will require a larger force to impose the displacement, leading to larger induced stresses. It is then clear that there is a relatively large stress concentration at the fixed bearing, where the reaction due to the imposed displacements is developed. Finally, it is seen that the girder achieves a state of tension beyond the fixed bearing. These stresses are identical to those presented in Figure 7.4 in the same span. This is to be expected, as axial displacements and stresses are unrelated between bearings 3 and 4.

It is also clear that the compressive stresses developed in the bottom flange are considerable. The peak compressive stress shown here is approximately 21 MPa. The bridge girders are composed of 345 MPa steel, so that the peak compressive stress is approximately 6% of the yield strength of the steel used. Although bottom flange stiffeners are always used in the region of peak stress shown here (at the fixed bearing), it must be remembered that these induced stresses are in addition to stresses arising under gravity loading. That is, flange buckling is probably precluded from occurring under these stresses, but localized yielding may still occur. Also, although tensile stresses near the end support will counter the compressive stresses shown here, it must be recalled that the tensile stresses will generally be small, as the gravity stresses reach zero values at the end of the span. Additionally, bottom flange stiffeners are not used in the end support regions to increase the buckling capacity of the bottom flange.

7.3.2 Slab Stresses

Shown in Figure 7.6 are slab stresses induced under thermal loading in addition to the longitudinal displacement restraint. The general shape of this curve appears to be the same as that of the curve of bottom flange stresses, reflected about a horizontal axis. Peak stresses at the supports are now tensile, instead of compressive.

Of interest here are the peak tensile stresses. For concrete with a compressive strength of 41.3 MPa, the cracking stress is nearly 4.0 MPa. It is then seen that, at the fixed bearing, the slab is at the verge of undergoing tensile cracking. This is significant. Although the thermal change imposed upon the structure for this analysis is somewhat conservative (i.e., the temperature change imposed is that which may reasonably be expected to occur over an entire year), the displacements imposed are typical values which were observed. The possibility of slab cracking can thus not be ruled out.
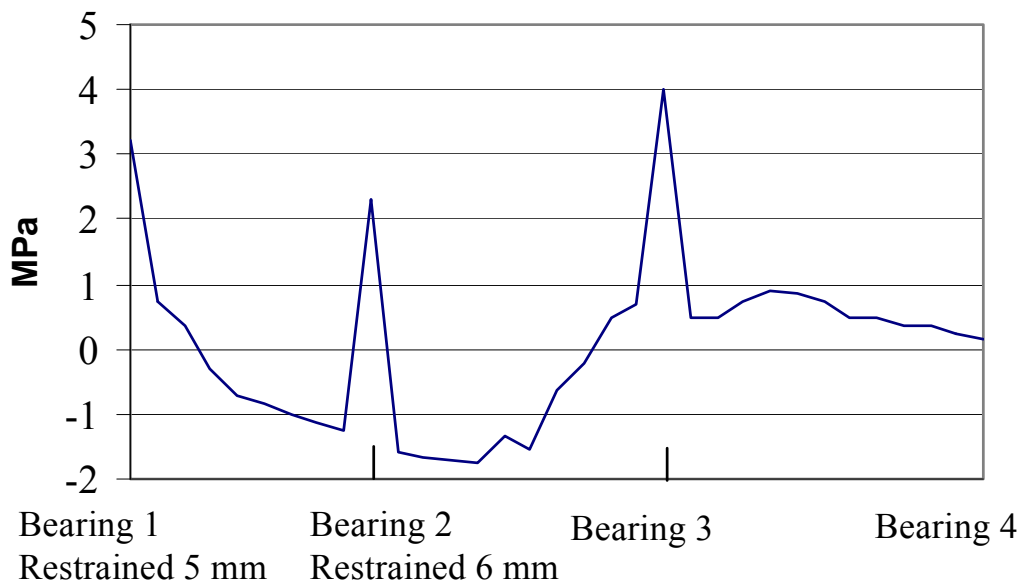
Figure 7.6 Slab Stresses Under Longitudinal Restraint

7.3.3 Remarks on Stress Output

The stress states reported here are only included for illustrative purposes, and for comparison between "frictionless" boundary conditions and restrained boundary conditions. The stresses shown are only to illustrate the changes which occur under the restraint of deformations. These would, of course, be impossible to quantify during the design phase of such a structure, and, as described previously, are in addition to those stresses which may be expected to occur under gravity loading. It has been seen that significant stresses may indeed result.

Finally, the stresses shown were all calculated under the assumption that the bridge piers are immovable supports. It was described that this analysis involves restraining the "free" deformations, computing the resulting forces imposed upon the girders, and running the analysis again with the forces included. In the real structure, however, these forces are resisted by the bridge piers. If the piers were to deflect appreciable amounts, the stresses induced under restrained deformations would be reduced. The instrumentation of the two previously-instrumented piers to measure pier deflections via plumb bobs was described in Chapter 2. Measurements of pier deflections during a day will be described next.

7.4 Measured Pier Deflections on August 12, 1998

7.4.1 Pier Flexural Stiffnesses

As described previously, the two instrumented piers are of different heights. The southern pier has a height of approximately 13.4 meters, while the northern pier has a height of approximately 9.75 meters. The northern pier has a large flare at the top, as there is an unfinished access ramp at this location. The contribution of the flared top to the stiffness of the pier was neglected. That is, its

height and dimensions were not included in the stiffness calculation. The inclusion of the flare effectively makes the pier infinitely stiff at the top. The largest pier bending occur at the base of the pier, not at the flare.

The southern pier has cross-sectional dimensions of 3.05 m x 1.8 m, with the weak axis oriented along the bridge's tangential direction. The northern pier has cross-sectional dimensions of 3.65 m x 2.4 m, with its weak axis also oriented along the bridge's tangential axis.

There are two extreme cases when considering the flexural stiffness of the piers with respect to displacements at the tops of the piers. The first is to consider the piers as cantilevers protruding from the ground. The stiffness of the piers in this case is $3EI/L^3$, where "L" is the height of the pier and "I" is the moment of inertia in the direction being considered. The second case is to consider the piers as fixed-ended, with a stiffness of $12EI/L^3$. Because, in theory, the bearings allow girder rotations to occur, it was assumed that the girders, acting through the bearings, offer no restraint to pier bending. Thus, pier stiffnesses were assumed as $3EI/L^3$. For concrete with a compressive strength of 41.3 MPa, the elastic modulus is 30,400 MPa. The moment of inertia of the northern pier, in the tangential direction, is $(3.65)(2.4)^3/12=4.20$ m^4. The moment of inertia in the transverse direction is $(2.4)(3.65)^3/12=9.72$ m^4. Thus, the stiffness of the northern pier, in the tangential direction, is $3(30,400)(4.20)/(9.75)^3=413.2$ kN/mm. The stiffness in the transverse direction is $3(30,400)(9.72)/(9.75)^3 =957$ kN/mm. In the same fashion, the longitudinal stiffness of the taller southern pier is 58 kN/mm, and the transverse stiffness is 161.4 kN/mm.

7.4.2   Field Measurements of Pier Deflections

The pier deflections from 6:00 until 18:00 on August 12 were monitored while the computerized instrumentation was also recording temperatures and

deformations. In a manner identical to that described in Chapter 5, an analysis was performed to determine theoretical displacements and rotations, for comparison to values recorded by the instrumentation. Longitudinal displacements of the inner girder at the end pier are shown in Figure 7.7.

It is clear that there are substantial differences between theoretical and measured displacements. Pier deflections resulting from SAP 2000-predicted reactions at the bearings were not computed. Instead, pier deflections were measured, and resulting forces at the pier caps will be computed. As will be seen shortly, this led to additional insight into the "real" behavior of the structure.
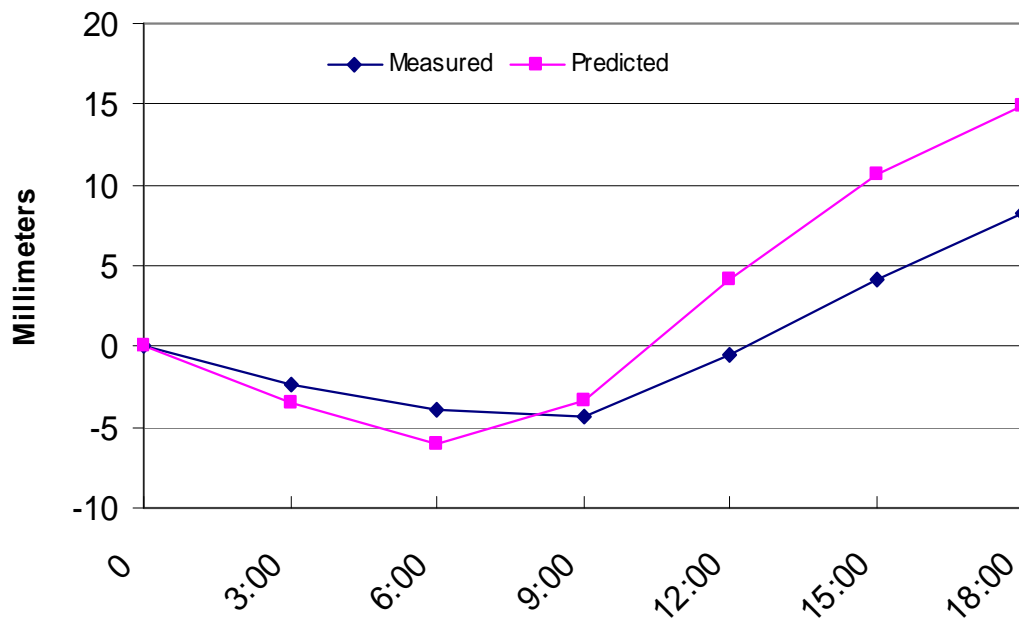
Figure 7.7 Measured And Predicted Inner Girder Translations At The End Pier, August 12, 1998 (Displacements At The Bearing)

7.4.2.1 Northern Pier Deflections

Measured displacements of the northern pier in the longitudinal direction are tabulated in Table 7.1. For purposes of this presentation, longitudinal displacements at both piers will be taken as positive in the northern direction and negative in the southern direction. It should also be noted that deflections are with respect to the bridge's position at 6:00. That is, the SAP 2000 analysis was carried out from midnight until 18:00, but plumb bob positions were taken relative to their positions at 6:00.

Table 7.1 Northern Pier Deflections On August 12, 1998

Time	Deflection
9:00	1.6 mm
12:00	3.2 mm
15:00	1.6 mm
18:00	1.6 mm

It is clear from the table that small displacements are measured. These deflections, when added to measured displacements at the bearing, should approach predicted values from the finite element model. Figure 7.8 shows the same curve of predicted displacements shown in Figure 7.7, along with a curve depicting the sum of pier deflections and measured displacements at the bearing. It is seen that these curves plot more closely to each other than the curves in Figure 7.7. The northern pier deflections, when added to measured displacements at the bearing, approximate values of girder displacement predicted by the finite element analysis. There is still some inevitable error. As described earlier, the

temperature representation used in the finite element analysis is approximate. Boundary conditions are not exactly correct, and the pier deflection monitoring system used was prone to error, as well. Nonetheless, the fact that the combination of girder displacement and pier deflection approximates predicted values of girder translation is evidence that the combination of these two factors is how the bridge accommodates temperature changes, at least at the northern pier. It will be recalled that there is a clogged expansion joint over this pier, and that there are concrete U-beams framing into the pier, supported by elastomeric bearing pads. These pads will prevent translations of the concrete beam ends, thus introducing more frictional forces at the pier cap. Also, the instrumentation used to monitor pier deflections is not perfect, and is prone to measurement error.
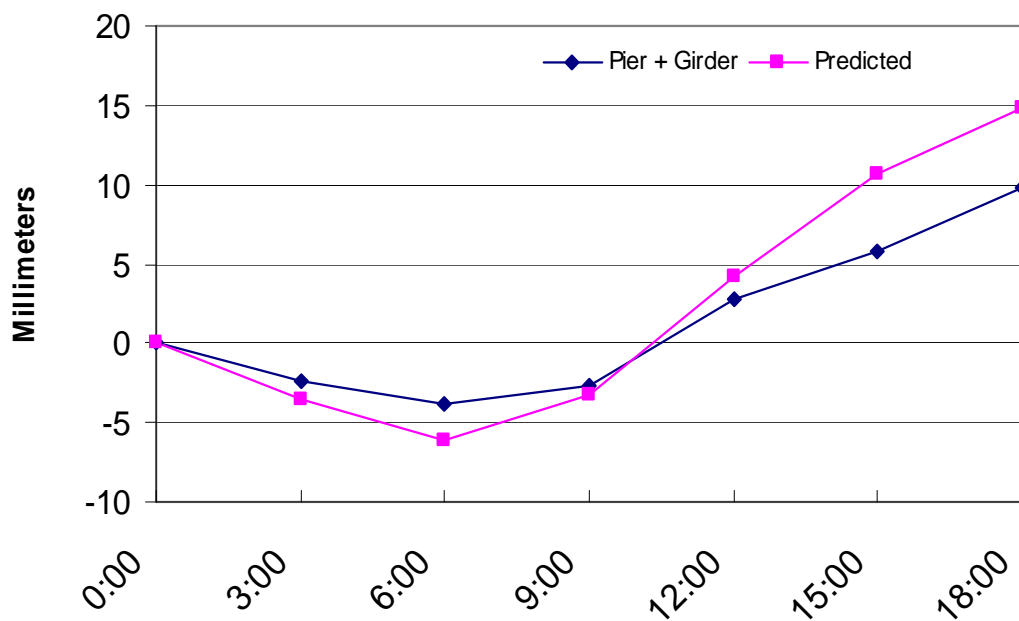
Figure 7.8 Predicted Deformations And A Curve Of Measured Displacements At The Bearing Plus Measured Pier Deflections

7.4.2.2 Southern Pier Deflections

Southern pier deflections in the longitudinal direction as measured during August 12 are tabulated in Table 7.2. The sign convention used is the same as that for end pier deflections. It is clear that larger deflections were measured at this pier. These deflections were added to deformations measured at the bearing on the southern pier as with measurements at the northern pier. Results are shown in Figure 7.9. It is clear from this chart that pier deflections, when added to girder translations at this location, exceed values predicted by the finite element analysis. This is an unexpected occurrence. Again, there are several possible causes of error in this analysis as described earlier, but it is seen that the measurements are significantly larger than the predicted values.

Table 7.2 Southern Pier Deflections On August 12, 1998

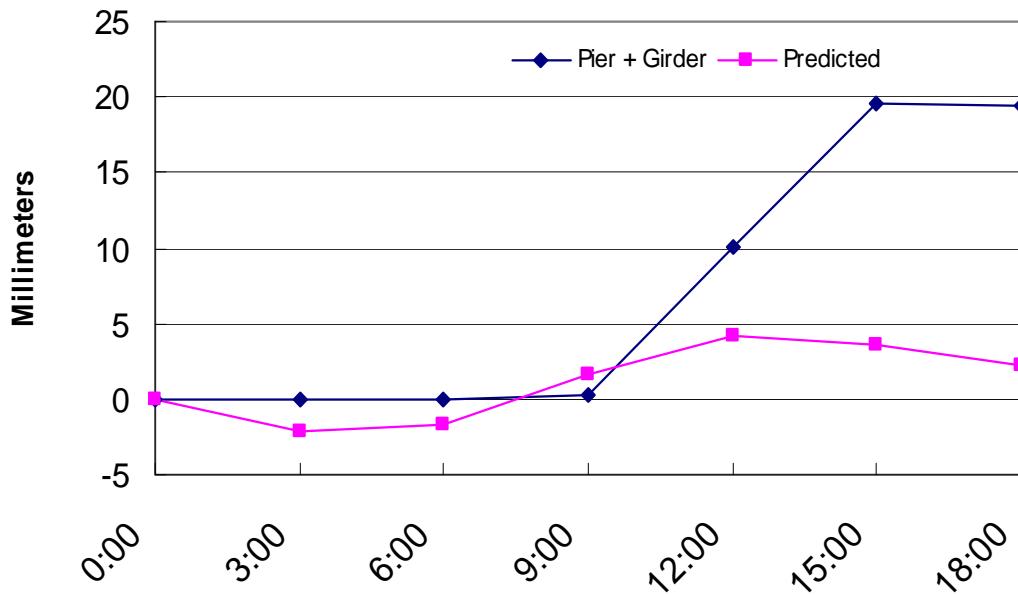| Time	Deflection
9:00	1.6 mm
12:00	9.5 mm
15:00	19.1 mm
18:00	19.1 mm

Figure 7.9 Predicted Deformations And A Curve Of Measured Displacements At The Bearing Plus Measured Pier Deflections

In determining causes for this result, several factors must be borne in mind. First is the bridge geometry. The condition at the northern pier, with concrete U-beams framing into the pier cap adjacent to the steel girders, is repeated at the opposite end pier. It may thus be hypothesized that the ends of the steel spans are stiffened by the presence of adjacent concrete beams. Also, the bearing which was nominally taken as fixed in this study (Bearing 3), is not fixed in the field condition. In fact, this bearing is supported by the tallest pier in this bridge. The pier adjacent to this is the "southern" pier, where these large deflections have been measured. These two piers are the most flexible in the system, and are located adjacent to piers which are more fixed than their idealized bearing conditions would indicate. It then seems possible that the taller piers, including the southern pier, are "bowing out" in space under thermal changes in the bridge

186

superstructure. This would explain the small girder deformations measured at the southern pier, while also explaining the relatively large deflections measured at the southern pier base. Friction in the system, including additional, unaccounted-for stiffness contributions, is more likely to be accommodated by the taller, more flexible "inner" piers.

7.5   Pier Lateral Forces

It is of interest to calculate lateral forces resulting from the measured pier deflections. This is performed using the simple relation $P=k\Delta$, where "k" is the lateral stiffness of the pier, and "Δ" is the measured deflection. Knowing measured pier deflections during August 12, pier forces at each time of measurement may be calculated. These are tabulated in Table 7.3 for the northern pier, and in Table 7.4 for the southern pier.

Table 7.3 Lateral Forces Imposed Upon The Northern Pier On August 12, 1998

Time	Lateral Force
9:00	661 kN
12:00	1322 kN
15:00	661 kN
18:00	661 kN

Table 7.4 Lateral Forces Imposed Upon The Southern Pier On August 12, 1998

Time	Lateral Force
9:00	93 kN
12:00	551 kN
15:00	1108 kN
18:00	1108 kN

It is clear that somewhat large forces result, particularly at the inner pier. It may thus be called into question whether the bearings could even transmit these lateral forces to the pier caps. However, is must be borne in mind that the pier stiffnesses were calculated under the assumption that the piers are perfect cantilevers, supported by rigid bases. This is never true in reality. In fact, small rotations at the base of the piers will greatly reduce the forces required at the tops of the piers to cause these deflections.

Consider the northern pier. It was described above that the height of this pier is 9.75 meters. A maximum deflection of 3.2 mm was measured during August 12. Thus, at the time of maximum measured deflection, a rotation, or tilting, of the pier's base of 3.2mm/9750mm=0.00033 radians will reduce the lateral force at the top of the pier to zero, allowing the pier to rotate as a rigid body. This is a small rotation, certainly possible in real field conditions.

Now consider the southern pier. The height of this pier is 13.4 m, and the largest measured deflection was 19.1 mm. Thus, a rotation of 19.1mm/13400mm=0.0014 radians at the base of the pier will allow the pier to rotate as a rigid body, allowing this deflection to occur in the absence of imposed forces at the pier cap. This also seems possible in the field condition. For both piers, the actual condition is likely somewhere between the extremes. That is, the piers are likely not rotating as rigid bodies, but there is very likely some rotation

occurring at the bases of the piers, drastically reducing the forces at the pier caps. It is thus possible for all measured displacements, both of the girder at the bearing and of the pier caps, to occur without requiring unrealistic imposed forces at the pier caps.

7.6   Summary and Conclusions

Stress states have been examined for typical differences between measured and theoretical values of longitudinal deformations at the instrumented bearings. Pier stiffnesses and deflections were also considered and illustrated. Conclusions may now be drawn on results presented in this chapter.

1. In the absence of pier deflections, significant changes in the stress states within the girders may result. Axial stresses induced in the inner girder at the end pier were examined, assuming the piers rigid. It is clear that changes in stress states occur when the predicted deformations are inhibited. The yield strength of the steel girders is 345 MPa. The induced stresses due to restraint of deformations do not greatly reduce the capacity of the section, but it will be recalled that these induced stresses are in addition to stresses already present due to gravity loading. These stresses would be impossible to calculate in the design of such a bridge, as it would not yet be known how the naturally-occurring deformations may be inhibited during the service life of the bridge. They are included here only to illustrate that stress states can indeed change significantly under restraint of deformations. It was also shown that, in the absence of pier deflections, the concrete slab over the fixed bearing may be at the verge of tensile cracking.

2. The instrumented piers are quite stiff, and pier deflections are occurring. Pier deflections have been measured, but deflection measurements are prone to error, so it is difficult to know with certainty their values. The instrumentation scheme

for monitoring pier was adequate to verify that pier deflections are occurring due to the restraint of deformations, however. Because the piers were idealized as cantilevers supported by rigid bases, it was found that large forces are often required to cause these deflections. It is doubtful that the bearings could transmit such forces to the pier caps. However, as was noted, relatively small rotations, or "tilts" of the pier bases will allow these deflections to occur. In the extreme case, these deflections may occur in the absence of lateral force, allowing the piers to rotate as rigid bodies.

3. It may be concluded that the bridge is accommodating thermally-induced deformations through a combination of girder deformations at the bearings, pier deflections, and the build-up of stresses within the girders. Some amount of force generated is also absorbed by the slab and concrete beams in an adjacent span, acting through the clogged expansion joint. The stress states shown were for two cases. One was the occurrence of stresses due to thermal loading only. These stresses arise because the bridge is not perfectly free to deform, but in fact has the restraint of transverse displacements at the end pier. The second case was the development of stresses due to the restraint of deformations, in accordance with measured deformations and theoretically-computed deformations. These stress states were computed based on the assumption that the bridge is supported by rigid piers. It was shown that in fact the piers are very stiff, but that pier deflections are occurring.

It was hypothesized that the concrete beams in adjacent spans, supported by elastomeric pads, stiffen the end piers of the steel spans somewhat. It was also hypothesized that friction in the bridge superstructure system is accommodated by relatively large deflections of the tall, flexible inner piers, such as the southern instrumented pier in this study.

The behavior of this bridge due to thermal changes over time has been analyzed exhaustively. Girder translations and rotations have been analyzed, as have pier deflections which help the superstructure accommodate thermal changes. The temperature distributions throughout the bridge have been analyzed in detail, as well. In the next chapter, summaries and conclusions will be drawn on this phase of Texas Department of Transportation Project 1395.

Chapter 8

Summary and Conclusions

8.1   Thermal Behavior of the Bridge

The instrumentation scheme used collected 37 bridge temperatures along with the local air temperature on an hourly basis. It was found that there are always temperature variations present throughout the bridge superstructure. The Emerson Mean Bridge Temperature, based on equilibrium principles, was evaluated for each data collection time, and it was discovered that the Emerson Mean Temperature of the bridge is always warmer than the local air temperature. The Emerson Mean Temperature approaches the air temperature in the early morning hours, and, due to radiant heating, increases above the air temperature as temperatures rise throughout the day.

There are often significant steel temperature variations across the width of the bridge cross-section. This is due to differential radiant heating across the section. Specifically, it was seen that, at 18:00 on March 10, the warmest point in the bridge section was some 22 Celsius degrees warmer than the air. Such large differences above the ambient temperature frequently occur. It will also be recalled that the bridge has no asphalt overlay. The inclusion of such a surface would likely lead to even larger gradients, due to the asphalt's solar energy absorption.

The slab warmed at a slower rate than the steel girders, but, due to the thermal conductivity properties of concrete, stayed warm longer. It was seen that the slab could remain some 3-5 Celsius degrees warmer than the air several hours after the air and steel had started to cool.

There is typically a slight lag between the times of maximum air temperature and maximum Emerson Mean Bridge Temperature. The outer girder and surrounding air will typically achieve their maximum temperatures at nearly the same time. The slab and inner girder, however, usually achieve their maximum temperatures simultaneously, and this time is typically one or two hours after the air temperature is a maximum. The slab and inner girder temperatures influence the Emerson Mean Bridge Temperature enough so that this mean temperature lags the air temperature.

It was found that the AASHTO-specified maximum temperature to be considered for this bridge is slightly conservative, but reasonable. The specified minimum temperature is somewhat more conservative. The bridge never reached negative mean temperatures, but the AASHTO-specified minimum for this bridge is -18° Celsius. This is somewhat conservative. The specified maximum of 50° Celsius was nearly reached, as the maximum Emerson Mean Bridge Temperature achieved was 44ºC.

Finally, it was seen that the highest daily Emerson Mean Bridge Temperature reached typically exceeded maximum ambient temperatures by 4-5 Celsius degrees. The lowest Emerson Mean Bridge Temperatures reached were typically 1-2 Celsius degrees warmer than the surrounding air.

8.2   Thermally-Induced Translation Behavior of the Bridge

The bridge was instrumented to record girder translations at the bearings in the longitudinal and transverse directions. A finite element model was developed to estimate recorded measurements. It was found that translation trends in both directions follow both temperature and theoretical trends. Displacement magnitudes in both directions, however, are smaller than those predicted by the model. Differences were seen to typically vary between 30-50% of theoretical

values. Reasons for these differences were hypothesized as friction in the bearings, and possible instrumentation (potentiometer) error. The system (either the bearings or the instrumentation) often appeared to "lock up" and failed to record daily maximum values of displacement that would be expected. The system will recover in time and continue to record displacement cycles. It was also noted that, at any particular time, it is impossible to discern whether the differences between measured and theoretical displacements are due to potentiometer error or friction in the system.

The potentiometers were also able to record appreciable ranges of displacement over time, though not as large as theory predicts. This was illustrated in detail in Chapter 5. The recorded temperatures of the bridge were used to compute extreme values of displacement, and these values were not matched by measured displacements. The possibility of pier deflections accommodating the thermal changes was noted and examined in Chapter 7. It was also found that the bearings, while accumulating translations through the year, will return to original positions over time.

It was discovered that predicted displacements of the instrumented "free" bearing were oriented along the chord from the fixed bearing. Measured displacements also appeared to occur along the chord. It was noted, however, that several factors preclude this from occurring reliably at all times, and that the chord-oriented measured displacements could be questionable. It was noted that measured displacements were smaller than predicted values. If these motions were allowed to occur freely, the directions of displacements may change. As noted by Roeder, there is wisdom in using unguided bearings to prevent damage to the bearings.

Finally, it was seen that the maximum range of recorded longitudinal displacements was some 40 millimeters. The maximum range of predicted longitudinal displacements was approximately 62 millimeters. This was

194

computed using three mean temperatures at each time step, namely, those of the inner girder, the outer girder, and the slab. It was noted that this is an approximate approach. As the bridge is curved and does not simply run in one direction, there will always be temperature differences along the length of the bridge which were not accounted for in the model. It was seen that, using this same approach, the maximum range of predicted transverse displacements was some 16 millimeters, while the maximum measured range was near 8 millimeters. The three-temperature approach used is essential for accurate predictions of transverse displacements. This was shown in Chapter 5, where the use of a single bridge temperature was shown to predict small values of transverse displacement. This is true even for the maximum range of ambient temperatures recorded, near 37 degrees Celsius.

Finally, if the bridge is treated as a straight element spanning between the "fixed" bearing and the guided bearing at the northern pier, it has an expansion length of approximately 135.3 meters. An estimation of the maximum longitudinal displacement the bridge would undergo, based on ambient temperature records and the relation $\Delta=\alpha(\Delta T)L$, is thus $(1.17\text{x}10^{-5}$ /ºC$)(37$ºC$)(135.3$ m$)=59$ millimeters. This closely approximates the finite element prediction of the maximum displacement, 62 millimeters.

8.3   Thermally-Induced Girder Rotations

It was found that measured rotations of the girders at the bearings followed temperature trends and theoretical trends well. Rotations were seen to occur in both directions, with the diaphragms at the piers forcing the girders to rotate together about the longitudinal axis of the bridge. Measured rotations were found to typically be somewhat smaller than theoretical rotation magnitudes. Transverse rotations, as expected, were small and this was contributed to the fact

that the presence of diaphragms linking the girders at both piers forces the girders to rotate as a unit in the transverse direction. Finally, it was found that all measured rotations due to thermal changes were at least one order of magnitude smaller than the maximum rotation magnitudes the pot bearings can safely allow.

8.4   Thermally-Induced Stresses and Pier Deflections

It was noted that, if thermally-induced girder deformations are restrained, significant stresses will arise in the girders and slab. Analyses were performed for typical values of longitudinal girder restraint and a 40ºC uniform temperature rise. While it was found that bottom flange plate buckling probably will not occur, there is an appreciable added compressive stress to the flange at the supports. Peak values were found to be approximately 25 MPa. It was also found that, for this somewhat conservative analysis, the concrete slab may be on the verge of cracking over the fixed bearing support.

It was also noted that pier deflections will reduce the induced stresses just described. To garner an idea of whether the piers are in fact deflecting, deflections were monitored on August 12, 1998, while the computerized instrumentation measured relevant temperatures and girder deformations. It was discovered that the piers do indeed deflect. Northern pier deflections, when added to measured girder deformations at the bearing, closely approximate predicted girder deformations at this location. However, southern pier deflections were rather large, and, when added to girder deformations measured at this location, significantly surpassed predicted girder deformations at this location. It was then hypothesized that the presence of concrete U-beams adjacent to the steel portions of this bridge stiffen the end piers somewhat, and that the taller, more flexible inner piers accommodate friction in the system by deflecting relatively large amounts. While it was noted that large deflections at these piers require

large forces at the pier caps, it was also recalled that the piers were treated as cantilevers with rigid bases. The pier supports are likely not this stiff in reality, and it was noted that relatively small rotations at the bases of the piers will significantly reduce the forces required at the pier caps to cause these deflections. In the limit, the piers may undergo rigid-body rotation, causing the measured deflections in the absence of any lateral force.

8.5   Conclusion

In conclusion, it was determined that the trapezoidal box girder bridge at Beltway 8 and Interstate 45 is accommodating thermal changes over time through a combination of girder deformations at the bearings, pier deflections, and induced stresses within the bridge superstructure, including the concrete spans adjacent to the instrumented spans. The clogged expansion joint allows the generated forces due to the restraint of deformations to be spread to the adjacent slab and concrete U-beams, while the instrumented girders and piers also absorb stresses and deflect. These concrete U-beams are likely stiffening the end piers of the steel spans somewhat. Significant deflections of the taller inner piers accommodate additional, unaccounted-for friction in the system. Large forces are not required to cause these rotations, thus, the bearings are not required to transmit these forces to the pier caps. If the bearings were required to transmit the forces, damage and or destruction of the bearings may result, however, the bearings appear to be free from this condition.

References

American Association of State Highway and Transportation Officials. *LRFD Bridge Design Specifications (SI Units).* Second Edition. Washington, D.C., 1998.

Billington, N.S. *Thermal Properties of Buildings.* Cleaver-Hume Press, Ltd., 1952.

Emerson, M. "Thermal Movements in Concrete Bridges-Field Measurements and Methods of Prediction." *Publication SP-70, Vol. 1.* American Concrete Institute, Detroit, MI. 1981.

Fu, H.C., et. al. "Thermal Behavior of Composite Bridges." *Journal of Structural Engineering,* Vol. 116, No. 12 (December 1990). American Society of Civil Engineers, New York, N.Y., pp. 3302-3323.

Moorty, Shashi, and Roeder, Charles W. "Temperature-Dependent Bridge Movements." *Journal of Structural Engineering,* Vol. 118, No. 4 (April 1992). American Society of Civil Engineers, New York, N.Y., pp. 1090-1105.

Roeder, Charles W. *Thermal Movement Design Procedure for Steel Bridges. Final Report prepared for the AISI Transportation and Infrastructure Committee.* Funded by the American Iron and Steel Institute Projects. 1998.

Roeder, Charles, and Stanton, John. *Steel Bridge Bearing Selection and Design Guide, Vol. II, Highway Structures Design Handbook.* American Iron and Steel Institute. 1996.

Thepchatri, Thaksin; Johnson, C. Philip; Matlock, Hudson. "Prediction of Temperature and Stresses in Highway Bridges By A Numerical Procedure Using Daily Weather Reports." Research Report 23-1, Preliminary Review Copy. Center for Highway Research, Austin, TX. 1977.

Will, Kenneth M.; Johnson, C. Philip; Matlock, Hudson. "Analytical and Experimental Investigation of the Thermal Response of Highway Bridges." Research Report 23-2, Preliminary Review Copy. Center for Highway Research, Austin, TX. 1977.